

EFFECT OF EXTENDED ENVIRONMENTAL EXPOSURE ON THE DURABILITY OF HIGH-STRENGTH SILICA FUME CONCRETE

*Ahmed M. Saleh and Mohammad H. Swellam
Structural Engineering Department, Cairo University

ABSTRACT

Durability of high strength silica fume concrete under different extended environmental exposure conditions is assessed through the measurement of the concrete compressive strength at different concrete ages and its water permeability. The progress of the compressive strength up to 875 days was monitored for three batches kept under three environmental conditions; namely, standard laboratory conditions, down town typically air polluted environment, and coastal exposure conditions of the Mediterranean with high chloride-sulfate content. The strength progression for the batch kept at lab conditions showed an increase in compressive strength followed by an almost steady state while the two batches kept under down town and coastal conditions showed an increase followed by a decrease in strength. Permeability was measured for the three batches at the age of 480 days. The batch kept at the lab conditions possessed the least permeability while the one exposed to coastal environment possessed the highest and was two and half times that of the batch kept under lab conditions.

KEYWORDS: High-strength concrete; silica fume concrete; concrete durability; compressive strength evolution; concrete permeability; environmental exposure.

INTRODUCTION

In spite of the many advantages that can be favorably utilized in the construction industry, the use of high strength concrete (HSC) is still limited within the Egyptian construction industry. Many special structures like long-span bridges and high-rise buildings can benefit from the high strength-to-weight ratio of HSC. The resulting structures are more slender and are favorably accepted in terms of aesthetics and cost saving. HSC has been produced from traditional constituents (sand, crushed stone, cements, and additives including silica fume). The positive effect of silica fume on the concrete properties is attributed to its filler effect, aggregate-mortar interface strength enhancement, and its pozzolanic action where it reacts with the calcium hydroxide to provide additional calcium silicate hydrate and hence hypothetically improves the long term concrete properties; concrete durability.

Several researchers [1 to 8] reported an increase in early strength for ages of 3 to 90 days where the concrete was subjected to laboratory conditions. Accordingly, one finds in the literature an implicit notion that the strength will be larger than the 28 days value at all subsequent concrete ages. In most cases, researchers reported an optimum silica replacement which lies between 15% and 25 % of the cement content leading to an increase in the 28-days strengths, sometimes in excess of 100 MPa [4 to 8]. Hooton [7], monitored the retrogression of strength beyond 365 days for mixes of low w/c ratio and high cement content kept under laboratory conditions. He reported a slight decrease of strength at 5 years which he explained as a typical scatter observed in long term strength tests and hence did not contradict the notion of progressive increase of strength.

* Corresponding author
Received Date:23/3/08
Acceptance Date:21/4/08

However, in [20], the reduction has been attributed to large shrinkage caused by the relatively unbalanced mix constituents. Trejo et al [9] and Bushlaibi [10] studied the effect of curing and early age environmental exposure on the mechanical properties of HSC up to 56 days. They observed that compressive strength is adversely affected when early age temperature and humidity are varied from standard lab curing conditions. However, all their tested samples showed increase in compressive strength till the age of 56 days.

Yogendran et al [8] reported a slight decrease in permeability (measured by air content) with the increase of silica fume content, while Mohamed et al [11] reported an increase in air content with the increase of silica fume. On the other hand, Bayasi et al [12] and Pigeon et al [13] reported a slight variation in air content of no specific trend with the variation of silica fume content. Such contradicting observations are attributed to the fact that major factors, other than silica content, such as w/c ratio, degree and method of compaction as well as type and content of plasticizer varied from one researcher to the other.

Durability of concrete structures may be examined by different lab tests including air permeability, chloride diffusion, carbonation, leaching with ammonium nitrate, etc. [14]. All lab tests are intended to measure durability indicators and to approximate actual exposure conditions. In this work, actual exposure conditions are utilized by placing the concrete samples in the real environment for sufficiently long period. Durability is monitored by measuring the concrete compressive strength development with time as well as by measuring the concrete permeability.

The progression of strength for three batches of a single concrete mix was monitored up to 875 days. The first batch was the control batch that was kept under lab conditions; the second batch was stored at a location down town Cairo, where air pollution is dominant throughout the year; while the third batch was stored at a location close to the shore of the Mediterranean. Water permeability was also measured for the three batches at the age of 480 days. The effects of extended environmental exposure on the progression of strength and permeability of HSC are reported in the following sections.

CONCRETE MIX DESIGN

Trial mixes were conducted aiming at the highest concrete strength that can be achieved using non-exotic locally available constituents. Several types of large aggregates including siliceous, crushed granite, crushed marble, crushed basalt, and crushed dolomite were used in the trial mixes. The aggregate type that produced the highest strength was the 10 to 20mm crushed dolomite, for which different mix proportions were investigated. It should be noted that for all studied aggregates and mixes, the failure surface possessed steep planes that passed through the large aggregates as shown in Fig. 1, indicating that no further increase in concrete strength can be achieved by enhancing the paste or interface strengths and any further increase in strength can only be realized when aggregates with higher crushing value are used.

The highest strength achieved at 28 days was about 80 MPa, the concrete mix is given in Table1. The indicated mix had a very high workability that no measure of slump could be made. Vibrators were used inside and outside of the moulds to drive the air bubbles out of the cast concrete.

Table 1: Concrete Mix for High-Strength Concrete

Constituents	Content per cubic meter
Large aggregates (Kg)	1040
Small aggregates (Kg)	520
Portland Cement (Kg)	550
Silica fume (Kg)	110
Water (liter)	132
Super plasticizer (liter)	20



(a) Crushed Basalt



(b) Crushed Dolomite

Fig. 1: Steep failure surfaces of standard cubes utilizing different types of large aggregates

EXPERIMENTAL PROGRAM

Three batches were prepared consisting of standard cubes and cylinders. Since the curing method was found to influence the mechanical properties of HSC [9, 10], all batches were similarly cured for two weeks in a water tank and were later moved to the required environmental exposure. The samples of the control batch were stored under lab conditions, outside but close to the curing tanks. As for the other two batches, one batch was placed within the Cairo down town area where air pollution due to traffic emissions is typically high. The samples were placed on a flat surface in open air about six meters above road level. The second batch was placed in an area west of Alexandria, close to the sea shore (about 400 meters away from the sea line). The samples were sprayed with sea water only upon arrival to the site then left to the natural conditions. Fig. 2 shows the storage conditions for the three batches. It should be noted that the specimens at Cairo down town and the sea shore batches were stored outdoor where they were subjected to natural solar radiation, temperature, humidity and rain of the actual environment. For the control batch, the progress of compressive strength was monitored up to 725 days, whereas the compressive strength of the other two batches was monitored up to 875 days.



(a) Controlled



(b) Air polluted



(c) Coastal

Fig. 2: Concrete samples located in different environments



(a) Specimens (½ standard cylinders) (b) Testing apparatus
Fig. 3: Specimens and apparatus used in the comparative permeability tests

Permeability testing was conducted at concrete age of 480 days, for the three batches, in a non-standard apparatus using half standard cylinders as shown in Fig. 3. The specimens were placed in the closed vessels of the apparatus and were subjected to pressurized water. The specimens were left under a pressure of 30 Bar for a period of 4½ to 6½ hours. Water that penetrated the concrete specimen was collected and its volume was measured at the end of the test period. The permeability is measured through an index given by Eq. 1 [15]. The permeability of different samples was compared, relative to each other, via the calculated index.

$$PI = \frac{Vh}{ptA} \tag{1}$$

where; *PI* is the Permeability Index (velocity units)
V is the volume of collected permeated water
h is the specimen height
p is the applied pressure head (height of water column)
t is the time to permeate
A is the cross sectional area of the specimen

RESULTS

The compressive strength was monitored up to 725 days for the control specimens and up to 875 days for the polluted air and coastal batches. Each test constituted 3 to 4 standard cubes, where the reported results are the mean value for the tested cubes. The permeability of the three batches was measured at the age of 480 days. Each permeability test constituted 4 half-cylinders, the results reported below are the average of the 4 tests. The 28-days strength was 82.2 MPa for the control batch, 83.4 MPa for the polluted air batch, and 84.0 MPa for the coastal batch. It is to be noted that no test results were excluded in any of the tested groups for strength or permeability measurements.

Effect of Environment on the progression of the Compressive Strength

Figs. 4 and 5 illustrate the observed progressive increase in the compressive strength with time where the absolute strength is represented in Fig. 4 while Fig. 5 represents the compressive strength normalized by the 28-days strength. The strength for the control batch increased with time where the strengths at 7, 28, 70, 190, 610 and 725 days where 72.1, 82.2, 90.0, 91.0, 95.5 and 95.2 MPa, respectively.

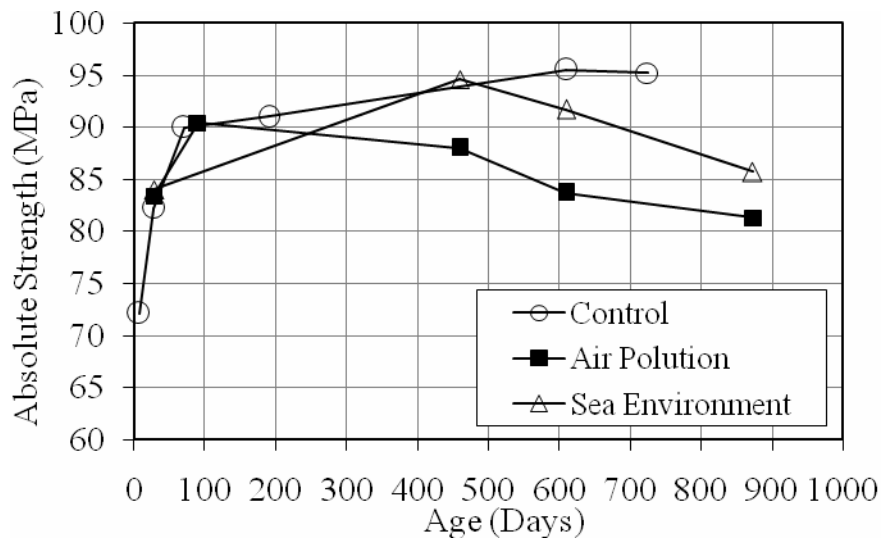


Fig. 4: Evolution of absolute strength with time for all batches

The strengths for the polluted air batch at 28, 90, 460, 610 and 875 days were 83.4, 90.4, 88.0, 83.7 and 81.3 MPa, respectively while the coastal batch provided strengths at 28, 460, 610 and 875 days equal to 84.0, 94.6, 91.7 and 85.7 MPa, respectively.

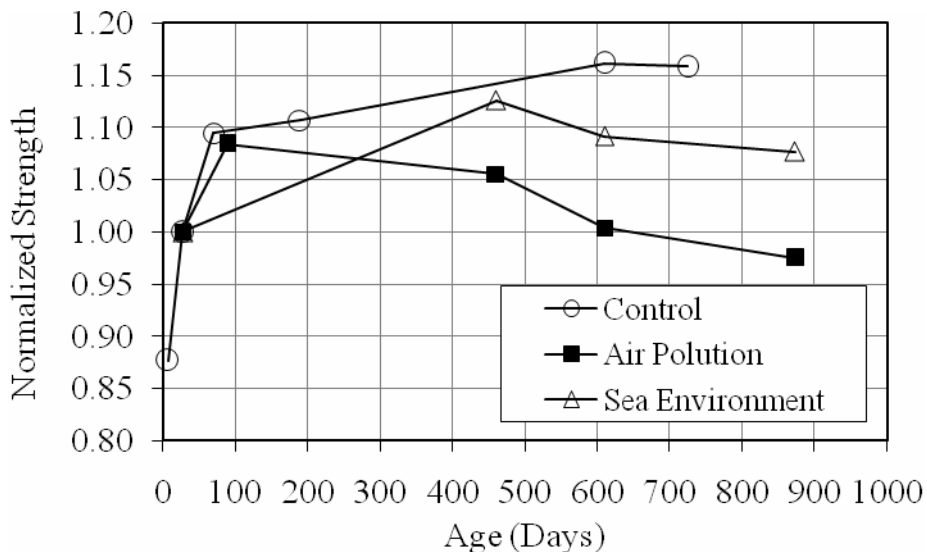


Fig. 5: Evolution of normalized strength with age for all batches

The 28-days strengths for the three batches were very close to each other at 82.2, 83.4, and 84.0 MPa. Figures 4 and 5 illustrate that a steady increase in absolute as well as normalized strengths for the control batch was observed up to 610 days followed by an almost constant strength at 725 days. On the other hand, retrogression of strength was observed for the polluted air batch as well as the coastal batch (both under relatively aggressive exposure conditions) where a decrease in strength was observed after long exposure. The control batch reached a steady state of about 95 MPa (1.156 relative strength). Under polluted air environment, after gaining relative strength up to 1.084 at 90 days, the relative strength at 460 days was only 1.055, which has further dropped to 1.004 and 0.975 at 610 and 875 days, respectively. Under coastal environment, a higher gain was observed at 460 days of relative strength as high as 1.126 which dropped to 1.02 at 875 days.

Effect of Environmental Exposure on Concrete Permeability

The permeability index for the three batches of concrete was measured at the age of 480 days. No permeability measurements were made at 28 days. The three batches are made of the same concrete mix, had similar manufacturing and curing conditions and of almost the same compressive strength, accordingly there is no reason to expect any significant difference in permeability of the three batches at this early age where the environmental effects are not measurable yet.

Three permeability indices were determined according to the test procedure specified in section 3 above; the results were $0.89\text{E-}9$, $1.1\text{E-}9$ and $2.24\text{E-}9$ mm/sec for the control, polluted air, and coastal batches, respectively.

The permeability index for the polluted air batch was higher than that of the control batch by 23%. Such a higher index indicates an adverse effect of carbonation of the environment at the Cairo down town location. On the other hand, a more severe effect is evident in the permeability index for the coastal batch, where a margin of 252% increase over the control batch was measured.

Values found in the literature for water permeability are based on different methods of measurement, accordingly a wide range of values is found. Gomes et al [16], classify different concrete grades at $1.0\text{E-}3$ mm/sec for high permeable concrete, $1.0\text{E-}3$ to $1.0\text{E-}4$ mm/sec for average permeable concrete, $1.0\text{E-}5$ to $1.0\text{E-}6$ mm/sec for low permeability concrete, $1.0\text{E-}6$ to $1.0\text{E-}7$ mm/sec for high impermeable concrete, and $1.0\text{E-}7$ to $1.0\text{E-}9$ mm/sec for higher impermeable concrete. In reference [17], the chloride diffusion coefficient is related to water permeability leading to specifying a value of $7.5\text{E-}7$ to $1.0\text{E-}9$ mm/sec for normal concrete and $1.4\text{E-}12$ to $2.0\text{E-}15$ mm/sec for high quality concrete. Neville [18] suggests that a maximum permeability of $1.5\text{E-}7$ mm/sec is often recommended in practice. Accordingly, the results obtained may all be considered representing "good" concrete according to Gomes et al [16] and Neville [18] but are all within the normal concrete grade according to [17].

In this study the conducted permeability test was not a standard test. However, the measured values reflect the relative effect of the considered environments. The effect of coastal environment is evident and raises the concern regarding the effectiveness of the concrete in protecting steel reinforcement against the migration of corroding agents from outside the concrete body. This is more pronounced when exposure is extended to longer periods of time as in the present tests.

DISCUSSION

The results obtained in this study demonstrate that there is an evident adverse effect of long term exposure of the HSC mix used to the considered natural environmental conditions that are not considered to be extremely severe to concrete structures. Since the control batch was kept under standard lab environment and it did not show any retrogression of strength, it is clear that this retrogression of strength was not an intrinsic property of the chosen mix and is solely attributed to the environmental exposure.

For the polluted air environment at Cairo down town, the observed reduction in strength may be attributed to the formation of the weak carbonic acid resulting in higher carbonation levels and consequently larger shrinkage [19]. Also, the carbonic acid formation and the subsequent higher carbonation level decrease the available amount of calcium hydroxide necessary for the reaction with silica fume to produce the sought long term calcium silicate hydrates that should have improved the concrete properties at long term.

For the coastal batch, the absolute strength was 94.6 MPa at 460 days which was higher than its 28-days strength followed by 91.7 MPa at 610 days and 85.7 MPa at 875 days. Such behavior may be attributed to the initial chloride's accelerator effect [19] which led to a progressive increase in strength until 460 days. This accelerator effect is then balanced and even overcome by the adverse effect of the sulfate attack which leads to the long term formation of gypsum and ettringite [19]. Gypsum and ettringite possess a volume larger than their components and expand upon imbibing water hence exerting internal pressure on hardened

concrete creating micro cracks that are expected to be the main reason for the strength retrogression observed at the ages of 610 and 875 days. This may also be the reason behind the two and half times increase in the permeability index for the coastal batch over the control batch. It should be noted that the ettringites become more water soluble in the presence of chlorides [19] and hence can easily be washed out by rain fall and/or during the permeability test leading to the high permeability index.

The results obtained in this study pose some questions that need to be addressed. First, how can the retrogression of strength be dealt with where strengths can drop with time to below the 28-days strength? Second, how does the retrogression of strength affect the credibility or the interpretation of results obtained from cores extracted long time after casting in environments similar to the studied conditions. Third, what are the nature and critical contents for pollutants that impose the retrogression threat and how can such threats be alleviated?

Further, the test results of this study suggest that when HSC containing silica fume is used in similar aggressive environments, a designer may not rely solely on the production of dense HSC and sufficient concrete cover to protect the steel reinforcement but should seek additional means to achieve the required structural durability.

CONCLUSIONS

The effect of environmental exposure and age on the strength and permeability of HSC were examined. Several observations were realized from the obtained test results:

1. Up to 610 days, concrete kept at the laboratory conditions developed the traditional progressive increase in compressive strength. Up to 610 days a 15% increase over the 28-days strength was observed after which the value almost remained constant up to 725 days,
2. Concrete cubes kept in polluted air environment showed a retrogression in strength to the extent that their 610 and 875 days compressive strength were only 1.004 and 0.975 of the 28 days strength,
3. Concrete cubes kept in coastal environment showed an initial increase in strength (12.6%) up to 460 days followed by a retrogression in strength at 610 and 875 days (1.092 and 1.077 of the 28 days strength),
4. Concrete samples kept at laboratory conditions provided the least permeability index of 0.89E-9 mm/sec. The concrete samples kept at coastal environment provided the highest permeability index of 2.24E-9 mm/sec, while at the polluted air environment the permeability index was 1.1E-9 mm/sec; all at the age of 480 days.

ACKNOWLEDGEMENT

The authors wish to thank the staff of the Concrete Research Lab, at Cairo University, for their efforts throughout the experimental work. Also, the Materials Lab at the National Housing and Building Research Centre is gratefully acknowledged for their support in conducting the permeability tests. Finally, Engineer M. Yehia is thanked for hosting the samples exposed to the coastal environment.

REFERENCES

1. Sellevold, E. J., and Radjy, F. F. (Aug. 1983), "Condensed Silica Fume in Concrete : Water Demand and Strength Development," Proceedings of the First International Conference on Fly Ash, Silica Fume, Slag and Other Mineral By-Products in Concrete, ACI Pubs. SP-79, Montebello, Canada, pp 677 – 694.
2. Molhotra, V. M. (1986), "Mechanical Properties, Freezing and Thawing Resistance of Non - Air-Entrained and Air-Entrained Condensed Silica Fume Concrete using ASTM Test C. 666," Cement, Concrete, and Aggregate.
3. Goldman, A., and Benture, A. (Sept- Oct 1989), "Bond Effects in High Strength Silica Fume Concretes," ACI Materials Journal, Vol. 86, No.5, pp 440-447.

4. Sandvik, M., Gjorv, O. E. (April 1986), "Effect of Condensed Silica Fume on the Strength Development of Concrete," Proc. Second International Conference on Fly Ash, Silica Fume, Slag, and other Mineral by-Products in Concrete, ACI SP-91, Madrid, Spain, pp 893 – 897.
5. Khalil, A. A. (1995), "Effect of Silica Fume on the Properties of Cementitious Concrete," M.Sc. Thesis, Al-Azhar University, Cairo, Egypt.
6. Wolseifer, J. (April 1984), "Ultra-High Strength Field Placeable Concrete with Silica Fume Admixture," Concrete International: Design & Construction, Vol. 6, No. 4, pp 25-31.
7. Hooton, R. D. (March 1993), "Influence of Silica Fume Replacement of Cement on Physical Properties and Resistance to Sulfate Attack, Freezing and Thawing, and Alkali-Silica Reactivity," ACI Materials Journal, pp 143-151.
8. Yogendran, V., Langan, B. W., Haque, M. N., and Ward, M. A. (March 1987), "Silica Fume in High Strength Concrete," ACI Materials Journal, pp 124-129.
9. Trejo, D., Moutassem, F., Hueste, M. B. D., Halmen, C., and Cline, D. B. H. (Nov-Dec 2007), "Influence of Environmental Exposure Conditions on Mechanical Properties of High-Strength Concrete," ACI Materials Journal, Vol. 104, No.6, pp 643-652.
10. Bushlaibi, A.H. (Jan. 2004), "Effects of Environmental and Curing Methods on the compressive Strength of Silica Fume High-strength Concrete," Advances in Cement Research, Vol. 16, No. 1, pp 17-22.
11. Mohamed, S. M. (1994), "Influence of Silica Fume on the Transition Zone between Mortar and Aggregate and on the Properties of Concrete," M.Sc. Thesis, Cairo University, Giza, Egypt.
12. Bayasi, Z. and Zhou, J. (July 1993), "Properties of Silica Fume Concrete and Mortar," ACI Materials Journal, pp 349-356.
13. Pigeon, M., Plante, P., and Plante, M. (Sept. 1989), "Air Void Stability, Part I: Influence of Silica Fume and other Parameters," ACI Materials Journal, pp 482-490.
14. Assié, S., Escadeillas, G., Marchese, G., and Waller, V. (Feb 2006), "Durability Properties of Low-resistance Self-Compacting Concrete," Magazine of Concrete Research, Vol. 58, No. 1, pp 1-7.
15. Matest Company, Italy, C430 series device manual (Water Permeability Testers), <http://www.matest.com/prodottovis.asp?cod=982&type=2&sec=4>, visited on 20 May 2008.
16. Gomes, A.M., Costa, J.O., Albertini, H. and Aguilar, J.E. (2003), "Permeability of Concrete: A study intended for the In-Situ Valuation using Portable Instruments and Traditional Techniques," International Symposium on Non-Destructive Testing in Civil Engineering (NDT-CE2003).
17. "Concrete Durability Report for Dubai Metro Project," (2006), CAPCIS Inc.
18. Neville, A. M. and Brooks, J.J. (1994), "Concrete Technology," ELBS edition, reprint, Longman Singapore.
19. Neville, A. M. (1981), "Properties of Concrete," The English Language Book Society and Pitman Publishing, Third Edition.
20. Neville, A. M. (1996), "Properties of Concrete," The English Language Book Society and Pitman Publishing, Fourth and Final Edition.

INFLUENCE OF SULFATE ATTACK ON CHLORIDE ION INGRESS IN HIGH-PERFORMANCE CONCRETE

Essam El-Rafey¹, *Rafik Abbas² and Maissa Salah El-Din³

1-Dean, Institute of Graduate Studies and Research, Alexandria University, Alexandria, Egypt.

2-Associate Professor, Institute of Graduate Studies and Research, Alexandria University, Egypt.

3-Central Lab and Research, Alexandria Water Co., Alexandria, Egypt.

ABSTRACT

This study was carried out to evaluate the influence of sulfate attack on chloride ingress in high-performance concrete. After water curing, the specimens were placed in three different test solutions, having the following compositions: 5.0% NaCl, 5.0% NaCl + 0.5% Na₂SO₄ and 5.0% NaCl + 20% Na₂SO₄. The deterioration of concrete due to combined attack were evaluated through change in compressive strength and expansion measurements. The concentrations of free chloride and sulfate penetrating specimens through diffusion were measured periodically, up to 18 months. Microstructure analysis was also carried out through X-ray diffraction and Scanning electron microscope. The experimental results showed that the presence of sulfate in the combined solution decreased the free chloride content at early exposure period, but the opposite was observed at latter exposure period. Addition of silica fume may significantly improve the resistance of concretes to combined attack. The content of C₃A in cement used in concrete proved to be an important factor in the concrete performance when subjected to combined attack. The high-performance concrete with its superior mix design (cement content and w/c ratio) confirmed its effectiveness in withstanding the influence of combined attack on concrete.

Keywords: High-Performance Concrete, Chloride ingress, Sulfate attack, Strength, Chemical Analysis, Microstructure Analysis.

INTRODUCTION

The application of high-performance concrete in high-rise buildings, bridges, and all other types of structures is increasingly growing; therefore, the demand for the research of its durability also increased. The durability of high-performance concrete is important because it determines the service life of the structures. Chloride ingress is of large concern when durability is considered. The chloride-induced corrosion can cause significant deterioration of reinforced concrete structures, resulting in costly repair. For this reason, the development of high-performance concrete capable of resisting chloride diffusion has been the subject of research for many years.

The ingress of chloride ion into concrete is slow if the concrete cover is not deteriorated. However, when the concrete cover is damaged by sulfate solution attack, which is commonly encountered in field constructions, chloride ion rapidly accesses to the surface of steel rebar embedded in concrete. The attack of sulfates on concrete is due to two principal reactions: the reaction of sulfate ions and Ca(OH)₂ to form gypsum and the reaction of the formed gypsum with calcium aluminate hydrates to form ettringite [1]. At present, many concrete constructions are severely deteriorated and lost its function only in several years, which is mainly caused by the concentrated salt solutions such as chloride and sulfate ions.

Corresponding author
Received Date:27/12/07
Acceptance Date:21/7/08

Many researches related to concrete deterioration and steel rebar corrosion are widely made in a sulfate solution or chloride solution [2-4]. However, little studies of the whole process of damage are done on concretes attacked by a combined salt solution of chloride and sulfate. Additionally, different viewpoints were expressed in these studies. The role of chloride ions in the presence of sulfate was frequently investigated, on the other hand the role of sulfate in the presence of chloride ions on the deterioration of concretes is not well established. Different scenarios have to be distinguished when assessing the influence of chlorides: (a) the case of externally applied chlorides, and (b) chlorides that are admixed during concrete production. Midgley and Illston [5] argued that for concretes incorporating chloride admixtures, the sulphates and chlorides in the system compete for reaction with C_3A resulting in a direct conversion of C_3A to ettringite and chloroaluminate (Friedel's salt, $C_3A \cdot CaCl_2 \cdot 10H_2O$). In the case of externally applied chlorides (such as deicer salt penetration or storage in chloride solution), there is no such competition between chloride and sulfate for C_3A . Instead the free chlorides entering concrete have a preferential reaction with any unreacted C_3A or its hydrates. Extensive review presented by Hillier et al. [6], has shown that the interaction of chloride ions and concrete could result in chloride ions being present in concrete in one of the following three forms: (a) Free chlorides in solution within the pore space, (b) Chlorides loosely bound (immobilized) by C-S-H, and (c) Chlorides strongly bound by C_3A hydrates mainly in the form of Friedel's salt, and to a lesser extent by C_4AF .

Limited experimental data developed by Al-Amoudi et al. [7] demonstrated that the damage caused in concrete by sulfate attack is reduced in the presence of chloride. They stated that the differences in the diffusion rates of sulfate and chloride ions is regarded as the main reason for the higher strength reduction and expansion observed in specimens placed in the sulfate solution compared with those placed in the sulfate-chloride solution. The rate of diffusion of chloride ions, being much higher than that of the sulfate ions, allows the chloride ions to permeate through the concrete surface much faster than the sulfate ions. Chlorides permeating into the concrete react with C_3A to form Friedel's salt as a result of which the quantity of C_3A available for the sulfate ions to react and form expansive ettringite is reduced. Feldman and Beaudoin [8] also reported that for the concrete stored in a composite solution for 12 months, the concurrent presence of sulfate and chloride ions in solution decreased the chloride ions ingress rate into plain concrete and concretes incorporating the partial replacement of cement with slag and silica fume. Tumidajski and Chan [9] showed a similar viewpoint about the ordinary Portland cement concrete based on the experimental results, while they also proposed that the presence of sulfate ion increased the chloride penetration and diffusivity in the slag concrete. In contrast, Dehwah et al. [10] considered that the presence of sulfate ions in the chloride solution did not influence the time to initiation of chloride-induced reinforcement corrosion, but the rate of corrosion increased with increasing sulfate concentration. The interaction between sulfate and chloride salt was quantitatively determined by Zuquan et al. [11]. Their experimental results showed that presence of sulfate in the combined solution increased the resistance to chloride ingress into concretes at early exposure period, but the opposition was observed at latter exposure period. Zibara [12] examined hydration products formed in cement pastes exposed to externally applied chlorides at normal temperatures. There were some findings showing that at high salt concentrations ettringite was partially consumed and replaced by Friedel's salt. Others disagree with the view that ettringite is influenced by chlorides. Midgley and Illston [5] reported that chlorides did not attack the ettringite when pastes were exposed to chloride penetration. Chloride concentrations of 3.0% and 15.0% NaCl were used in their study. Obviously, chloride ingress and deterioration of concretes would change with the different research circumstances.

The current work was conducted to investigate the effect of sulfate on chloride ingress in high-performance concrete incorporating silica fume, which is commonly used nowadays. It also addressed the influence of cement composition and concrete mix design on combined attack. Compressive strength, expansion of specimens, chloride ingress, sulfate content along with phase transformations were monitored. X-ray diffraction (XRD) and Scanning electron microscope (SEM) techniques were used to evaluate the damage process of concretes caused by mixed chloride and sulfate ions.

EXPERIMENTAL PROGRAM

Materials and Specimens Preparation

Commercial ordinary Portland cement type CEM I (32.5 R) was applied to all concretes. The cement phase composition was as follow: C₃S 47.4%, C₂S 26.1%, C₃A 9.8%, C₄AF 10.4%. The fineness was 315 m²/kg. The Silica fume was in powder form with an average of 93% silicon dioxide, 2.10 specific gravity and average specific surface of 20,000 m²/kg. The superplasticizer used was a sulfonated naphthalene formaldehyde superplasticizer with 39% solids content and a specific gravity of 1.19. The coarse aggregate used was crushed limestone with a maximum size of 20 mm and specific gravity of 2.57. The fine aggregate used was natural siliceous with a fineness modulus of 2.6 and specific gravity of 2.63.

Five HPC mixes and one conventional concrete mix (CNC) were examined. The HPC mixes complies with the United States Federal Highway Administration HPC Performance Grades 1 and 2 [13]. The mixture proportions and the corresponding compressive strengths of the concretes are given in table 1. The concrete mixes were prepared using a tilting drum mixer of 0.15 cubic meter capacity. The superplasticizer was incorporated in all HPC mixes and the content was adjusted to achieve a slump of 175 ± 25mm. Concrete was then cast in moulds and vibrated to ensure good compaction. The following specimens, for each concrete mix, were cast:

- 100 mm cubes for compressive strength measurements;
- 75 × 150 mm cylinders to determine the chloride and sulfate concentration;
- 75 × 75 × 285 mm concrete prisms to determine length change.

After casting, the specimens were covered with wet burlap for a period of 24 hours and then demolded. Concrete specimens were cured in water at 23 ± 2°C for 28 days.

Table 1: Mix proportions, slump and the 28-days compressive strengths, chloride and sulfate contents.

Ingredients (kg/m ³)	Mix No.					
	CNC	HPC1	HPC2	HPC3	HPC4	HPC5
Cement	400	400	400	450	450	450
SF	—	40	40	45	45	45
Water	195	154	142	173	145.5	135
Fine aggregate	660	700	685	660	665	700
Coarse aggregate	1015	1045	1035	1015	1025	1070
Superplasticizer (% of cement wt.)	—	2.2	2.75	2.0	2.4	2.85
w/c ratio	0.49	0.39	0.36	0.39	0.33	0.30
Slump (mm)	180	210	180	200	170	150
28-days compressive strength (MPa)	44.7	65.8	72.3	69.0	77.4	85.0
Chloride content (% cement)	0.07	0.07	0.06	0.08	0.08	0.08
Sulfate content (% cement)	2.65	2.93	2.86	2.79	2.74	2.89

Test Solutions

After water curing, the specimens were placed in three test solutions, having the following compositions:

- Solution No.1: 5.0% NaCl (chloride environment).
- Solution No.2: 5.0% NaCl + 0.5% Na₂SO₄ (chloride-low-sulfate environment).
- Solution No.3: 5.0% NaCl + 20% Na₂SO₄ (chloride-high-sulfate environment).

All the solutions contained NaCl and varying concentrations of sodium sulfate, in order to systematically evaluate the effect of sulfate ions on the chloride ingress and concrete deterioration. The surrounding surface of cylinders was isolated by epoxy coating, to ensure that the penetration of aggressive solutions will occur in the longitudinal direction of the cylinders. All mixes were immersed in the solutions for 18 months and tests were performed throughout this period. Solutions were changed after 7, and 14 days of immersion of concrete specimens; then at four-week intervals up to 18 months.

Testing Procedure

Compressive strengths, free chloride (water-soluble chloride) and sulfate contents for different concrete mixtures were measured at the end of curing period and before immersion in aggressive solutions.

Compressive strength test: Compressive tests were carried out on cube specimens at the end of curing period, and at three months intervals after immersion in aggressive solutions. Three cubes were tested for every mix at the required age.

Expansion measurements: The change in length of concrete prisms was measured according to ASTM C-490. Initial measurements were conducted after 28 days water curing. Then, all specimens were immersed into different aggressive solutions; periodical measurements were carried out with intervals not longer than two weeks.

Free chloride and sulfate contents: Samples were obtained from the cylindrical specimens to determine free chloride and sulfate contents in concretes at the end of curing period and at three months intervals after immersion in aggressive solutions. Samples were obtained using an industrial drill, housing a 20 mm diameter tungsten-tipped drill bit. Each concrete specimen was drilled longitudinally in 10 mm stages on each of the two faces of the concrete cylinder, to a maximum depth of 50 mm. The resulting powder from each depth was collected to give a sample of approximately 15.0 g. Each sample was then stored in airtight plastic bags until required for free chloride and sulfate analysis. The sulfate and the free chloride (water-soluble chloride) contents were gravimetrically determined [14]. Powder samples collected by drilling from different depths were mixed thoroughly, and a representative sample was used to measure the sulfate content. The background sulfate content of the concrete after water curing was subtracted from the obtained results.

Microstructure analysis of cement hydrates: The morphological changes in cement hydrates due to chloride and sulfate exposure were investigated using X-ray diffraction (XRD) and scanning electron microscope (SEM). The latter was equipped with an energy dispersive X-ray analyzer (EDXA) which provides semi-quantitative information on the elemental composition of concrete at the point of inspection. Mix HPC1, as high-performance concrete with 400 kg/m³ cement content and 0.39 w/c ratio, was selected to this investigation to insure the rapid attack. The powder at 15 mm depth was collected to perform the XRD analysis. Five powder samples were collected and analyzed: after curing in tap water; after 12 and 15 month of immersion in chloride solution; and after 12 and 18 month of immersion in chloride high-sulfate environment.

TESTS RESULTS

The results obtained from investigating the durability of high-performance concrete (HPC) are presented and compared to those of conventional concrete. The cube compressive strength, the mean chloride and sulfate contents, expressed as percentage of cement weight, after 28 days of water curing, are presented in table 1.

Change in Compressive Strength

The cube compressive strength of each mix throughout 18 months of immersion in different aggressive environments is given in table 2. The change in strength, expressed as a percentage of the 28-days results, is illustrated in fig. 1. Results revealed that change in compressive strength for concrete mixes stored in pure sodium chloride is mainly affected by the cement content and the w/c ratio. Mix CNC has a higher w/c ratio than the HPC mixes (w/c ratio = 0.49), and as a result, it showed a strength gain up to nine months then a plateau up to eighteen months. Mixes HPC1, and HPC3 have the same w/c ratio of 0.39 but with different cement content. They showed strength gain by 18.2 % and 14.8 %, respectively after twelve months of immersion. Mixes HPC2, and HPC4 have different w/c ratio of 0.36 and 0.33 and different cement content of 400 and 450 kg/m³, respectively. Mix HPC4 has a lower percentage gain in the strength than that of mix HPC2. However, the order of magnitude of strength gain

expressed in MPa, is actually much higher. Mix HPC5 has the lowest w/c ratio among all other mixes (w/c=0.3) and 450 kg/m³ cement content. This mix showed the lowest percent of strength gain between all mixes; however, it exhibited the highest strength. It was found that the concrete mixes gain a high percentage of compressive strength at early ages than at later ages, depending on the cement content and the w/c ratio. The strength increase is mainly due to the accelerating action of chloride ions with the calcium aluminates or calcium silicates. The decrease of compressive strength of the different mixes is mainly attributed to the formation of calcium chloroaluminate hydrate. This phase usually leads to softening of the paste. The liberated CaCl₂ acts as an accelerator at early ages, and by the increase of its amount, it acts in the reverse direction [15].

Table 2: Compressive strength of concrete mixes immersed in different solutions (MPa).

Mix No.	28-days strength	Immersion duration in 5% NaCl (months)				Immersion duration in 5%NaCl + 0.5%Na ₂ SO ₄ (months)				Immersion duration in 5%NaCl + 2.0%Na ₂ SO ₄ (months)			
		3	9	12	18	3	9	12	18	3	9	12	18
CNC	44.7	48.0	52.6	52.6	51.7	47.0	48.2	47.8	45.8	46.9	47.3	45.6	42.6
HPC1	65.8	70.4	75.4	77.8	76.8	69.1	73.7	73.0	71.1	70.1	71.4	71.1	69.1
HPC2	72.3	78.8	81.6	83.5	82.8	78.1	80.1	79.6	77.7	78.1	79.1	78.9	76.0
HPC3	69.0	73.3	78.6	79.2	78.5	72.7	76.9	76.5	75.8	71.8	75.8	75.3	74.0
HPC4	77.4	81.8	88.1	89.2	88.4	81.3	86.0	84.6	83.7	80.0	83.9	84.4	82.1
HPC5	85.0	89.3	92.9	94.4	94.8	88.7	91.1	91.0	91.3	88.4	89.7	90.3	89.5

As shown in fig. 1, the effect of sulfate attack was confirmed through the observed change in strength after twelve months of immersion in case of chloride-low sulfate solution and nine months for chloride-high sulfate solution. The reduction in strength was in direct relation with sulfate content, i.e., the higher the sulfate in the solution the higher and earlier the change in strength. For HPC mixes, slight reduction in strength was obvious after 12 months of immersion. Up to this stage, no significant difference was observed between HPC specimens immersed in low and high-sulfate environment. At later ages, the effect of sulfate attack on the strength of HPC was noticeable, with higher reduction for specimens stored in high-sulfate solution. From the previously mentioned results, it is obvious that conventional concrete and HPC mixes stored in sodium chloride-high sulfate environment exhibited lower strength than those stored in sodium chloride-low sulfate environment, and the latter one exhibited lower strength than those stored in pure sodium chloride.

After eighteen months of exposure, visual inspection of HPC specimens did not reveal any sign of severe concrete deterioration. However, some surface scaling was observed mostly on conventional concrete specimens and occasionally on HPC specimens exposed to sodium chloride-high sulfate environment.

It is well established that calcium aluminates hydrate reacts with sulfates and forms ettringite. A second type of reaction occurs between the calcium hydroxide and sulfates and forming gypsum. Gypsum reacts with calcium aluminates hydrate and forms again ettringite. The formation of gypsum and ettringite lead to a consequent disruption of the hardened cement paste. Deterioration of concrete due to sulfate attack is similar to eating away of the hydrated cement paste and progressively reducing it to a cohesionless granular mass leaving the aggregates exposed. This type of deterioration may lead to reduction in the cross-sectional area of the structural component (i.e., loss in weight of concrete) and decrease in strength and this explains the reduction of compressive strength of concrete specimens immersed in chloride-sulfate environments than in case of pure chloride environment [16].

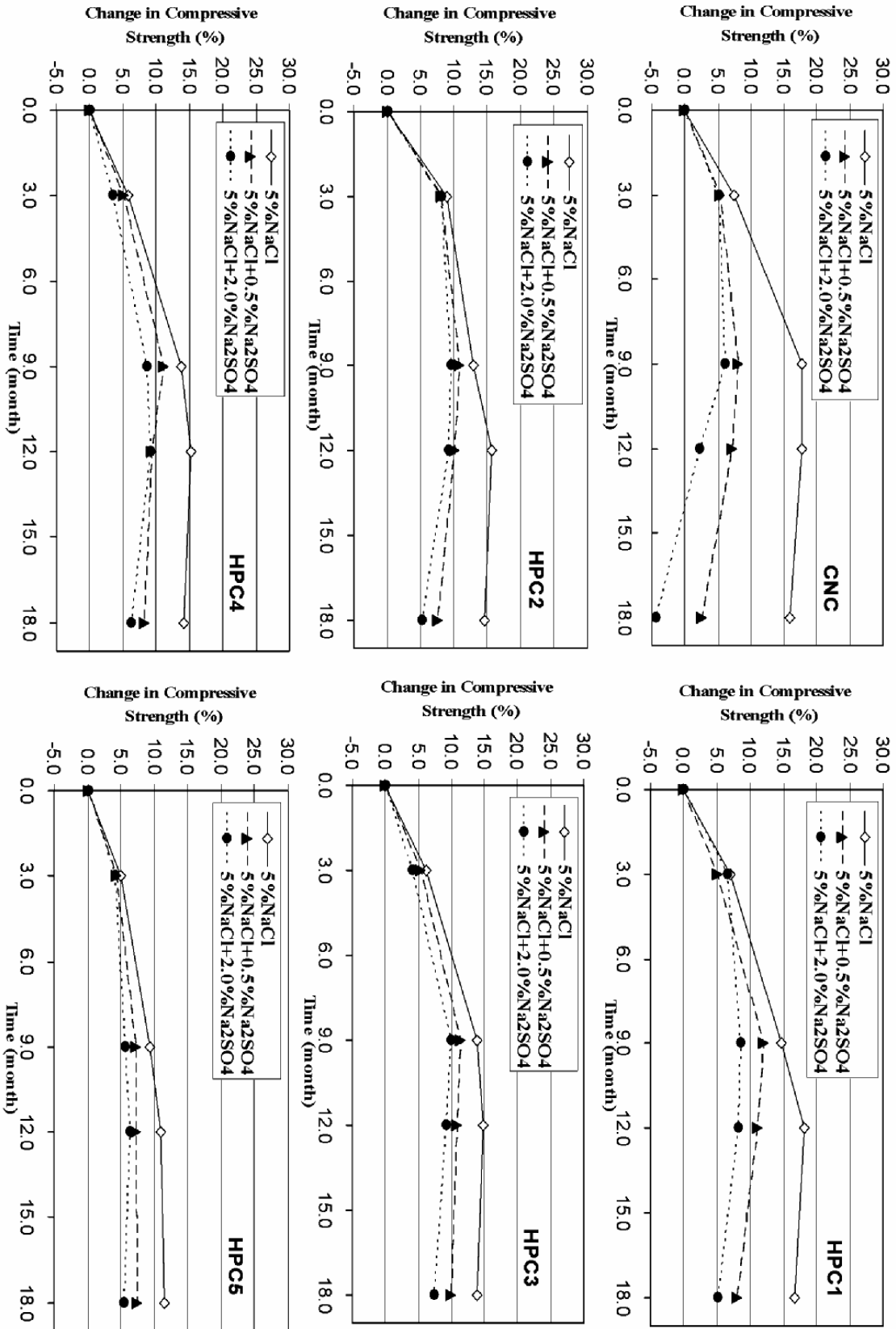


Fig. 1: Change in compressive strength of different mixes expressed as a percentage of the initial strength.

Expansion Measurements

The expansion of concrete immersed in pure sodium chloride, sodium chloride with low-sulfate and with high-sulfate environments are shown in fig. 2. Each figure presents one of the investigated mixes exposed to three different aggressive environments up to eighteen months of immersion. It is clear that the conventional concrete mix exhibited a typical behavior when subjected to different aggressive environment.

The highest expansion was manifested by specimens immersed in sodium chloride high-sulfate solution, besides, the lowest expansion values by specimens stored in chloride solution. Specimens stored in sodium chloride low-sulfate solution exhibited intermediate expansion values. HPC mixes followed the same trend with expansion values lower than the conventional concrete, depending on the cement content and the w/c ratio of each mix. The latter properties are found to be of primary importance in governing the expansion rate of HPC mixes in chloride-sulfate environment. Besides, it is clear that the difference in expansion values for specimens subjected to low and high-sulfate environments diminish as the cement content increases and/or decreasing the w/c ratio. For instance, the difference in expansion values of mix HPC5 subjected to low and high-sulfate solutions showed the lowest difference, as shown in fig. 2.

The rate of expansion at early ages was higher for conventional concrete than HPC mixes. It is noticeable that the expansion rates at early ages decrease as the cement content increases and/or decreasing the w/c ratio. This proves the effectiveness of these factors on the performance of HPC mixes in aggressive environment. It is important to note that the expansion values exhibited by these mixes confirm the formation of expansion products resulting from sulfate attack on hydrated cement, as will be confirmed by the sulfate penetration measurements presented in the next section.

Chloride Ingress

Table (3) presents the percentage of free chloride content for the investigated concrete mixes immersed in different aggressive environments for eighteen months at different depth intervals. Results are also illustrated in figs. 3-6, each figure represents the results of free chloride content, expressed as percent of cement weight, versus penetration depth at 6, 12, 15 and 18 months of immersion for conventional concrete (CNC), HPC1 and HPC5.

Based on the experimental data and after three months of exposure to different test solutions, the conventional concrete immersed in chloride solution showed a higher free chloride content than those exposed to chloride-sulfate solution. This was noticed in the outer layers; however, free chloride content was equal at inner layers, regardless of the solution composition. HPC mixes showed higher chloride contents at the outer depths when immersed in chloride solution. No significant difference in free chloride content was noticed for the HPC mixes at inner depths and in different environments.

After six months of immersion, it is clear that the free chloride content at outer layer for conventional concrete specimens immersed in pure chloride solution was higher than for specimens immersed in chloride-sulfate solutions, as shown in fig. 3. The effect of sulfate on the percentage of free chloride content was effective on the outer layers, where it suppresses the ingress of chloride ions in combined solutions. On the other hand, the difference in free chloride content between conventional concrete and the HPC mixes was obvious, where the free chloride contents for HPC mixes were lower by an average value of 50% than the control mix. It is clear that the concentration of free chloride decreased at inner depths, and reached a steady value at a depth of 15 mm.

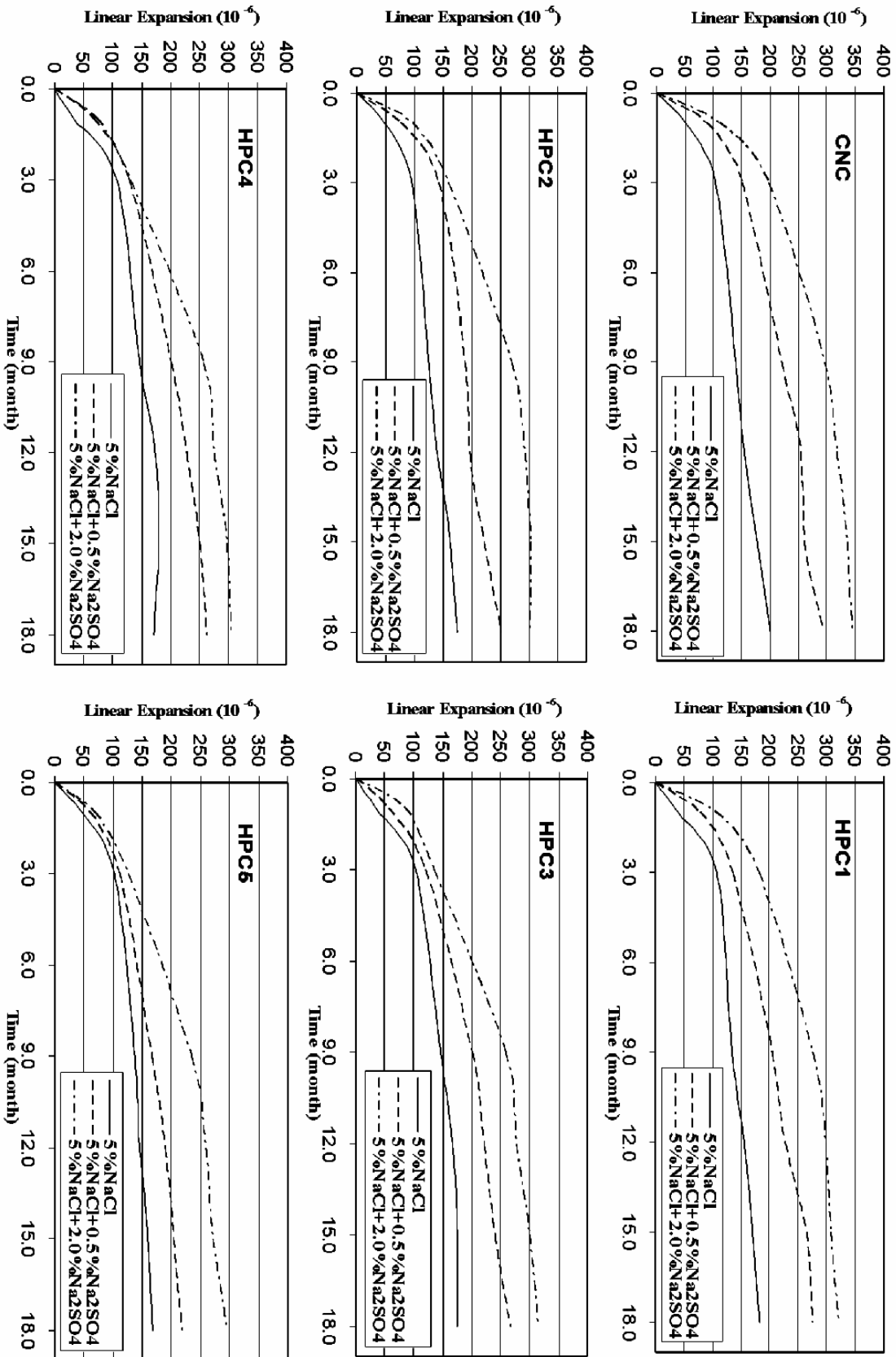


Fig. 2: Expansion of different mixes immersed in aggressive solutions.

Table 3: Free chloride content expressed as percent of cement weight for concrete specimens immersed in different solutions.

Mix No.	Depth (mm)	28-days Content	Immersion duration in 5% NaCl (months)						Immersion duration in 5%NaCl + 0.5%Na ₂ SO ₄ (months)						Immersion duration in 5%NaCl + 2.0%Na ₂ SO ₄ (months)					
			3	6	9	12	15	18	3	6	9	12	15	18	3	6	9	12	15	18
CNC	5.0	0.07	0.51	0.76	1.19	1.30	1.54	1.73	0.41	0.69	1.18	1.43	1.79	2.07	0.37	0.61	0.98	1.20	1.99	2.36
	15.0		0.34	0.35	0.58	0.71	0.99	1.12	0.22	0.34	0.53	0.78	1.15	1.31	0.20	0.27	0.41	0.58	1.25	1.48
	25.0		0.16	0.23	0.31	0.40	0.58	0.60	0.11	0.17	0.27	0.35	0.57	0.69	0.09	0.16	0.20	0.32	0.64	0.75
HPC1	35.0	0.07	0.09	0.12	0.19	0.23	0.27	0.32	0.08	0.11	0.16	0.21	0.28	0.39	0.09	0.09	0.16	0.19	0.32	0.46
	45.0		0.09	0.11	0.12	0.18	0.21	0.23	0.07	0.08	0.11	0.16	0.21	0.25	0.07	0.07	0.10	0.18	0.24	0.29
	5.0		0.32	0.57	0.93	1.10	1.43	1.60	0.30	0.37	0.80	1.03	1.60	1.85	0.28	0.34	0.67	1.00	1.61	1.98
HPC2	15.0	0.06	0.19	0.29	0.42	0.58	0.74	0.90	0.18	0.19	0.37	0.53	0.69	0.97	0.17	0.20	0.35	0.42	0.68	1.01
	25.0		0.11	0.15	0.20	0.30	0.32	0.46	0.08	0.14	0.18	0.22	0.36	0.48	0.09	0.12	0.13	0.19	0.41	0.58
	35.0		0.08	0.09	0.10	0.21	0.24	0.28	0.07	0.07	0.09	0.14	0.23	0.31	0.08	0.08	0.09	0.19	0.26	0.38
HPC3	45.0	0.08	0.09	0.09	0.09	0.12	0.15	0.17	0.07	0.07	0.08	0.12	0.18	0.20	0.08	0.09	0.07	0.12	0.18	0.23
	5.0		0.30	0.42	0.86	1.00	1.40	1.63	0.28	0.33	0.68	0.97	1.46	1.69	0.25	0.29	0.57	0.86	1.44	1.75
	15.0		0.18	0.19	0.38	0.42	0.66	0.83	0.15	0.17	0.31	0.36	0.61	0.74	0.15	0.17	0.28	0.32	0.54	0.82
HPC4	25.0	0.08	0.10	0.14	0.18	0.29	0.35	0.39	0.09	0.11	0.16	0.25	0.33	0.36	0.09	0.11	0.14	0.24	0.37	0.51
	35.0		0.09	0.09	0.11	0.20	0.24	0.28	0.07	0.08	0.09	0.12	0.26	0.29	0.09	0.08	0.09	0.13	0.27	0.35
	45.0		0.08	0.09	0.10	0.11	0.13	0.16	0.07	0.07	0.07	0.10	0.17	0.19	0.08	0.08	0.09	0.10	0.18	0.24
HPC5	5.0	0.08	0.31	0.44	0.88	1.14	1.35	1.65	0.25	0.39	0.69	0.96	1.38	1.68	0.24	0.33	0.56	0.94	1.36	1.78
	15.0		0.16	0.25	0.37	0.53	0.62	0.76	0.11	0.18	0.33	0.48	0.59	0.71	0.13	0.17	0.27	0.39	0.55	0.86
	25.0		0.09	0.18	0.23	0.30	0.33	0.38	0.08	0.13	0.23	0.26	0.36	0.41	0.10	0.13	0.16	0.21	0.35	0.49
HPC6	35.0	0.08	0.08	0.10	0.12	0.18	0.24	0.26	0.07	0.07	0.11	0.13	0.21	0.25	0.09	0.10	0.11	0.13	0.23	0.32
	45.0		0.08	0.09	0.10	0.12	0.13	0.16	0.07	0.07	0.08	0.10	0.15	0.17	0.09	0.06	0.07	0.10	0.13	0.21
	5.0		0.28	0.41	0.74	0.91	1.37	1.58	0.24	0.31	0.63	0.83	1.38	1.68	0.24	0.28	0.55	0.76	1.28	1.72
HPC7	15.0	0.08	0.15	0.21	0.31	0.44	0.54	0.62	0.13	0.19	0.27	0.36	0.48	0.64	0.12	0.18	0.23	0.34	0.49	0.72
	25.0		0.10	0.14	0.20	0.27	0.33	0.35	0.08	0.13	0.19	0.22	0.31	0.38	0.08	0.13	0.14	0.21	0.35	0.39
	35.0		0.09	0.11	0.13	0.15	0.23	0.26	0.06	0.08	0.10	0.14	0.22	0.25	0.08	0.10	0.09	0.12	0.24	0.24
HPC8	45.0	0.08	0.08	0.09	0.10	0.11	0.12	0.14	0.05	0.06	0.07	0.10	0.15	0.16	0.08	0.08	0.10	0.11	0.14	0.18
	5.0		0.24	0.39	0.70	0.84	1.25	1.49	0.21	0.32	0.53	0.69	1.28	1.54	0.21	0.28	0.47	0.65	1.24	1.63
	15.0		0.13	0.19	0.31	0.43	0.49	0.59	0.11	0.15	0.29	0.37	0.45	0.61	0.10	0.13	0.22	0.32	0.43	0.64
HPC9	25.0	0.08	0.12	0.13	0.22	0.25	0.29	0.29	0.09	0.10	0.18	0.23	0.27	0.29	0.09	0.11	0.16	0.23	0.25	0.31
	35.0		0.10	0.08	0.14	0.15	0.20	0.21	0.08	0.09	0.10	0.13	0.22	0.23	0.09	0.10	0.11	0.12	0.22	0.24
	45.0		0.08	0.08	0.09	0.09	0.11	0.12	0.08	0.09	0.10	0.11	0.12	0.14	0.08	0.09	0.11	0.10	0.13	0.15

After nine months of immersion, the values of free chloride for conventional concrete immersed in both chloride and chloride low-sulfate solutions were similar at outer layers (5 and 15mm) and higher at inner layers than the values exhibited by specimens immersed in chloride high-sulfate solution. The previously mentioned observation for conventional concrete was not observed in any of HPC mixes, where specimens immersed in chloride solution showed the highest free chloride content.

As shown in fig. 4, the percent of chloride content at the surface layer (up to 15mm) of CNC mix is higher for specimens immersed in chloride low-sulfate solution than those stored in both chloride and chloride high-sulfate solutions, for twelve months. This may be due to the effect of sulfate attack that took twelve months of immersion in aggressive environments to be effective. At inner depths, the percentages of free chloride content were higher for specimens immersed in chloride solution than the other environments. This was observed in depths ranging from 25 to 45mm. Regarding HPC1 mix, specimens immersed in chloride solution showed higher free chloride content than the values exhibited by specimens immersed in other solutions. However, it is clear that the free chloride content of specimens immersed in chloride-sulfate solutions manifested a noticeable increase up to 15mm. Up to this immersing duration, the free chloride content for mix HPC5, regardless of the type of aggressive solution, did not show the steep drop in values observed at surface layers in other mixes. Usually, this steep decrease is due to the higher content of free chloride content at the outer layer. The ingress of chloride is known to be high in this layer, where the latter acts as reservoir of chloride for inner depths.

The free chloride content for specimens stored for fifteen months in different aggressive environments are presented in fig. 5. It is clear that the free chloride contents of conventional concrete (CNC) were higher for specimens immersed in chloride-sulfate solutions compared to those immersed in chloride solution. This may result from the effect of sulfate attack. The free chloride content of mix HPC5, with its higher cement content and lower w/c ratio, manifested a different behavior. The chloride content was similar for all specimens, regardless the aggressive environments they were exposed. This proves the delayed sulfate attack on high performance concrete despite of the high C_3A content of the used cement.

The free chloride contents after eighteen months of immersion in different aggressive environments are presented in fig. 6. As observed after fifteen months of immersion, the free chloride contents of conventional concrete (CNC) were higher for specimens immersed in chloride-sulfate solutions compared to those immersed in other solutions. Similar trend is observed for HPC1 mix except with lower free chloride content than conventional concrete mix. However, the free chloride content was higher in HPC1 than HPC5. The latter showed higher chloride content at outer layer, for specimens stored in chloride high-sulfate solution than those stored in other solutions. At inner depths, the HPC5 specimens manifested similar chloride content, regardless of the solution composition.

Change in Sulfate Content

Sulfate content of different concrete mixes immersed in different aggressive environments for eighteen months are illustrated in fig. 7, each figure represents the results of sulfate content versus immersion duration (3, 6, 9, 12, 15 and 18 months) up to 50mm depth. It is important to note that the background sulfate content of concrete was subtracted from the obtained results to facilitate the tracing of sulfate penetration from the surrounding environment. It is clear that the values of sulfate content at high-sulfate environment are higher than of low-sulfate environment. This may be due to the presence of high percentage of sulfate that leads to more cracks in the sample and as a result, the penetration of sulfate ions increased. From the obtained results, it can be found that, the amount of sulfate increases with the immersion time in different aggressive environments. However, the rate of increase in sulfate content was high at early ages for specimens stored in both solutions. CNC specimens stored in chloride low-sulfate solution exhibited high rate in sulfate penetration up to nine months and a slower rate at latter ages. This duration for CNC specimens stored in chloride high-sulfate solution was extended up to twelve months. Mix HPC1 has the same trend as the CNC mix at all environments but with lower values.

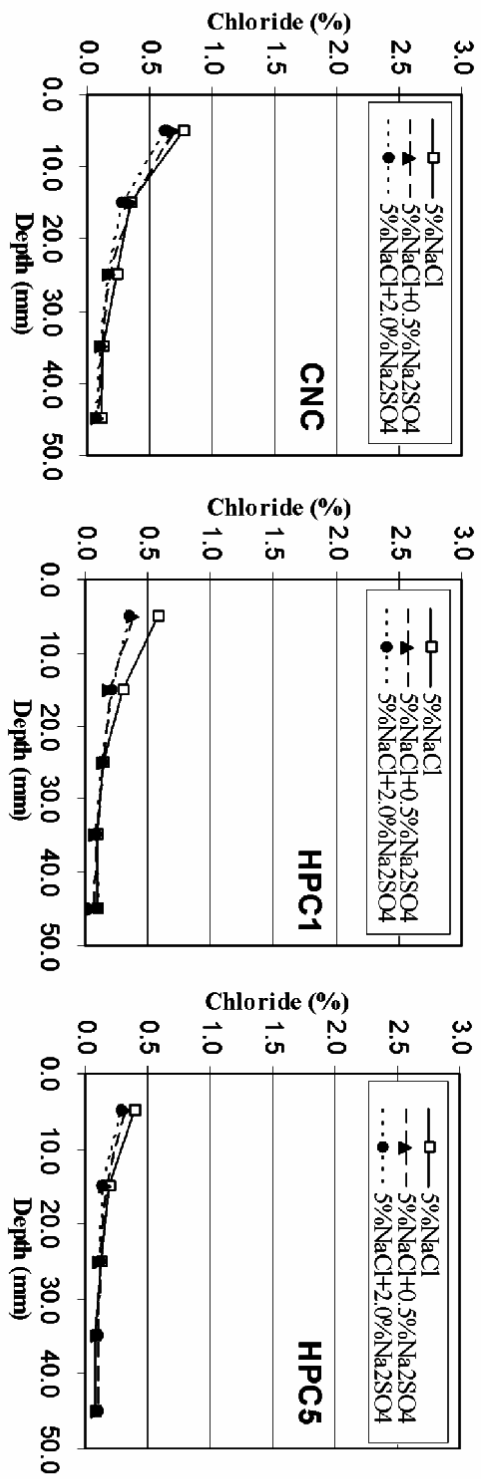


Fig. 3: Free chloride content expressed as percent of cement weight at different depths and after six months of exposure.

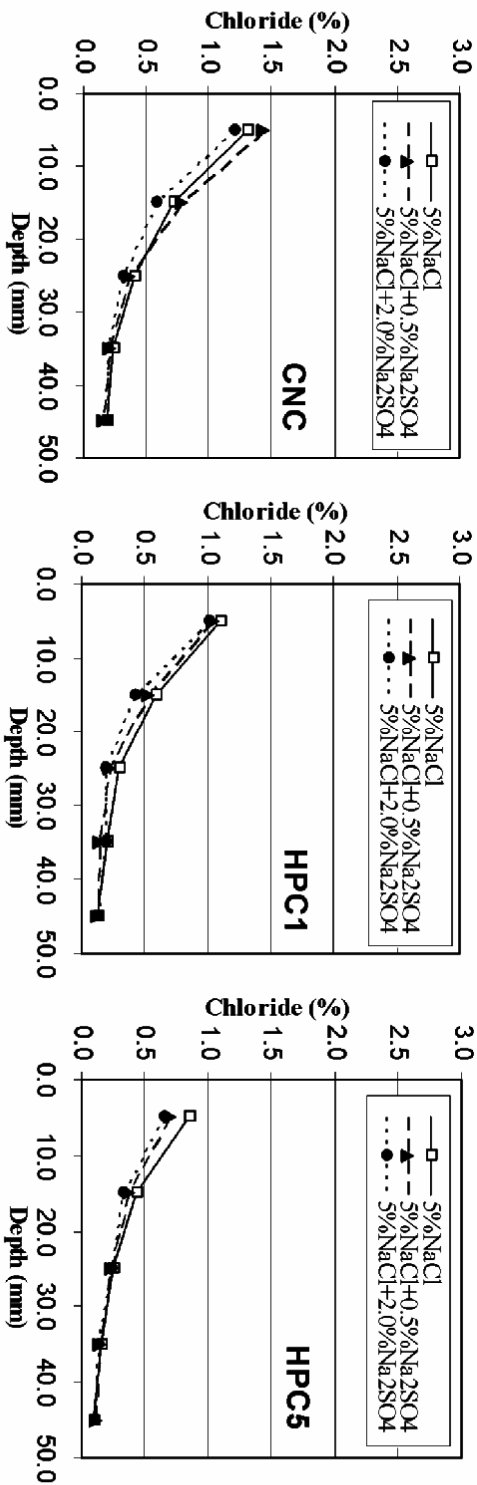


Fig. 4: Free chloride content expressed as percent of cement weight at different depths and after twelve months of exposure.

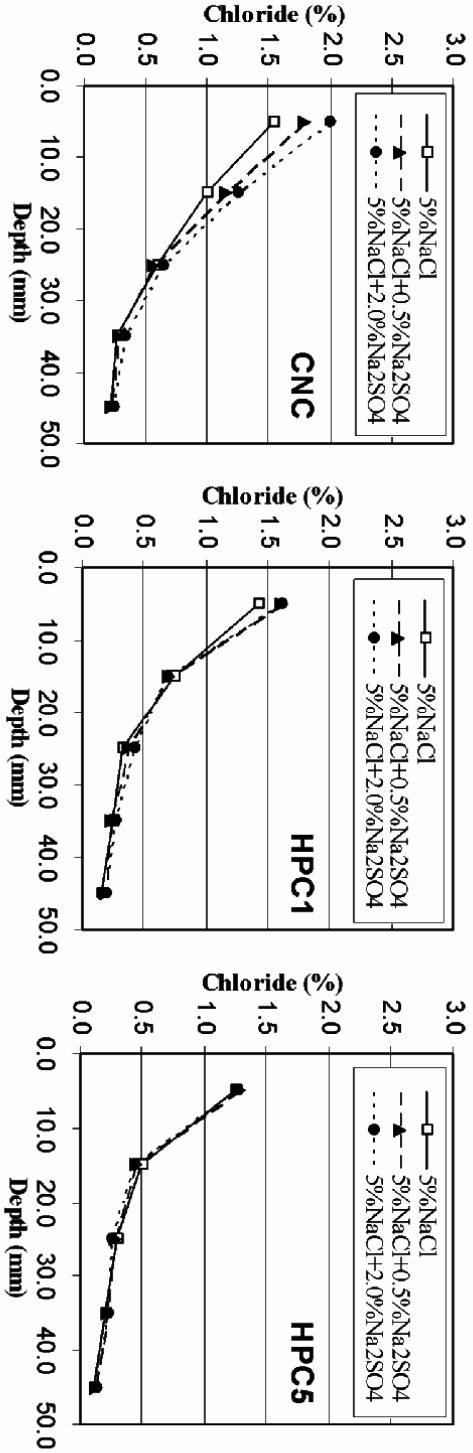


Fig. 5: Free chloride content expressed as percent of cement weight at different depths and after fifteen months of exposure.

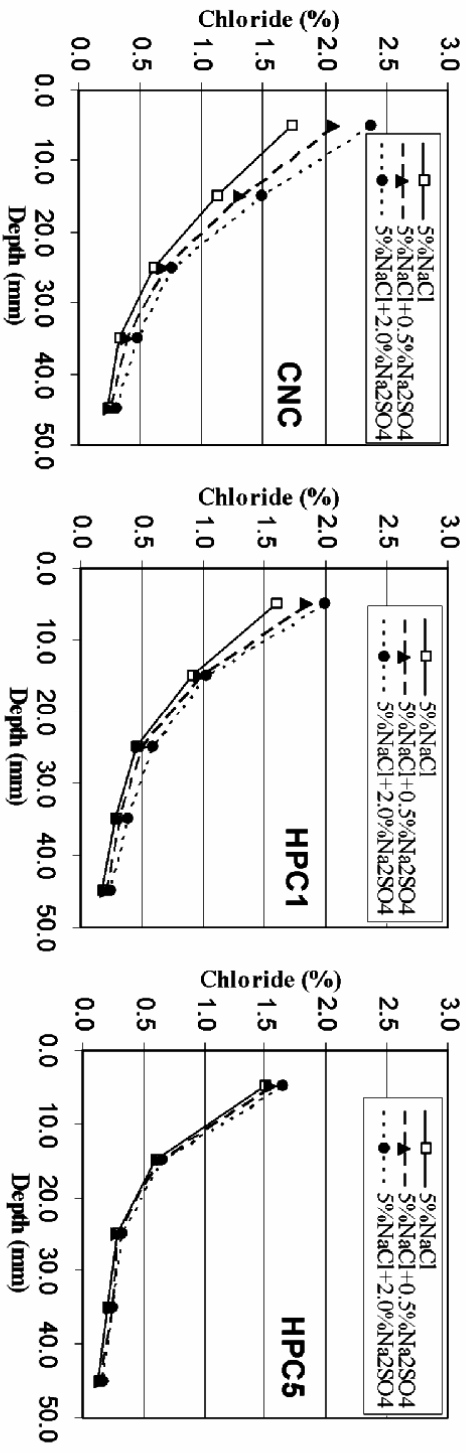


Fig. 6: Free chloride content expressed as percent of cement weight at different depths and after eighteen months of exposure.

On the other hand, the rate of increase in sulfate content for HPC5 mix stored in chloride sulfate solution was almost steady during the testing period, and with lower rate than conventional concrete. The effect of low w/c ratio, which is the main characteristic of HPC mixes prove its positive impact in decreasing the rate and percentage of sulfate penetration. Besides, it is obvious that the presence of chloride in the surrounding solutions did not mitigate the sulfate penetration. This may be detected by the difference in sulfate content encountered with increasing the sulfate content in the surrounding environment. As stated in previous results, the presence of chloride ions either in the surrounding environment or in the pore solution did not exhibited any positive effect in mitigating the penetration of the sulfate ions [17].

The type of cement (CEM I 32.5 R) which was used throughout this investigation with its high amount of tricalcium-aluminate component (9.88%) can react with sulfate ions to form ettringite. It is clear that the C_3A has an important role on sulfate attack; cements of low C_3A are recommended in situations where the concrete are exposed to sulfate environments. However, cements with low C_3A generally have a higher C_3S/C_2S ratio. An increase in the C_3S content of cement, therefore, generates a significantly higher quantity of calcium hydroxide. The produced calcium hydroxide may directly be combined with the sulfate ions leading to the formation of gypsum, leading to the reduction of stiffness and strength. However, the presence of silica fume, with its pozzolanic activity, may diminish this effect by the reaction with calcium hydroxide. It is well known that dense, low water to cement (w/c) ratio concrete is recommended for any construction from durability perspective. This is because all the deterioration phenomena are directly related to the permeability of concrete.

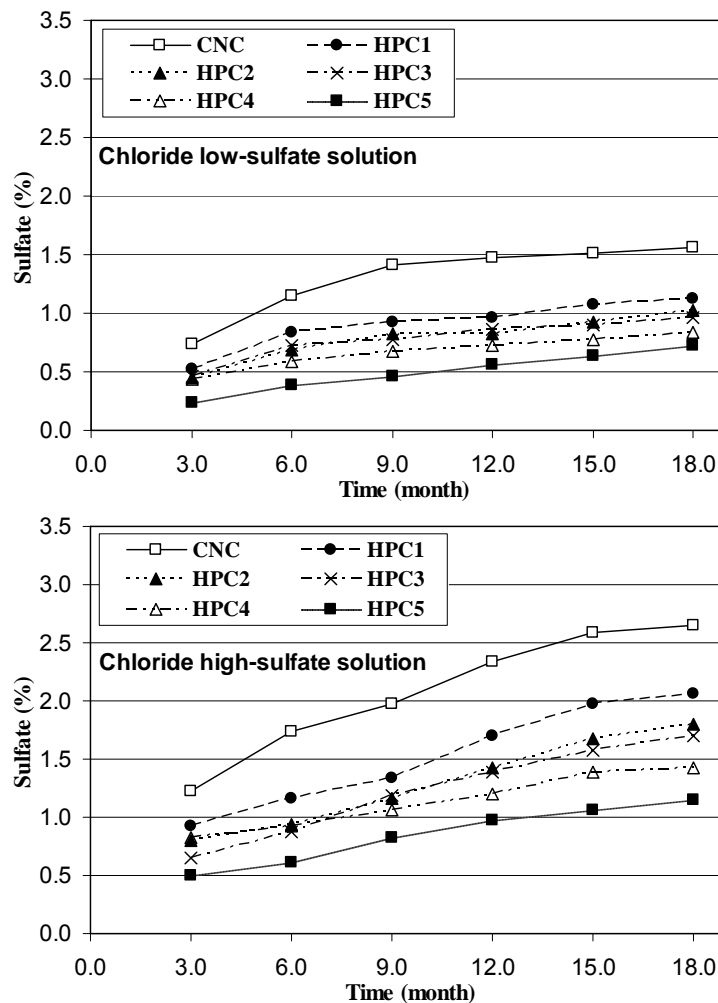


Fig. 7: Change in sulfate content for different mixes expressed as percent of cement.

Microstructure Change of HPC Exposed to Combined Solutions

The X-Ray diffraction (XRD) analysis was performed on the powder collected from drilling of the isolated cylindrical specimens from HPC1 at 15mm depth. The designated depth (i.e, 15 mm) was expected to be a stable media for reaction between the aggressive ions and the hydration products, where superficial part of specimens is usually characterized by its higher content of surrounding solution.

The XRD patterns of the HPC1 mix is illustrated in fig. 8. Quartz (Q) and Calcite (C) are the main phases found in all patterns. The presence of these two phases is due to the existence of sand and limestone, which were used as fine and coarse aggregate, respectively. The XRD pattern of HPC specimen cured in water for 28 days is shown in fig. 8 (a). It is clear that a typical pattern is obtained, where portlandite (P), anhydrous cement (AC) are present and easily detected. Fig. 8 (b and c) show the XRD patterns of HPC specimens immersed in 5% sodium chloride solution for a period of 12 and 15 months, respectively. Both patterns demonstrate the presence of the main hydration products: Portlandite and with almost no traces of anhydrous cement. Besides, Friedel's salt (CCA), which is a typical phase found in concrete subjected to chloride environment [18] is clearly identified in both patterns.

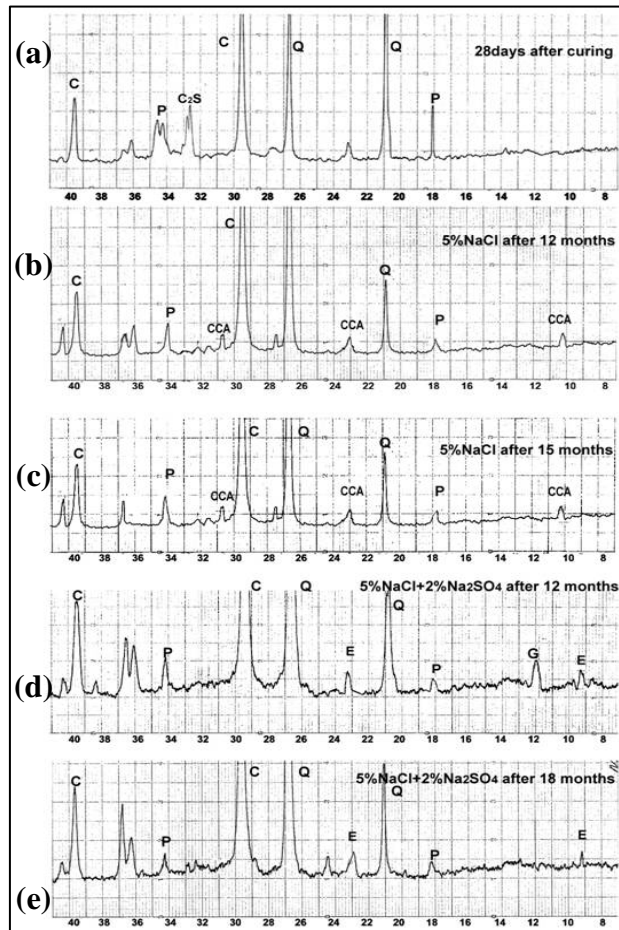


Fig. 8: X-Ray Diffraction patterns of HPC1 mix.

Quartz (Q), Calcite (C), Portlandite (P), Friedel's salt (CCA), Gypsum (G) and Ettringite (E). (a) after 28-days of water curing, (b) after 12 month of immersion in chloride solution, (c) after 15 month of immersion in chloride solution, (d) after 12 month of immersion in chloride high-sulfate solution, and (e) after 18 month of immersion in chloride high-sulfate solution.

The XRD patterns of HPC specimens immersed in chloride high-sulfate solution for a period of 15 and 18 months are presented in fig. 8 (d and e), respectively. Both patterns revealed the presence of Gypsum (G) and Ettringite (E) phases, which are the typical phases usually found in concrete mixtures made of Ordinary Portland cement, regardless of the low C_3A content, and subjected to sulfate attack. The Friedel's salt phase was not found in these patterns. This observation is questionable, where it is believed that the use of OPC cement with a specified content of C_3A will increase the resistance of concrete towards sulfate attack in the presence of chloride, through the formation of stable Friedel's salt [7]. However, recent studies supported the obtained results and proved that the sulfoaluminate (Ettringite) is the dominant phase under combined attack, when using OPC with high C_3A content [17-20]. In other words, the disruption in concrete structure caused by sulfate attack is unavoidable when using cement with high C_3A content.

The morphological changes in cement hydrates were also investigated using scanning electron microscope (SEM). Fig. 9 shows the SEM micrograph of the HPC1 mix before immersion in different aggressive solutions. The energy dispersive spectrum (EDS) of the area indicated the presence of mainly calcium (Ca) in addition to silica (Si). A dense morphology of the calcium-silicate hydrate (C-S-H) is clear. Fig. 10 (a and b) shows the microstructure and the related EDS spectrum of HPC1 mix immersed in chloride solution for fifteen months. The EDXA of the area indicates the presence of mainly calcium (Ca) in addition to silica (Si). Morphology of the calcium-silicate hydrate (C-S-H) was noted. The EDS indicated the relative heights of the chloride (Cl), aluminum (Al) and calcium peaks, which proves the presence of Friedel's salt. The latter is present due to the effect of chloride environment. The EDS spectrum also indicated the presence of mainly oxygen (O) in addition to calcium (Ca) and carbon (C) which denotes for calcium carbonate. Calcium carbonate is a typical phase of limestone (coarse aggregate).

Fig 11 (a and b) show the microstructure and the related EDS spectrum of HPC1 mix immersed in chloride high-sulfate solution for a period of eighteen months. The EDS spectrum of the area, shown in each figure with the relative heights of the calcium, sulfate and aluminum peaks with an approximate ratio of 6:3:1 indicated that the needle-like crystals are ettringite crystals. The ettringite crystals can be seen in the pore of fig. 11 (a). It is expected that after longer period of exposure, pores will be completely filled up by needle-like crystals, and with the further development of exposure period, it will result in occurrence of cracking. Although, chloride ions were present in the solution, the existence of Friedel's salt was not recognized in any specimens, only traces of chloride (Cl), which may result from free or loosely bound chloride [6,21].

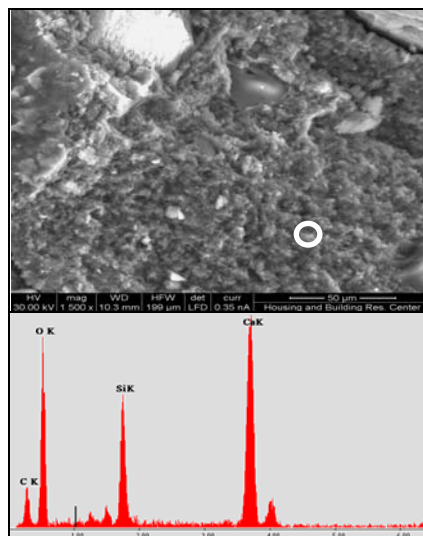


Fig. 9: SEM and EDS of HPC1 mix after water curing for 28 days.

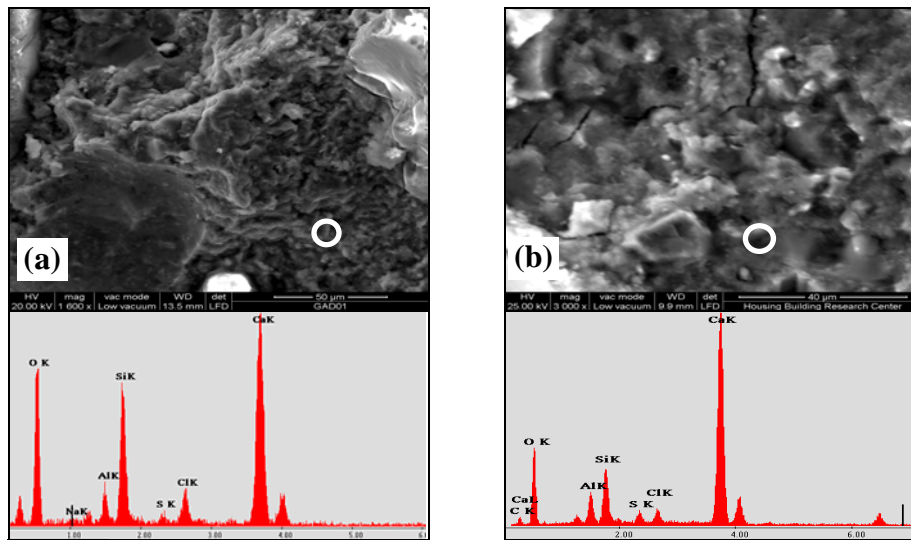


Fig. 10: SEM and EDS of HPC1 immersed in 5% sodium chloride solution for 15 months.

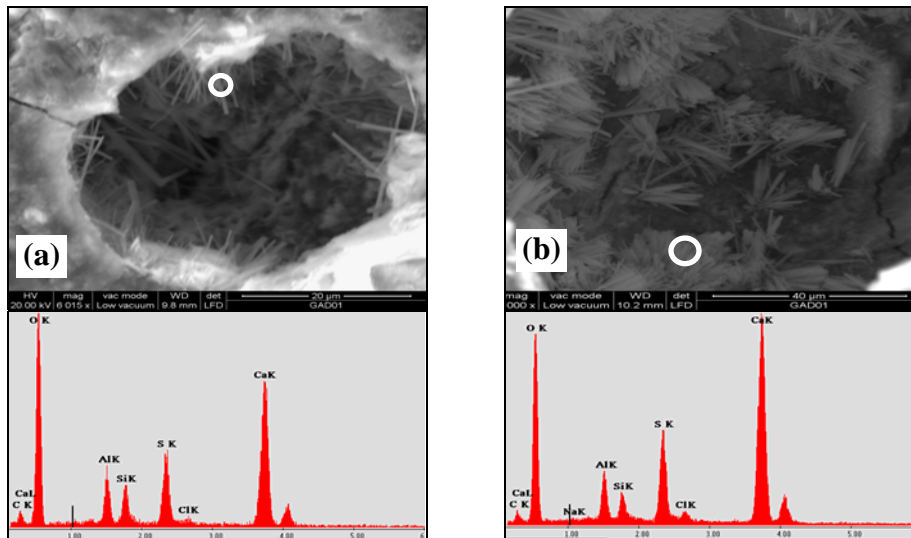


Fig. 11: SEM and EDS of HPC1 immersed in 5% sodium chloride + 2.0% sodium sulfate solution for eighteen months.

DISCUSSION

The experimental results presented in this paper indicate that sulfate negatively affected the compressive strength of HPC, although, its effect was delayed to latter exposure periods. Length change measurements also confirmed the previous results. The expansion rate of HPC, compared to conventional concrete, was slow at early exposure periods, than increased at latter exposure period. Besides, the change in sulfate content in the investigated HPC mixes supported the previous findings. The change in sulfate content increased steadily during the exposure period. Nevertheless, these outcomes must be considered in conjunction with the composition of HPC and the sulfate concentration in the surrounding environment. The efficiency of HPC composition was also confirmed through visual inspection. Where, surface scaling was occasionally observed on HPC specimens exposed to sodium chloride-high sulfate environment only at latter exposure period.

Measurements of free chloride content in conventional concrete and HPC subjected to combined solution indicated that the sulfate has a pronounced effect on the chloride profiles. In the presence of sulfate, the content of free chloride was reduced at early exposure periods and at various depths. This behavior was observed in both conventional and high-performance concretes. This may be attributed to two respects: (a) diffusion rate of each ion in co-diffusion of sulfate and chloride was less than that in single-diffusion for concretes, and (b) gradual formation of ettringite crystal in early exposure period leads to compacted microstructure of concretes, which decreases the ingress of chloride into concretes to some extent.

Additionally, it was clear that at early exposure periods, the free chloride content was higher for specimens immersed in chloride-low sulfate solutions than those immersed in chloride-high sulfate solution. This may be due to the deposition of sodium sulfate salt on the specimens' surface that may hinder or delay the penetration of aggressive salts into concrete specimens.

At latter exposure period, the free chloride content in conventional concrete increased at the outer depths in the following order; chloride high-sulfate solution, chloride low-sulfate solution than in chloride solution. High-performance concrete followed this trend but with lower values and slower rate compared to conventional concrete. This may be due to initiation of expansion and cracking, resulting from sulfate attack, consequently the ingress of chloride ions increase. Similar behavior was reported by Al-Amoudi [22]. Microstructural analysis proved the presence of sulfate attack expansive phase (ettringite) and showed the absence of Friedel's salt phase in HPC specimens subjected to combined solution at latter exposure periods. Recent studies supported the obtained results and proposed that the Friedel's salt may be unstable in the presence of sulfate and that the disruption caused by sulfate attack is unavoidable with the high C_3A content [17,20]. Consequently, the content of C_3A in cement proved to be of high importance in controlling the damage of concrete under the combined attack of sulfate and chloride. The chloride binding capacity of C_3A in the form of Friedel's salt and accordingly the mitigation of sulfate attack needs to be investigated. The reduction of C_3A content introduced by the latest version of the Egyptian code for concrete structure design to be in the range between 5 to 8% seems reasonable. Nevertheless, the utilization of other types of cements (e.g., blastfurnace slag cement, pozzolanic cement) and production of dense concrete may also provide durability of concrete under combined attack.

The results also indicated that the introduction of silica fume decreased the ingress of chloride into high-performance concrete. This may be attributed to the fact that silica fume would react with $Ca(OH)_2$ to produce the calcium silicate gel which can improve the compaction of concretes, hence, decreasing the chloride ingress.

CONCLUSIONS

Based on the study reported here, the following conclusions may be drawn:

- The effect of sulfate on chloride ingress at early exposure period is different from that at latter exposure period.
- At early exposure period, the presence of sulfate in combined solution decreased the concentration of free chloride in concrete.
- At later exposure period, the presence of sulfate in combined solution lead to the formation of sulfate attack products and as a result increased the free chloride content.
- The presence of chloride ions did not mitigate the sulfate attack or hinder the formation of sulfate attack products.
- The content of C_3A in ordinary Portland cement used in concrete subjected to combined attack needs to be assessed, due to its significance in controlling the damage of concrete under the combined attack.
- The high-performance concrete with its superior performance and composition (cement content and w/c ratio) proved to be effective in withstanding the influence of combined chloride and sulfate attack.

REFERENCES

1. Hekala, E.E., Kishar, E. and Mostafa, H. (2002), "Magnesium sulfate attack on hardened blended cement pastes under different circumstances", *Cement and Concrete Research*, 32, pp. 1421–1427.
2. Santhanam, M., Menashi, C. and Olek, J. (2002), "Mechanism of sulfate attack: a fresh look Part 1. Summary of experimental results", *Cement and Concrete Research*, 32, pp. 915–921.
3. Santhanam, M., Menashi, C. and Olek, J. (2003), "Mechanism of sulfate attack: a fresh look Part 2. proposed mechanisms", *Cement and Concrete Research*, 33, pp. 341–346.
4. Shamsad, A. (2003), "Reinforcement corrosion in concrete structures, its monitoring and service life prediction - a review", *Cement & Concrete Composites*, 25 (4–5), pp. 459–471.
5. Midgley, H.G. and Illston, J.M. (1983) "The penetration of chlorides into hardened cement pastes", *Cement & Concrete Research*, 14, pp. 546–558.
6. Hillier, S. R., Sangha, C. M., Plunkett, B. A. and Walden, P. J. (2000), "Effect of concrete curing on chloride ion ingress", *Magazine of Concrete Research*, 52 (5), pp. 321-327.
7. Al-Amoudi, O.B., Masiehuddin, M. and Abdui-Al Y. (1995), "Role of chloride ions on expansion and strength reduction in plain and blended cements in sulfate environments", *Construction and Building Materials*, 9 (1), pp. 25–33.
8. Feldman, R. and Beaudoin, J. (1991), "Effect of cement blends on chloride and sulfate ion diffusion in concrete", *Il Cemento*, 88, pp. 3–18.
9. Tumidajski, P. and Chan, G.W. (1996), "Effect of sulfate and carbon dioxide on chloride diffusivity", *Cement & Concrete Research*, 26, pp. 551–556.
10. Dehwah, H.A.F., Maslehuddin, M. and Austin, S.A. (2002), "Long-term effect of sulfate ions and associated cation type on chloride-induced reinforcement corrosion in Portland cement concretes", *Cement & Concrete Composites*, 24, pp. 17–25.
11. Zuquan, J., Wei, S., Yunsheng, Z., Jinyang, J. and Jianzhong, L. (2007), "Interaction between sulfate and chloride solution attack of concretes with and without fly ash", *Cement & Concrete Research*, 37, pp. 1223-1232.
12. Zibara, H. (2001), "Binding of externally applied chlorides by pastes", PhD Thesis, Department of Civil Engineering, University of Toronto, Canada.
13. Federal Highway Administration (FHWA) (2005), "High performance concrete, structural designers' guide", <http://knowledge.fhwa.dot.gov/cops/hpcx.nsf/all+documents/>, accessed Feb. 3, 2008.
14. Salah El-Din, M. (2008), "Diffusion of chloride ion into high-performance concrete", M.Sc. Thesis, Institute of Graduate Studies and Research, Alexandria University, Egypt.
15. El-Shimy, E. (1992) "Blended cements and their resistance to aggressive media", PhD Thesis, Faculty of Science, Zagazig University, Egypt.
16. Manu, S., Menashi, D. and Jan, O., (2003) "Mechanism of sulfate attack: a fresh look, Part2: proposed mechanism", *Cement & Concrete Research*, 33, pp. 341-346.
17. Brown, P.W. and Badger, S. (2000), "The distributions of bound sulfates and chlorides in concrete subjected to mixed NaCl, MgSO₄, Na₂SO₄ attack", *Cement & Concrete Research*, 30, pp. 1535-1542.
18. Brown, P.W. and Doer, A. (2000), "Chemical changes in concrete due to the ingress of aggressive species", *Cement & Concrete Research*, 30, pp. 411-418.
19. Mohammed, T., Hamada, H., and Yamaji, T. (2004), "Concrete after 30 Years of Exposure – Part I: Mineralogy, Microstructures, and Interfaces", *ACI Materials Journal*, 101, pp. 3-12.
20. Mohammed, T., Hamada, H., and Yamaji, T. (2004), "Concrete after 30 Years of Exposure – Part II: Chloride Ingress and Corrosion of Steel Bars", *ACI Materials Journal*, 101, pp. 13-18.
21. Dehwah, H.A.F. (2007), "Effect of Sulfate Concentration and Associated Cation Type on Concrete Deterioration and Morphological Changes in Cement Hydrates", *Construction and Building Materials*, 21, pp. 29-39.
22. Al-Amoudi O. S. (2002), "Attack on plain and blended cements exposed to aggressive sulfate environments", *Cement & Concrete Composites*, 24, pp. 305-316.

EFFECT OF ELEVATED TEMPERATURE ON MECHANICAL PROPERTIES OF BLENDED CEMENT MORTAR

M.S. Morsy, *A. M. Rashad and S. S. Shebl
Housing & Building National Research Center, Egypt
E-Mail: alaarashad@yahoo.com

ABSTRACT

An experimental investigation was conducted to evaluate the performance of mortars composed of ordinary Portland cement (OPC) partially replaced with metakaolin (MK) and / or silica fume (SF) exposed to elevated temperature. Eighteen different mixtures were designed to have a mortar flow of $94 \pm 5\%$. The mortars had binder: sand ratios of 1:5.23. Three specimens from each mix were tested for compressive strength at ambient temperature, control sample. The other specimens were exposed to a gradual increase in temperature to 200 °C, 400 °C, 600 °C and 800 °C for two hours duration in an electrical symmetrical furnace. The residual compressive strength was evaluated for all samples. The optimum mixtures for improving residual compressive strength using MK and / or SF as cement replacement are reported.

Keywords: Elevated Temperature Resistance; Silica Fume; Metakaolin, Mortar; Blended Cement.

INTRODUCTION

Occasionally, concrete structures are subjected to high temperatures (reactor vessels, thermal shock, fire, coal gasification vessels, some industrial applications, etc.). In most cases, such elevated temperatures result in considerable damage to concrete structures and masonry walls. Recently, high-strength concrete and high-strength mortar are widely used in different parts of civil engineering structures. As they become more commonly used, the risk of being exposed to high temperatures also increases. Thus, better understanding the behavior of high-strength mortar at high temperatures gains importance for predicting the mortar properties.

Mineral additions for the manufacturing of concrete generally include both natural pozzolans of volcanic origin and artificial pozzolans such as fly ash and silica fume. Currently, other alternatives to these materials are being investigated using clay minerals (i.e., kaolinite, montmorillonite, illite that can be thermally activated by dehydration in the temperature range of 700 to 800 °C). The most typical example is kaolin, which upon heating produces metakaolin (MK). The properties of MK as a pozzolanic material have been reported previously [1-5]. Also, the influence of curing temperature on reaction rate constants and on the behavior and stability of hydration phases have been studied [6]. MK shows a high level of pozzolanic activity, similar to SF. For this reason, it is very important to quantify the heat evolution during hydration in MK/cement systems. Also, as reported by Gruber et al. and Boddy et al., the performance of concrete incorporating MK, at appropriate replacement levels, is similar to that of concrete containing silica fume [4-5]. When used as a partial replacement for OPC,

* Corresponding author
Received Date:27/1/08
Acceptance Date:11/3/08

metakaolin is capable of reacting with portlandite to form supplementary calcium-silicate-hydrate (C-S-H) similar in composition and structure to those obtained from Portland cement [7].

Metakaolin has also been used for making cementitious materials called hydroceramics, i.e. ceramic-like materials synthesized from a solid aluminosilicate and an alkali-rich solution at low temperature, < 100 °C. It has been reported that metakaolin of high lime reactivity (6–7.5 MPa) can be produced by thermal decomposition of kaolin, a naturally occurring clay basically containing kaolinite $[Al_2O_3-Si_2O_5(OH)_4]$ mineral and trace of silica and other minerals which can be blended with high quantity of fly ash (over 45%) lime and industrial gypsum to form strong binder of low leachability [8-9].

In the particular case of MK, it appears to have excellent potential as an active addition for producing mortars and concretes [10]. However, this material shows a particular nature in its chemical and mineralogical composition. The hydrated phases (C_2ASH_8 and C_4AH_{13}), formed during the pozzolanic reaction at early curing periods, tend to be present as metastable phases. With longer curing times, the conversion of these hydrates to hydrogarnet (stable phase) can be expected [11]. This transformation will depend on different factors (for example, temperature reached inside the specimen).

Metakaolin is typically incorporated into concrete to replace 5% to 20%, by mass. MK improves concrete performance by reacting with calcium hydroxide to form secondary C-S-H. Because of its white color, high-reactivity MK does not darken concrete as SF typically does (the white-colored SF is very limited in tonnage), which makes it suitable for color-matching and other architectural applications [12-13].

Since the early 1970s, silica fume, a by-product of the silicon metal and ferro-silicon alloy industries, has been used as a mineral admixture in concrete to enhance strength and low permeability. There are other properties that are favourably affected by the incorporation of silica fume, including: modulus of elasticity [14] drying shrinkage [15] bonding (concrete steel) [16] and resistance to reinforcing steel corrosion and sodium sulfate attack due to low permeability to water and chloride ions [17-18]. However, there are some unfavourable properties associated with the addition of silica fume to concrete, such as loss of slump and reduction in ductility [19]. During the last 10 years, the use of silica fume in cement and concrete has increased. The application of silica fume as a mineral admixture in concrete is almost a routine nowadays for the production of tailor-made high-performance concretes [20-26].

The aim of the current research work is to determine the effect of elevated temperature on compressive strength of blended cement mortar containing MK and SF used in binary and ternary blends with Portland cement. The cement replacement was 0%, 5%, 10%, 20% and 30%, by mass of binder.

EXPERIMENTAL DETAILS

An experimental program was designed to investigate the residual compressive strength of blended cement mortar containing MK and SF following exposed to elevated temperatures. For this purpose, 8 mortar mixtures were prepared with 0%, 5%, 10%, 20% and 30% combinations of MK and SF, by mass of cement. Each mix comprised five groups. The first group was tested directly in ambient temperature to determine the compressive strength after curing. The second, third, fourth and fifth groups were tested after two hours exposure at 200 °C, 400 °C, 600 °C and 800 °C for two hours respectively.

Materials

Cement

The cement used in this research was OPC complying with ASTM C-150 requirements Type I. The chemical composition and physical properties of OPC are shown in Table 1.

Kaolin

A sample of kaolin (K) clay collected from Sina quarry was ground to a Blaine fineness of 3500 cm²/gm. Figure 1 shows the diffractograms of the K sample analyzed by X-ray diffraction

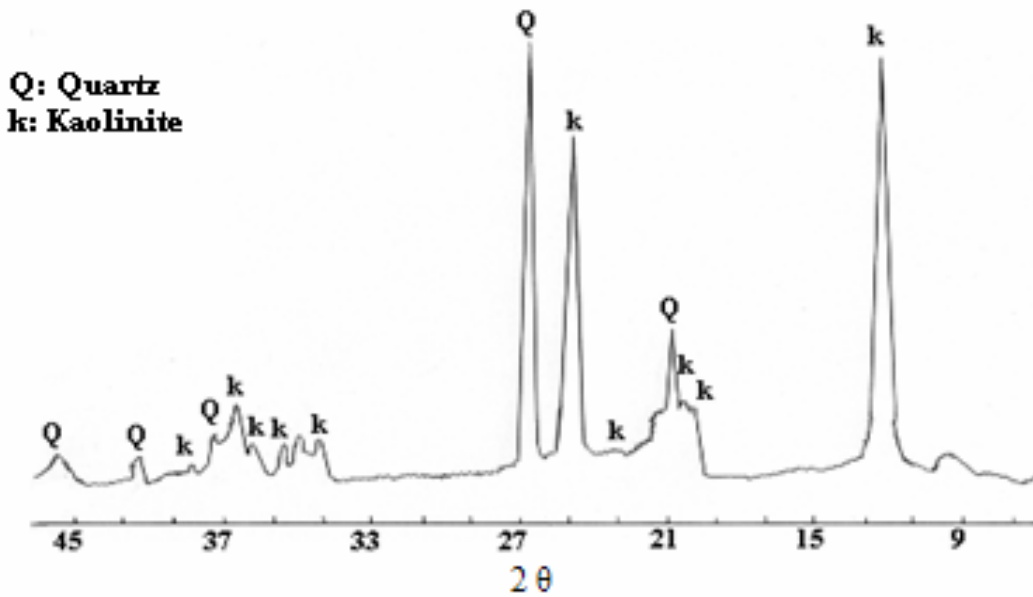


Fig. 1: X- Ray Diffraction of Kaolin

Metakaolin

The ground clay samples; kaolin, were thermally treated in an electrical furnace at 850 °C for a period of 2 hours then cooled gradually. Figure 2 shows the diffractograms of MK sample analyzed by X-ray diffraction. The chemical compositions and physical properties of these materials are shown in Table 1.

Silica Fume

Silica fume was supplied from our local Egyptian production. Its chemical oxide compositions and physical properties are given in Table 1.

Sand

Natural sand was used with nominal size of 5 mm, specific gravity of 2.65 and volumetric weight of 1.57 t/m³. The gradation of fine aggregate satisfied ASTM C 33 requirements.

Table 1: Chemical Compositions and Physical Properties of Cementitious Materials

Chemical composition (%)	OPC	MK	SF
SiO ₂	20.39	58.52	96.1
Al ₂ O ₃	5.6	35.54	0.5
Fe ₂ O ₃	3.43	1.15	0.7
CaO	63.07	1.24	0.21
MgO	2.91	0.19	-
Na ₂ O	0.38	0.25	0.31
K ₂ O	0.35	0.05	0.49
SO ₃	0.7	0.06	0.1
C ₃ A	9.04	-	-
P ₂ O ₅	-	0.09	-
TiO ₂	-	0.04	-
Loss on ignition	2.06	2.74	1.14
Specific gravity	3.15	2.34	2.32
Specific surface (cm ² /gm)	2500	3500	225000

Preparation of Cement Mortar, Testing and Evaluation

The cement mortars were cast using 5x5x5 cm cubes. The blended cement and standard triple graded sand in the proportion 1: 5.23 by weight at $94 \pm 5\%$ flow [27]. After 24 hours moist curing, the cubes were demoulded and cured in water until testing. The mix proportions of the 18 mortar mixtures are shown in Table 2.

Mixture of Cement–Metakaolin–Silica Fume

The OPC was partially substituted by combination mixtures of metakaolin and silica fume with 5, 10, 15, 20 and 30 %, by mass of OPC.

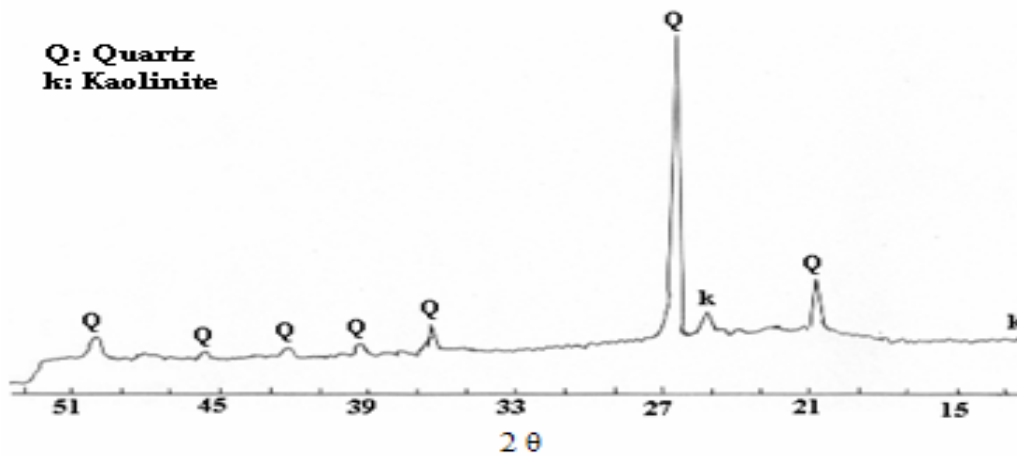


Fig. 2: X- Ray Diffraction of Metakaolin

Table 2: Mix Proportions of Mortar Mixtures

Mix	Blended Cement			Batched quantities (kg/m ³)				Water Binder Ratio
	%OPC	%MK	%SF	OPC	MK	SF	Sand	
M0	100	0	0	300	0	0	1570	1.082
M51	95	5	0	285	15	0	1570	1.0502
M52	95	0	5	285	0	15	1570	0.9867
M101	90	10	0	270	30	0	1570	1.140
M102	90	5	5	270	15	15	1570	0.9867
M103	90	0	10	270	0	30	1570	1.0
M201	80	20	0	240	60	0	1570	0.9957
M202	80	15	5	240	45	15	1570	0.9973
M203	80	10	10	240	30	30	1570	1.0342
M204	80	5	15	240	15	45	1570	1.0673
M205	80	0	20	240	0	60	1570	1.1323
M301	70	30	0	210	90	0	1570	1.062
M302	70	25	5	210	75	15	1570	1.0607
M303	70	20	10	210	60	30	1570	1.0763
M304	70	15	15	210	45	45	1570	1.1333
M305	70	10	20	210	30	60	1570	1.1827
M306	70	5	25	210	15	75	1570	1.1333
M307	70	0	30	210	0	90	1570	1.3156

Curing and Heating Regimes

The specimens were demolded after 24 h of casting and cured under water at 25 °C in a water tank. After 28 days of water curing, they were transferred to an environmental chamber maintained at 25 °C and 75% relative humidity. The specimens were dried at 105 °C for 24 hours then thermally treated in an electric furnace at 200, 400, 600 and 800 °C for 2 hours to achieve the thermal steady state [28]. The heating rate was set at 2.5°C/min based on the experience of our previous research [29]. The specimens were allowed to cool naturally to room temperature.

TEST RESULTS AND DISCUSSION

There are three test methods available for finding the residual compressive strength of concrete subjected to elevated temperatures: stressed test, unstressed test, and unstressed residual strength test. The first two tests are suitable for assessing strength during high temperatures, while the later is excellent for finding the residual properties after exposure high temperature. It was found that the last method can lead to the lowest strength and may be more suitable for getting the limiting values for residual strength, and hence was selected for this research [30].

Figure 3 illustrates the residual compressive strength of control and blended cement mortars with 5% pozzolana replacement exposed to elevated temperature. It is clear that, the residual compressive strength increases as the treatment temperature increases up to 200 °C then decreases as the treatment temperature increases up to 800 °C.

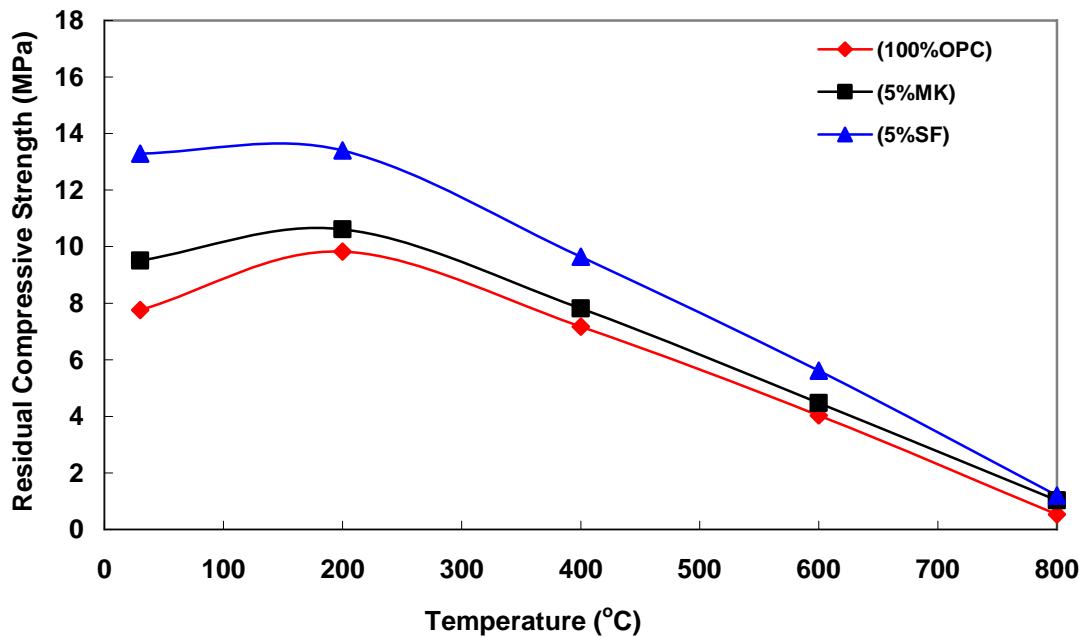


Fig. 3: Residual Compressive Strength of Control and Blended Mortars of 5% Replacement Exposed to Elevated Temperature

Obviously, the blended cement mortars of mixes showed an increase in compressive strength at 200 °C. This increase may be due to the hydration of unhydrated MK and/or SF particles which were activated as a result of temperature rise. A similar increase in strength was observed in 100% OPC mortar. This increase may be due to further hydration of unhydrated cement grains as a result of steam effect under the condition of the so-called internal autoclaving formed in cement paste [31]. The residual compressive strength of blended cement mortar is better than

the control mortar. The pozzolanic activity of this silica fume is more than this metakaolin. This is due to the plain surface area of silica fume is greater than that of metakaolin. However, the replacement of OPC by 5% SF and/or MK, improved the residual compressive strength of mortars.

Figure 4 shows the residual compressive strength of control and blended cement mortars of 10% pozzolana replacement exposed to elevated temperature. The residual compressive strength increases as the treatment temperature increases up to 200 °C, then decreases as the treatment temperature increases up to 800 °C. However, the replacement of OPC by MK and SF can improved the residual compressive strength of blended cement mortars after exposure to elevated temperature. Evidently, the increases of compressive strength are due to the internal autoclaved process in OPC mortar; which leads to hydration of unhydrated cement grains. The improvement in residual compressive strength of the blended cement mortar is due to pozzolanic activity. The decreases in residual compressive strength are due to dehydration of hydrated cement product. The residual strength depends on the type and the percentage of pozzolanic mixtures

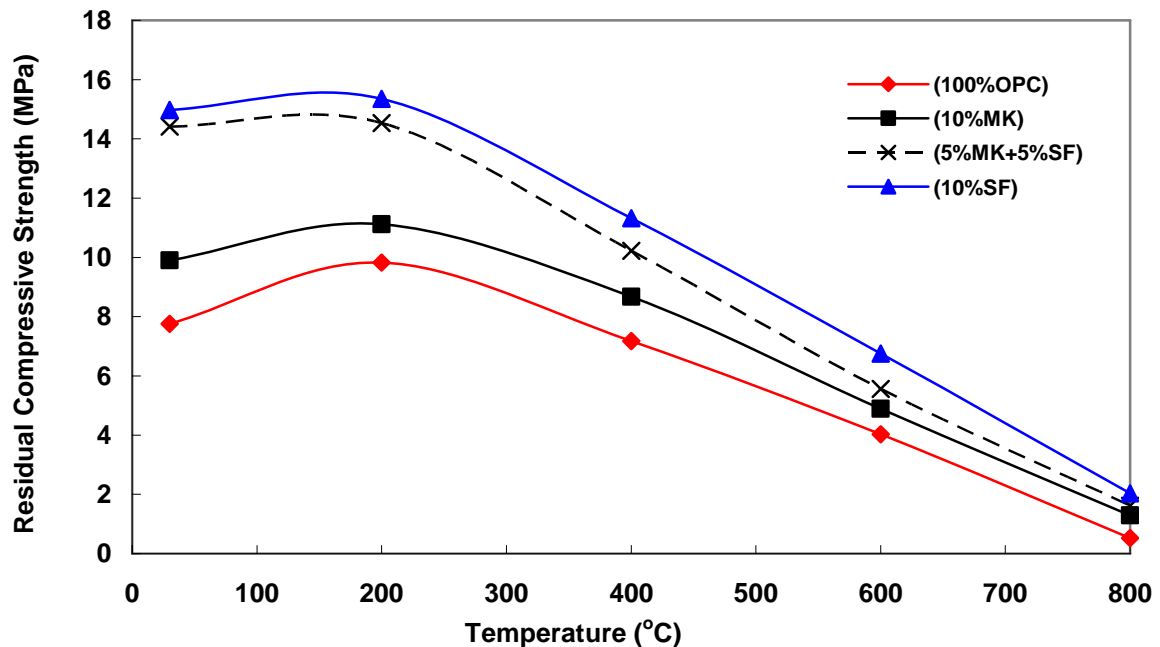


Fig. 4: Residual Compressive Strength of Control and Blended Mortars of 10% Replacement Exposed to Elevated Temperature

The replacement of OPC by 10% SF proves to be the most effective replacement to improve residual compressive strength. The combination of 5% MK and 5% SF replacement of OPC have lower residual strength than 10% SF. In blended cement mortar containing 10% MK, the residual strength is lower than 10% SF and combination of 5% MK and 5% SF.

Figure 5 demonstrates the residual compressive strength of control and blended cement mortars of 20% pozzolana replacement exposed to elevated temperature. It is clear that, the residual compressive strength of control and blended mortars of 20% pozzolana replacement exposed to elevated temperature increases as the exposure temperature increases up to 200 °C followed by a gradual decrease as the temperature increases up to 800 °C. The replacement of OPC by 20% pozzolana, by an equal combination of MK and SF (10% MK +10% SF), gave the optimum residual compressive strength. The replacement of OPC by 20% SF also gave the optimum residual compressive strength. The replacement of OPC, by a combination of 5% MK

and 15% SF showed a higher residual compressive strength than the separate replacement of 20% MK and the combination replacement of 15% MK and 5% SF.

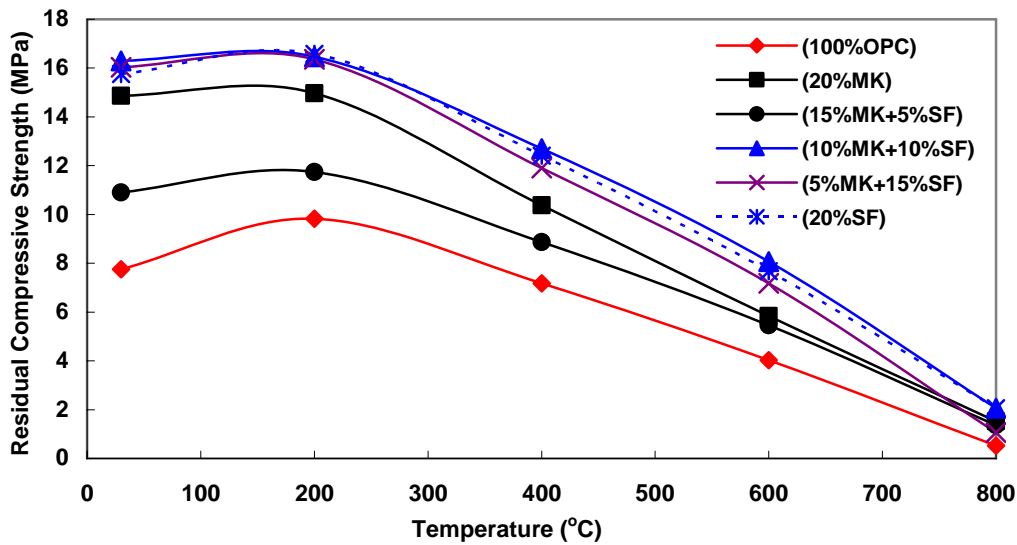


Fig. 5: Residual Compressive Strength of Control and Blended Mortars of 20% Replacement Exposed to Elevated Temperature

Figure 6 shows the residual compressive strength of control and blended cement mortars containing 30% pozzolana replacement exposed to elevated temperature. It is clear that, the residual compressive strength corresponding to mortar of different combinations of MK and SF subjected to different exposure temperatures increases as the temperature increases up to 200 °C then decreases as the temperature increases up to 800 °C. The combination of 5% MK and 25% SF seemed to be the optimum cement replacement that gave the maximum residual strength. Where 30% separate cement replacement with SF came in second place. The combination of 10% MK and 20% SF, combination of 20% MK and 10% SF came in the third and fourth place respectively. The equal combination of MK (15%) and SF and separate replacement of MK came in the fifth place. The pure OPC mortar came in the sixth place. Finally, the combination of 25% MK and 5% SF came in the last place according to their residual compressive strength.

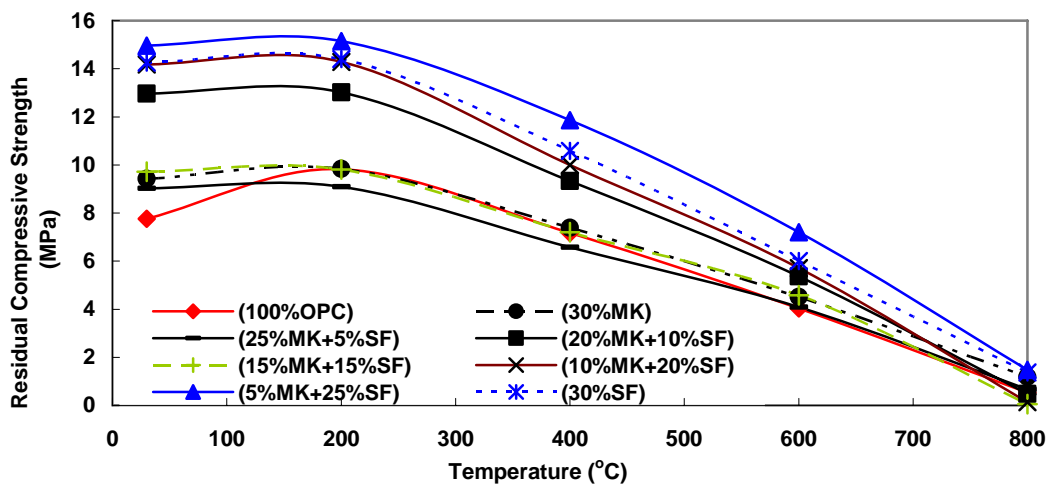


Fig. 6: Residual Compressive Strength of Control and Blended Mortars of 30% Replacement Exposed to Elevated Temperature

Figure 7 collects the maximum mixtures plotted through Fig 3 to 6. It is clearly apparent that the optimum replacement of OPC by 20% as equal combinations of MK and SF and by separate replacement of SF. The combination of 25% MK and 5% SF came in the second place. The separate OPC replacement by 10% SF came in the third place. Finally, 5% SF came in the last place.

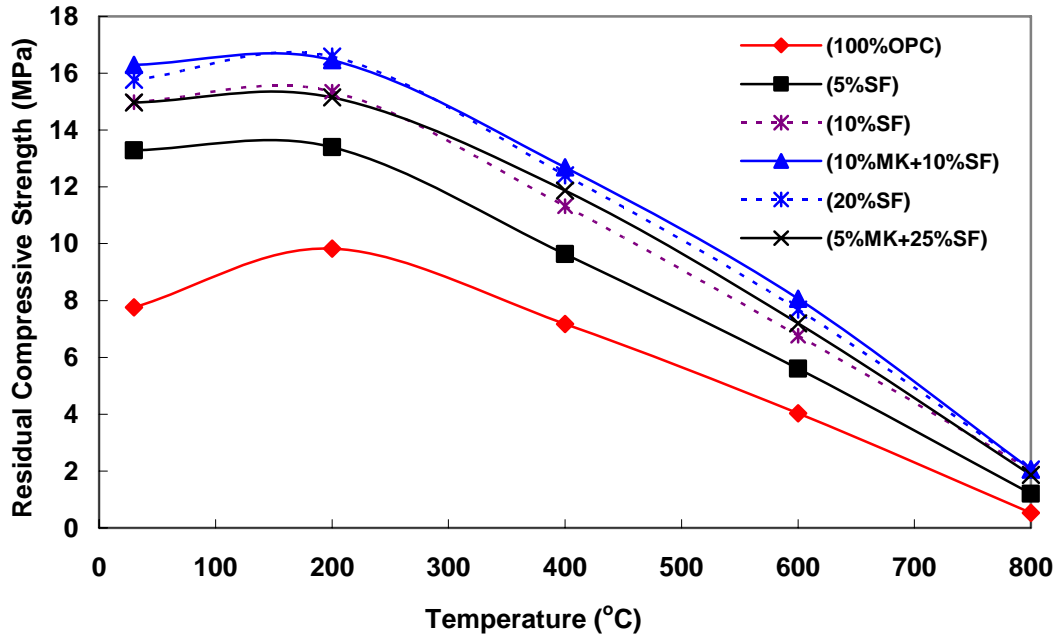


Fig. 7: Maximum Residual Compressive Strength of Mortars for Various Replacements Exposed to Elevated Temperature

CONCLUSIONS

The following conclusions can be drawn from the present study:

1. At cement replaced by 20% by mass of equal combinations of MK and SF gave the best control and residual compressive strength. This blend came in the first place.
2. Based on the mechanical properties of SF blended mortar, a 20% separate SF content seems to be, generally, more favorable than the other investigated ratios. This blend came in the second place.
3. At cement replaced by 30% by mass, the optimal combination of 5% MK and 25% SF gave a good control and residual compressive strength. This blend came in second place.
4. The 10% cement replacement by separate SF improves compressive strength before and after exposed to elevated temperature. This blended came in the Third place.
5. The 5% cement replacement by SF came in the fourth place for the residual compressive strength.
6. The studied MK and SF have a very positive effect on the mortar strength at the age of 28 days and after exposed to elevated temperature.

REFERENCES

1. Caldarone M. A. and Gruber K. .A., (1995), "High Reactivity Metakaolin (HRM) for High Performances Concrete", in: V.M. Malhotra (Ed.), Fifth CANMET/ ACI Intern. Conference on Fly Ash, Silica Fume, Slag and Natural Pozzolans in Concrete, Milwaukee, WI, Vol. 2, pp. 815–827.
2. Ambroise J., Murat M. and Pera J., (1996), "Investigations on Synthetic Binders Obtained by Middle-Temperature Thermal Dissociation of Clay Minerals", *Silicates Industriels* (7–8), 99–107.

3. Murat M., (1983), "Preliminary Investigation on MK", *Cem Concr Res* 13 (2), 259–266.
4. Gruber K. A., Ramlochan T., Boddy A., Hooton R.D., M.D.A. (2001), "Thomas, Increasing Concrete Durability with High-Reactive Metakaolin", *Cem. Concr. Compos.* 23 (6), 479– 484.
5. Boddy A., Hooton R. D. and Gruber K. A., (2001), "Long-Term Testing of the Chloride-Penetration Resistance of Concrete Containing High-Reactive Metakaolin", *Cem. Concr. Res.* 31 (5), 759–765.
6. Frías M., Cabrera J.G., January (2002), "The Effect of Temperature on the Hydration Rate and Stability of the Hydration Phases of Metakaolin-Lime-Water Systems", *Cement and Concrete Research*, Volume 32, Issue 1, 133-138.
7. De Silva P.S., and Glasser F.P., (1992), "Pozzolanic Activation of Metakaolin", *Adv Cem Res* 4 (16), 167-178.
8. Wild S., Khatib J. M. and Jones A., (1966), "Relative Strength and Pozzolanic Activity and Cement Hydration in Superplasticised Metakaolin Concrete", *Cem. Concr. Res.* 26 (10), 1537– 1544.
9. Singh M., Garg M., (1999), "Cementitious Binder From Fly Ash and other Industrial Wastes", *Cem. Concr. Res.* 29, 309- 314.
10. Zhang M. H., Malhotra V., (1995), "Characteristics of a Thermally Activated Alumino-Silicate Pozzolanic Material and Its Use in Concrete", *Cem Concr Res* 25 (8), 1713– 1725.
11. Silva P.S., Glasser F.P., (1993), "Phase Relations in the System $\text{CaO-Al}_2\text{O}_3\text{-SiO}_2\text{-H}_2\text{O}$ Relevant To MK-Calcium Hydroxide Hydration", *Cem Concr Res* 23 (3), 627–639.
12. Bai, J.; Wild, S.; Sabir, B. B.; and Kinuthia, J. M., (1999), "Workability of Concrete Incorporating Pulverized Fuel Ash and Metakaolin", *Magazine of Concrete Research*, V. 51, No. 3, pp. 207-216.
13. Thomas, M. D. A.; Gruber, K. A.; and Hooton, R. D., (1997), "The Use of High-Reactivity Metakaolin in High-Performance Concrete", *High-Strength Concrete, Proceedings of First International Conference*, A. Azizinamini, D. Darwin, and C. French, eds., ASCE, Kona, Hawaii, pp. 517-530.
14. Galeota D. and Giammatteo M. M. (1989), "Stress-Strain Relationship of Normal and Lightweight Concrete with Silica Fume under Uniaxial Compression Fly Ash, Silica Fume, Slag, and Natural Pozzolans in Concrete", SP-114. American Concrete Institute, Detroit, pp. 991-1011.
15. Bentur A. and Goldman A. (1989), "Curing effects, strength, and physical properties of high strength silica fume concrete. *ASCE Materials Journal*, 1, No. 46, 46-58.
16. Robins P. J. and Austin S. A. (1986), "Bond of Lightweight Aggregate Concrete Containing Condensed Silica Fume, Fly Ash, Silica Fume, Slag, and Natural Pozzolans in Concrete", SP-91. American Concrete Institute, Detroit, pp. 941-958
17. Berke N. S. (1989), "Resistance of Microsilica Concrete to Steel Corrosion, Erosion, and Chemical Attack. Fly Ash, Silica Fume, Slag, and Natural Pozzolans in Concrete", SP-114. ACI, Detroit, pp. 861-886.
18. Cohen M. D. and Bentur A., (1988), "Durability of Portland Cement - Silica Fume Pastes in Magnesium Sulfate Attack and Sodium Sulfate Solution". *ACI Materials Journal*, 85, No. 3, 148-157.
19. Xie J., Elwi A. E. and Macgregor J. G. (1995), "Mechanical Properties of Three High-Strength Concretes Containing Silica Fume", *ACI Materials Journal*, 92, No. 2, 135-145.
20. Chakraborty A. M., and Dutta S. C., (2001), "Study on Silica Fume Modified Mortar with Various Indian Cement Cured at Different Temperature", *Building and Environment* 36, 375-382.
21. Yogendran V, Langan B. W, Haque M. N. and Ward M. A., (1987), "Silica Fume in High-Strength Concrete", *ACI Materials Journal*; 84(2):124-9.
22. Toutanji H. A. and El-Korchi T., (1995), "The Influence of Silica Fume on the Compressive Strength of Cement Paste and Mortar", *Cement and Concrete Research*; 25(7):1591-602.
23. Wild S., Sabir B. B. and Khatib J. M., (1995), "Factors Influencing Strength Development of Concrete Containing Silica Fume", *Cement and Concrete Research*; 25(7):1567-80.

24. Marzouk H. M. and Hussein A. (1990), "Properties of High Strength Concrete at Low Temperatures", *ACI Materials Journal*; 87(2):167-71.
25. Khatri R. P., Sirivivatnanon V. and Gross W. (1995), "Effect of Different Supplementary Cementitious Materials on Mechanical Properties of High Performance Concrete", *Cement and Concrete Research*; 25(1):209-20.
26. Detwiler R. and Mehta P. K., (1989), "Chemical and Physical Effects of Silica Fume on the Mechanical behaviour of Concrete". *ACI Materials Journal*; 86(6):609-14.
27. ASTM C230/C230M-03 Standard Specification for Flow Table for Use in Tests of Hydraulic Cement.
28. Mohamedbhai GTG. (1986), "Effect of Exposure Time and Rates of Heating and Cooling on Residual Strength of Heated Concrete", *Mag Concr Res*; 38(136):151-8.
29. Chan S.Y.N., Peng, G.F.M. Anson, (1999), "Residual Strength and Pore Structure of High-Strength Concrete and Normal-Strength Concrete after Exposure to High Temperatures", *Cem. Concr. Compos.* 21, 23-27.
30. Phan L.T., (1996), "Fire Performance of High Strength Concrete": A Report of the State-of-the-Art, Building and Fire Research Laboratory, National Institute of Standards and Technology, Maryland.
31. Nimityongskul, P. and Daladar, T. U., January (1995), "Use of Coconut Husk Ash Corn Cob Ash and Peanut Shell Ash as Cement Replacement", *Journal of ferrocement*, Vol. 25, No. 1, 35-44.

SHRINKAGE AND IMPACT RESISTANCE OF HIGH STRENGTH CONCRETE WITH POLYPROPYLENE FIBERS

Amr A.F. Shaheen¹, Aly A.Emam¹ and *Ibrahim M. Metwally²
*1-Strength of Material Institute 2-Reinforced Concrete Institute
Housing & Building National Research Center,*

ABSTRACT

Current trends in construction projects require the use of high strength concrete. Achieving such task mandates the use of proportionally high cement content, which comes with a band of problems such as high rate of plastic shrinkage and rapid development of micro-cracks. The focus of the present investigation is the differences in mechanical properties of high-strength concrete and ordinary strength concrete and the effect of using polypropylene fibers in the manufacturing of high-strength concrete. Three mixtures of concrete were cast to be representative of ordinary concrete, high strength concrete with and without polypropylene fibers. The samples were tested for compressive strength at 7, 28 and 90 days and splitting tensile strength at 7 and 28 days. Plastic shrinkage was monitored for 24 hours immediately after casting and impact resistance was determined after 28 days.

The results indicate that high strength concrete with and without polypropylene fibers has better mechanical properties than ordinary concrete especially for compressive strength, tensile strength and impact. The plastic shrinkage for high strength without polypropylene fibers was higher than that of ordinary concrete. The study signifies that using polypropylene fibers can improve plastic shrinkage and reduce the formation of micro-cracking of high strength concrete. Moreover, the fibers significantly improve concrete impact resistance.

Keywords

Mechanical properties; high-strength concrete; polypropylene fibers; compressive strength; splitting tensile strength; impact; plastic shrinkage.

Introduction

The current technology makes it possible to produce high-strength concrete with compressive strength that meets the demands of the recent structural design practice. To produce concretes with high strength requires using ultra-fine cementitious materials such as silica fume [1], and a low water to binder ratio (the binder being defined as the Portland cement together with any supplementary cementing material). Generally, for high strength concrete, the binder content is higher than that for normal-strength concrete. Moreover, the use of superplasticizer is required to provide adequate workability [2-7].

The main objective of this study is to investigate the influence of the condensed silica fume dust and polypropylene fibers on compressive strength, splitting tensile strength, plastic shrinkage and impact resistance of high strength concrete. Of meticulous interest herein is the monitoring of plastic shrinkage of high-strength concrete with and without polypropylene fibers.

* Corresponding author
Received Date:23/3/08
Acceptance Date:11/6/08

In this regard, the results presented by Bruno et al [8] indicated that very high values of plastic shrinkage can exist leading to drastic micro cracking in high strength concrete.

To reduce plastic shrinkage cracking, the most widely accepted method is the use of randomly distributed fibers, particularly fine synthetic fibers in reasonable volume fraction. The most commonly used fibers to control plastic shrinkage cracking are steel, nylon, polyester, cellulose fibers, PVA, polypropylene, and polyolefin [9].

It has been demonstrated that fibrillated polypropylene fibers significantly reduce the plastic shrinkage of concrete. The mechanisms by which polypropylene fibers reduce plastic shrinkage can be summarized as follows:

1. Increasing tensile strain capacity of fresh concrete beyond the tensile strains caused by shrinkage as shown schematically in Fig. 1. In the study detailed in reference [10], fresh concrete was cast around a threaded steel rod and strain was applied to the rod. Crack initiation within fresh concrete was observed to determine its strain capacity;
2. The regulation of bleed water rise by the reduction of coarse aggregate consolidation. Therefore, higher water retention by fresh concrete is achieved, resulting in better resistance to shrinkage[11]. Polypropylene fibers cause fresh concrete to bleed less and set faster, thereby reducing its time of exposure to plastic shrinkage. With these effects, the quantity of harmful capillaries formed by bleeding is reduced and intergranular friction is increased [12]; and
3. Arresting of micro cracks and capillaries, thereby restraining their potential expansion and development into plastic shrinkage cracks [13].

The uniform dispersion of fibers within fresh concrete is essential to their role in plastic shrinkage crack reduction. Achieving enhanced mixture uniformity with the application of fibrillated polypropylene fiber prevents localized expansion and development of capillaries and micro cracks into shrinkage cracks. Two effects of fibrillated polypropylene fibers upon plastic shrinkage can be distinguished: (i) Their influence in reducing free plastic shrinkage strain; and (ii) Their effect in resisting the resultant plastic shrinkage cracking strain/stress [14].

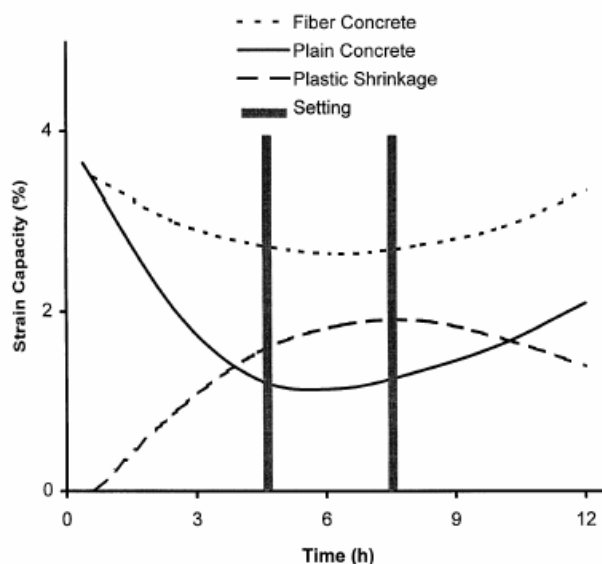


Fig. 1: Effect of polypropylene fibers on strain capacity of fresh concrete, [10].

Polypropylene fibers have significant influence in enhancing other mechanical properties of concrete as reported by Soroushian et al.[15], they concluded that Polypropylene fibers increased the flexural and impact strengths, and decreased the compressive strength, of

concrete materials; with 1% fiber volume fraction of polypropylene fibers, the average flexural and impact strengths were 1.21 and 5.8 times greater, respectively, and the average compressive strength was reduced by 23% in comparison with plain concrete without fibers. The present research focuses on making a comparison among the three concrete grades, with respect to plastic shrinkage, compressive strength, tensile strength, and impact resistance. The first grade is traditional conventional concrete mix without any admixtures with an average compressive strength of 300 kg/cm², the second is high strength concrete mix with silica fume, and the third is high strength concrete mix with silica fume and polypropylene fibers.

Experimental Program

Three mixes were cast to evaluate the advantages of adopted approach of adding silica fume and polypropylene fibers on the compressive strength, splitting tensile strength, impact and plastic shrinkage of concrete.

Materials

Ordinary Portland cement complying with the Egyptian Standard Specification 4756- 1/2005 is used through out the present work. The Pozzolanic material was silica fume, which has been used in the high strength mixes in a ratio 15% of cement weight as an additive material to improve the properties of concrete. It must be noted that a ratio of 15% SF in high-strength concrete is in line with literature e.g. Ref. [16] and [17]. The coarse aggregate was dolomite crushed stone with maximum grain size of 20 mm, and the fine aggregate was natural siliceous sand with a fineness modulus of 2.6, their relative proportions were 1.5:1, respectively. The water/cementitious ratio was taken 0.61 for the control mix (A1), then the ratio was reduced to 0.29 of binder cement materials for the second and third mixes (A2 and A3). This mandated the use of BVF as a superplasticizer additive (complying to ASTM C494 Type A,F) to reduce water content in the mix to get the desired strength for the concrete mix. Polypropylene fibers were added by an amount of 2 kg/m³ to concrete in the third mix to improve the plastic shrinkage of concrete.

Mix Proportions

In the first mix, neither pozzolanic admixture, nor superplasticizer additive or polypropylene fibers was used to produce the control mix. In the other two mixes high cement content, silica fume, superplasticizer additive were employed for achieving a high strength concrete. The third mix is typically the same as the second one except for adding polypropylene fibers to investigate its influence on concrete properties, especially plastic shrinkage and impact resistance. Proportions of all the mixes are outlined in Table (1).

Specimens Preparation and Testing

The three mixes were cast according to their proportions given in Table (1). After mixing, the slump test was performed and then, oiled steel molds of different specimens were filled and compacted. After 24 hours, the specimens were demoulded and immersed in water at room temperature for curing until testing. Nine cubes 150 mm were prepared to be tested for compressive strength according to ISO 4012 after 7, 28 and 90 days (three cubes for each age). Six cylinders 150 mm in diameter and 300 mm in height were cast to be tested for splitting tensile strength according to BS-1881 part 117 after 7 and 28 days (three cylinders for each age). Three beams with square cross-section (100x100 mm) and 500 mm span were prepared for impact testing according to ACI Committee 544.2R (1999) after 28 days. Three cylinders of diameter 100 mm and 200 mm in height were cast for plastic shrinkage monitoring immediately after casting and for a period of 24 hours. Plastic shrinkage test was carried out in accordance with ASTM C827-01a (2005), [18], and both schematic and experimental setup are shown in Figure (2).

Table 1: Proportions of concrete mixes

Mix		Mixture constituents					
Designation	Type	Cement kg/m ³	SF ¹ (kg/m ³)	Sand/ stone	SP ²	Water/ cementitious materials ratio	Polyprop. fibers (kg/m ³)
A1	Control	350	-	1:1.5	-	0.61	-
A2	HS ³	600	90	1:1.5	4	0.29	-
A3	HS with Polyprop. fibers	600	90	1:1.5	4	0.29	2.0

SF¹=silica fume, SP²=superplastizer (% of cementitious materials), and HS³=high strength

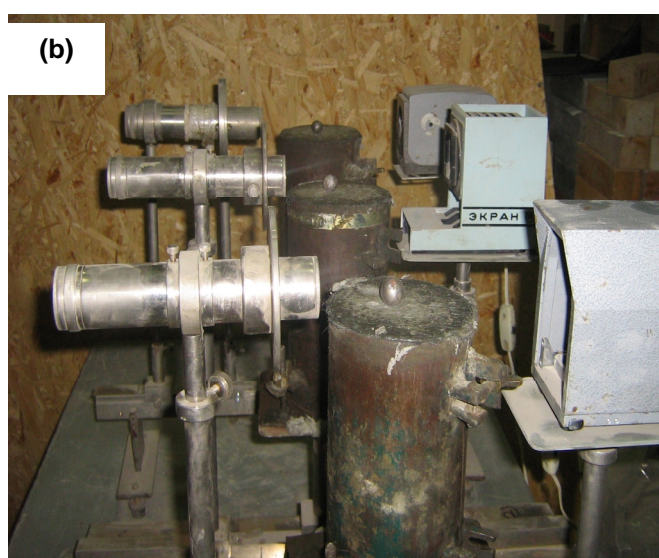
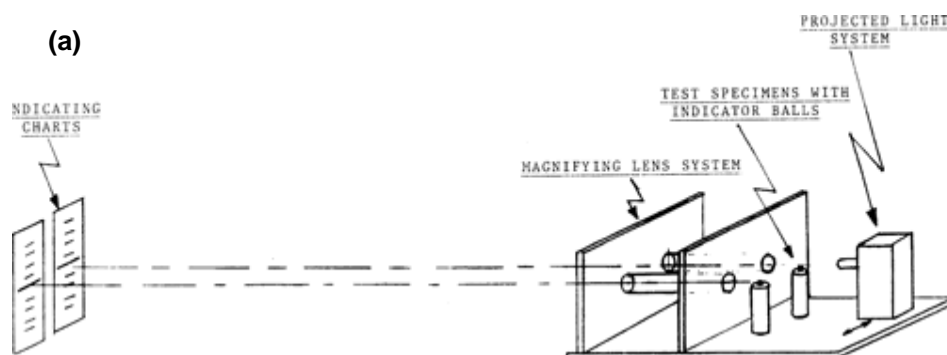


Fig. 2: Plastic Shrinkage Monitoring setup; (a) schematic and (b) experimental.

Test Results and Discussion

Compressive Strength

As a material parameter, the concrete compressive strength governs almost all other mechanical properties. Commercial production of concrete with high and ultra-high strength became a necessity to meet the never ending demand for urban expansion and development. In the current study a moderate high strength concrete (80 MPa.) was developed by manipulating the mix ingredients and using additives. This was achieved by increasing the cement content to 600 kg/m^3 (compared to 350 kg/m^3 for the control mix) and adding 15% silica fume along with 4% superplasticizer. The additives reduced water to cementitious materials ratio (w/cm) to 0.29, while maintaining a reasonable workability (slump about 100 mm.). Comparing the compressive strength for the developed three mixes (A1, A2, and A3), indicates that the gain in the compressive strength for A2 and A3 is over 100% as depicted in Figures (3) and (4). Moreover, the figures show that adding the polypropylene fibers has no significant influence on the compressive strength.

Tensile Strength

The same trend outlined above is observed for splitting tensile strength. Figures (5) and (6) show that the gain in the tensile strength for High Strength Concrete (HSC) is over 100% relative to ordinary concrete. The influence of adding polypropylene fibers is insignificant for tensile strength (comparing A3 and A2) as it improves the splitting tensile strength by only 5%. These results are expected and very much inline with literature [11,12]. It is worth mentioning that many concrete codes of practice underestimate the concrete tensile strength for HSC. Empirical relations given by such codes are mainly intended for ordinary concrete, e.g. ACI estimates tensile strength as $7.5\sqrt{f'_{cu}}$ and the new trend for HSC is to use $11\sqrt{f'_{cu}}$ in psi units.

Impact

Drop weight impact test was carried out on simple concrete beam structural configuration. The total impact weight was about 2 kg. with semispherical impactor end. The impact energy is the weight of the impactor multiplied by the sum of drop heights until beam failure. Then, a dimensionless impact factor was calculated as the ratio of impact energy of A2 and A3 relative to the control specimen A1. As illustrated in Figure (7), the impact resistance of HSC mixes A2 and A3 has been improved by 6 and 13 times; respectively relative to the control mix A1. Moreover, adding polypropylene fibers doubled the impact resistance. Despite the very limited number of test specimens, this result is very significant and shows a general trend that polypropylene fibers can greatly improve absorbed impact energy. As a note of caution, a more statistically significant number of samples should be considered before drawing a definite conclusion regarding the cited results.

Plastic Shrinkage

As it has been mentioned earlier, adding polypropylene fibers causes fresh concrete bleed less which leads to reducing capillaries formed by bleeding and hence a reduction in micro-cracks. Moreover, the mix sets faster and the end result is better resistance to plastic shrinkage. In the current study, plastic shrinkage readings have been recorded over a period of 24 hours immediately after casting. At each time point, the reading is the average of three samples for each mix. Then, a plastic shrinkage dimensionless factor is calculated using mix A1 as a reference. As depicted in figures (8) and (9), it can be seen that the first four hours after casting is the most influential period at which most plastic shrinkage occurs. Comparing the results of

mix A2 (cement content of 600 kg/m^3) with mix A1 (cement content 350 kg/m^3), an increase in plastic shrinkage between 20% and 60% is observed. On the other hand, adding polypropylene fibers (mix A3) reduces shrinkage by about 20% relative to A2 (i.e. the same cement content). It is worthy to mention that after 4 hours of casting the mix A3 gives the same result as mix A1 (with just over half the cement content). This result is a clear reflection of the mechanism created by adding the fibers which results in reducing plastic shrinkage and hence, micro-cracking of concrete.

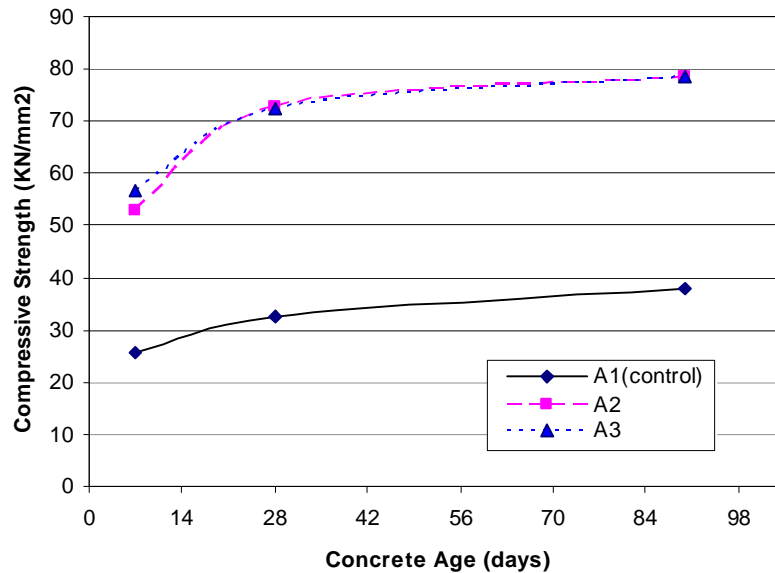


Fig. 3: Variation of Compressive Strength for Different Mixes over Time

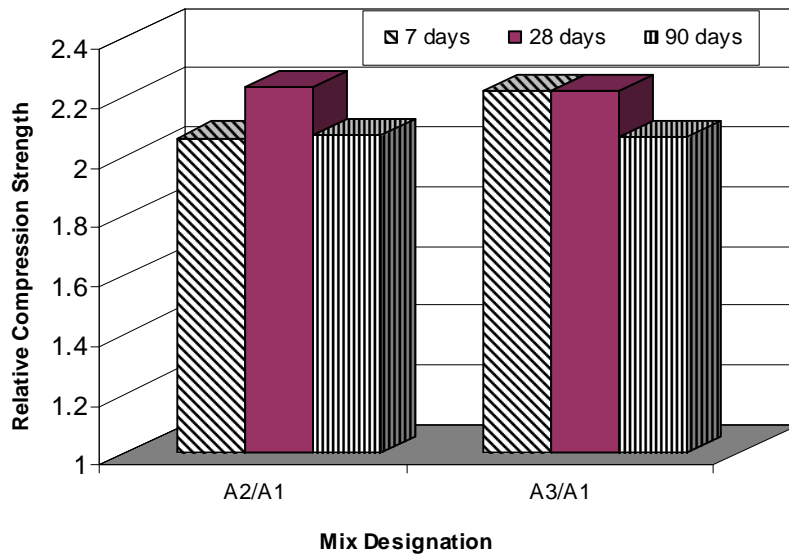


Fig. 4: Relative Compression Strength chart for Different Mixes over Time

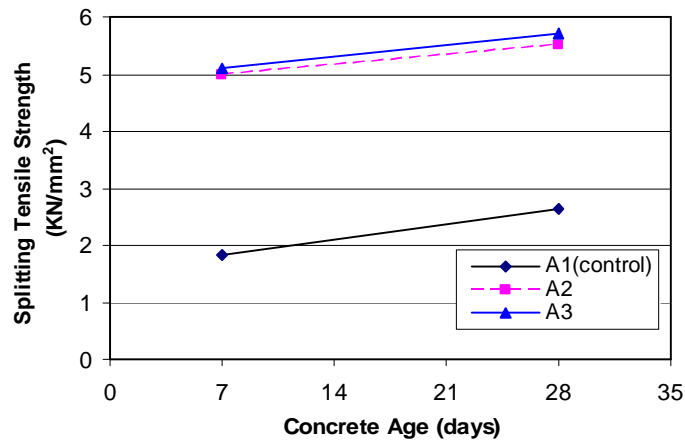


Fig. 5: Variation of Tensile Strength for Different Mixes over Time

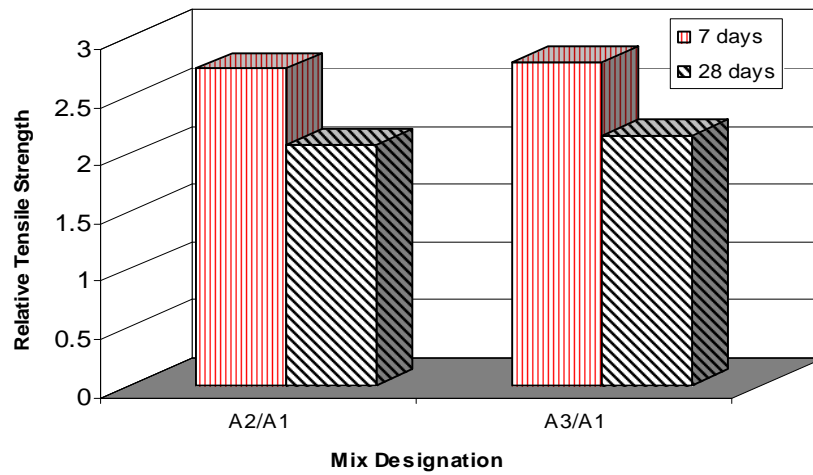


Fig. 6: Relative Tensile Strength Chart for Different Mixes over Time

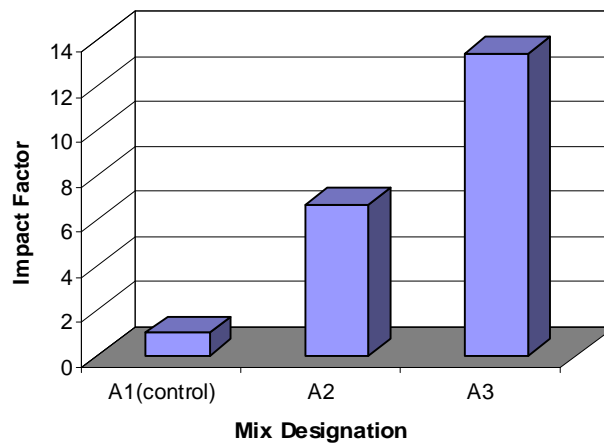


Fig. 7: Variation of Impact Factor for Different Mixes

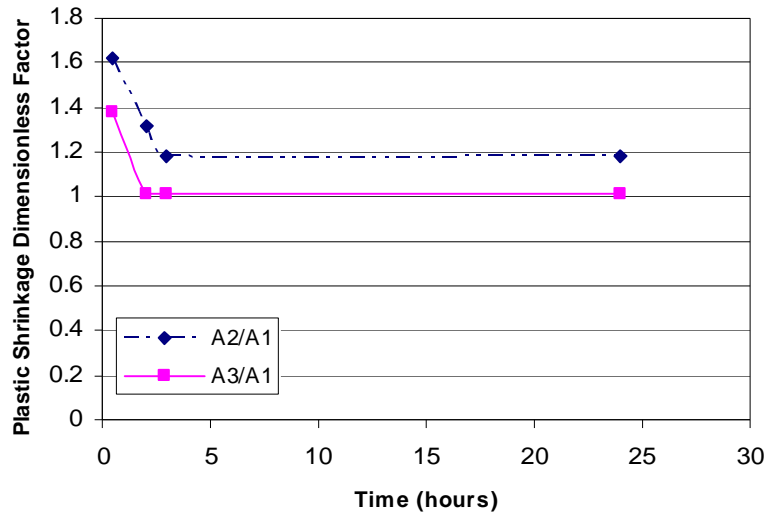


Fig. 8: Variation of Dimensionless Plastic Shrinkage Factor over Time

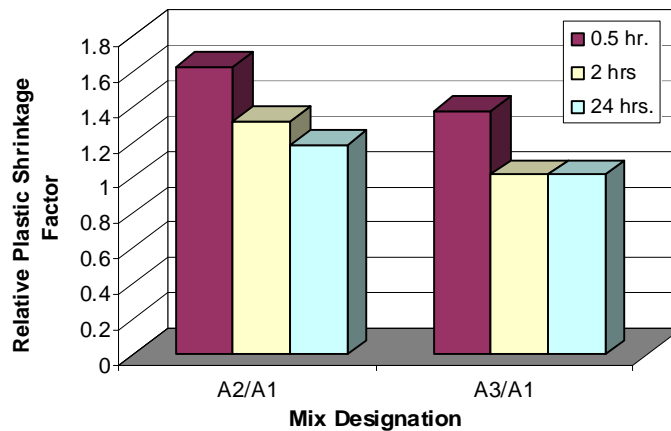


Fig. 9: Dimensionless Plastic Shrinkage Factor Chart

Conclusions

In the current study, a moderate HSC has been developed with compressive strength of about 80 MPa. Using crushed stone aggregate and some admixtures to reduce w/c ratio and improve workability. The influence of adding polypropylene fibers to HSC on impact resistance as well as plastic shrinkage has been investigated. The results indicate that the fibers have no significance on either the compressive strength or the splitting tensile strength. On the other hand, the fibers influence on both the impact resistance and plastic shrinkage is remarkable. The absorbed impact energy during drop weight test is more than doubled. Moreover, the concrete plastic shrinkage is reduced by over 20%, which results in less micro-cracking. It is also worthy to mention that adding the fibers compensates for the resulting increase of plastic shrinkage due to almost doubling the cement content needed for HSC.

REFERENCES

1. Roles, S.; Mbessa, M.; Ambroisa, J.; and Pera, J., 1999, "Influence of Ultra-Fine Particle Type on Properties of Very-High-Strength Concrete", SP 186-39, High Performance Concrete, ACI, pp.671-685
2. Zeghib, R., and Nacer-Bey, M., "Study and Formulation of High Performance Concrete with Various Ultra-Fine Admixtures", Fifth CANMET/ACI International Conference on Superplasticizers and Chemical Admixtures in Concrete", Supplementary papers, Rome, 1997, pp. 286-293.
3. Lang, E., and Geisseler, J., "Use of Blast Furnace Slag Cement with High Slag Content for High-Performance Concrete", 4th International Symposium on Utilization of High-Strength/High-Performance Concrete, Paris, 1996, pp. 213-222.
4. Novokshchenov, V., "Factors Controlling the Compressive Strength of Silica Fume Concrete in the Range 100-150 MPa", Magazine of Concrete Research, 1992, 44, No. 158, pp. 53-61.
5. Shah, S. P., and Ahmed, S. H., "High Performance Concrete: Properties and Application", 1994, Mc Graw-Hill, Inc, London, 403 p.
6. Gjorv, O. E., "High-Strength Concrete", In: Advances in Concrete Technology, 2nd Edition, CANMET, Editor: V. M. Mlotra, 1994, p. 19-82.
7. De Larrard, F., "Formulation et propriétés des béton a tres hautes performances", Rapport de recherché du laboatoire Central des Ponts et Chaussees, Paris, No., 149, 1988, 350p.
8. Bruno, V., Chabannet, M., Ambroise, J. and Pera, J., "Betons Tres Haute Performance (BTHP): Microfissuration et durabilite", 2nd CANMET/ACI International Conference on Durability of Concrete, Supplementary Papers, Montreal, 1991, pp. 175-193.
9. Naaman, A. E., Wongtanakitcharoen, T., and Hauser, G., "Influence of Different Fibers on Plastic Shrinkage Cracking of Concrete", ACI Materials Journal, V.102, No. 1, Jan-Feb. 2005, pp.49-58.
10. Webster, T., personal communication, Webster Engineering Associates, Independence, Ohio, Mar. 2001.
11. Zollo, R.; Ilter, J.; and Bouchacourt, G., "Plastic and Drying Shrinkage in Concrete Containing Collated Fibrillated Polypropylene Fiber," Third International Symposium on Developments in Fiber Reinforced Cement and Concrete, RILEM Symposium FRC 86, V. 1, July 1986.
12. Soroushian, P.; Mirza, F.; and Alhozaimy, A., "Plastic Shrinkage Cracking of Polypropylene Fiber Reinforced Concrete," ACI Materials Journal, V. 92, No. 5, Sept.-Oct. 1995, pp. 553-560.
13. Bayasi, Z., and Zeng, J., "Application of Polypropylene Fibers for Reduction of Shrinkage Cracking of Concrete," International Conference on Reinforced Concrete Materials in Hot Climates, United Arab Emirates University, Nov. 1994, pp. 441-452.
14. Bayasi, Z., and McIntyre, M., "Application of Fibrillated Polypropylene Fibers for Restraint of Plastic Shrinkage Cracking in Silica Fume Concrete", ACI Materials Journal, V. 99, No. 4, July-August 2002, pp.337-344.
15. Soroushian, P., Khan, A., and Hsu, J., "Mechanical Properties of Concrete Materials Reinforced with Polypropylene or Polyethylene fibers" , ACI Materials Journal, V. 89, No. 6, Nov. – Dec. 1992, pp. 535-540
16. Wei, S., P., Ganghua and D., Dajun, 1997, "Effect of the Combined Use of Ultra-Fine Fly Ash and Silica Fume on Strength of HPC", SP 172-16, High Performance Concrete, ACI, pp.299-312.
17. Sabir, B.B., 1995, "High-Strength Condensed Silica Fume Concrete", Magazine of Concrete Research, Vol. 47, No. 172, pp. 219-226.
18. ASTM C827-01a 2005 "Standard Test Method for Change in Height at Early Ages of Cylindrical Specimens of Cementitious Mixtures" ASTM International, PA, USA.

EFFECT OF CONCRETE CHARACTERISTIC STRENGTH ON RESIDUAL LOAD CAPACITY OF COLUMNS SUBJECTED TO FIRE LOAD USING NUMERICAL ANALYSIS

M. A. A.El Aziz¹, K. M. Osman², *S. M. Elzeiny³ and A. Serag⁴

1- Associate Professor, Fayoum University, Faculty of Engineering, Civil Department, Fayoum, Egypt.

2- Assistant Professor, Fayoum University, Faculty of Engineering, Civil Department, Fayoum, Egypt.

3- Assistant Professor, Housing and Building National Research Center, Cairo, Egypt

4- PhD Candidate, Fayoum University, Faculty of Engineering, Civil Department, Fayoum, Egypt.

Email: shmelzny@gmail.com

ABSTRACT

The current research work deals with the effect of variant concrete characteristic strength and different column cross-sectional dimensions (rectangularity ratio) of scalar reinforced concrete short columns model on the residual load capacity after firing using numerical analysis. The numerical analysis was conducted using three dimensional nonlinear F.E.A program (Ansys10). The temperature distribution in the concrete columns sections is according to *ISO-834 Standard Fire curve*. The temperature introduced to F.E.A program is 600°C with 20 min of firing time. In the beginning, a comparison between previous experimental work and numerical analysis using F.E.A. program was done to show the conformity. Next, an extensive numerical analysis was done for twenty seven scalar models classified to three groups according to column dimensions, fire duration, and concrete characteristic strength. The present study indicated that, the high effect of concrete characteristic strength and rectangularity ratio on columns residual load capacity after firing.

Keywords: Reinforced Concrete, Columns, Fire, Numerical Analysis, Residual Load Capacity.

INTRODUCTION

Current design of reinforced concrete structures is concerned with the behavior of ultimate strength and ductility under severe loading condition in view of the safety of structures and economy. One of the most important structural elements in the structures which play a significant role is the column.

The stress analysis in the field of structural engineering is invariably complex, and for many of the problems it is extremely difficult and tedious to obtain analytical solutions. In these situations, engineers usually resort to numerical methods to solve the problems. With the advancement of computers, one of the most powerful techniques that have been developed in the field of engineering analysis is the finite element method. The finite element method is essentially a process thought which a continuum with infinite degrees of freedom can be approximated to be an assemblage of sub-regions (or elements) each with a specified but no finite number of unknowns. This essential simplicity in both physical interpolation and mathematical form has undoubtedly been as much behind its popularity. Now, finite element method is being a general method and can be used for the analysis of structures and solids of complex shapes and complicated boundary conditions.

Fire is the main problem to be faced in the combustibility of contents and failure of the structure. The extent of consequential damage depends primarily on structural performance of building

* Corresponding author
Received Date:26/12/07
Acceptance Date:20/5/08

both during and after the fire. The behavior of concrete elements exposed to fire depends on its mix composition, size of cross section, concrete cover, percentage of reinforcement, and thermal properties. It has been determined by complex interactions during heating process. The modes of concrete failure under fire exposure are being varied according to the nature of the fire, the loading system, and the type of structure^[1].

Due to high temperature, shrinkage may be formed in the material, and expansion may cause buckling or crushing of the concrete structure. So, the design of reinforced concrete columns under fire conditions is generally made on the basis of national and international recommendations.^[2 to 10]

VERIFICATION OF PAST EXPERIMENTAL RESULTS WITH NUMERICAL ANALYSIS

Farid, et. al.,^[10], performed a numerical analysis using finite element method in order to verify the past experimental test results. The software program (ANSYS^[11]) used in the analysis was based on plastic model. The model can be precisely used to predict both the hardening and softening behavior of concrete. The available experimental work was made by both of Khalil, et. al.,^[12], and Mohamed, et. al.,^[13]. Biaxial compression test was carried out with six specimens. The dimensions and details of reinforcement for all specimens, load eccentricities and the material properties are shown in table (1).

Table 1: Tested Specimens details.

Col No.	Section (mmxmm)	Height (mm)	F _{cu} (MPa)	Ver. Rft.	Stirrups	Fire Exposure Time
C1	100x100	1000	25.43	4 ϕ 6	ϕ 2.7@7cm	At 10 min At 20 min
C2	100x400	1000	25.43	14 ϕ 6	ϕ 2.7@7cm	At 10 min At 20 min
C3	100x250	1000	25.43	10 ϕ 6	ϕ 2.7@7cm	At 5 min At 10 min At 15 min At 20 min
C4	150x150	1000	30	4 ϕ 10	ϕ 6@10cm	At 15 min
C5	150x150	1000	37.5	4 ϕ 10	ϕ 6@10cm	At 15 min
C6	150x150	1000	30	4 ϕ 12	ϕ 6@10cm	At 15 min

Element Used in Modeling Concrete

Solid or three-dimensional elements are used to simulate concrete elements. This element enables the solution of problems for a general three-dimensional stress analysis. In the three-dimensional stress analysis, finite element analysis provides a powerful tool for getting numerical solution. The eight-node isoperimetric element is one of simplest and its performance in situations where bending is involved can be improved by the addition of incompatible nodes similar to the quadrilateral elements. For this reason, the eight-node isoperimetric element is utilized in the current research work to simulate concrete material.

Element Used in Modeling Reinforcement

Three-dimensional truss element is used to simulate the reinforcement inside the concrete element. This element was used to get the axial force and axial strain occurred inside the steel bar due to any state of load.

Descertization of Elements

Figure (1) is showing the modeling of the reinforced concrete columns. From the above figure it can be noticed the configuration of mesh used for modeling the concrete elements, the internal reinforcement bars.

Comparisons between Experimental Work and Numerical Analysis

Table (2) shows the results of the crushing load failure before firing and residual load capacity for firing columns model from experimental tests and numerical analysis made by Farid, et. al.,[10]. Figure (2) shows a sample of the comparison between numerical and experimental results. Figure (3) shows a sample of the residual load capacity, deformed shape, and the first crack for sample of tested column models. By analyzing, we found that the max % error from the comparative study between experimental test results and finite element analysis study by using ANSYS program is 6.27 %, which show good agreement with test results.

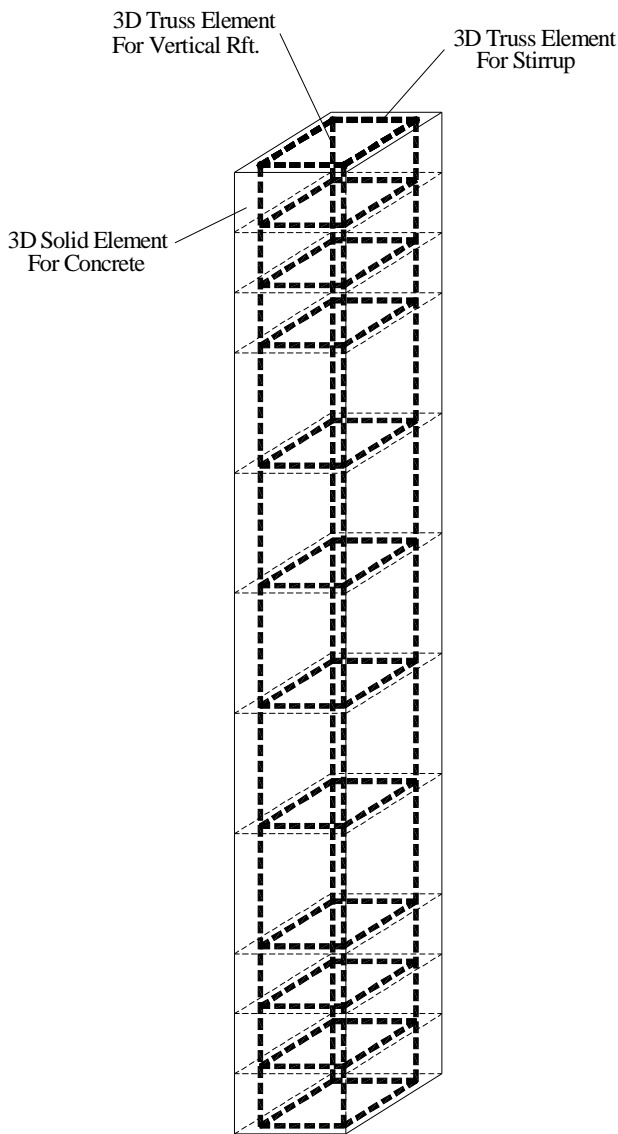
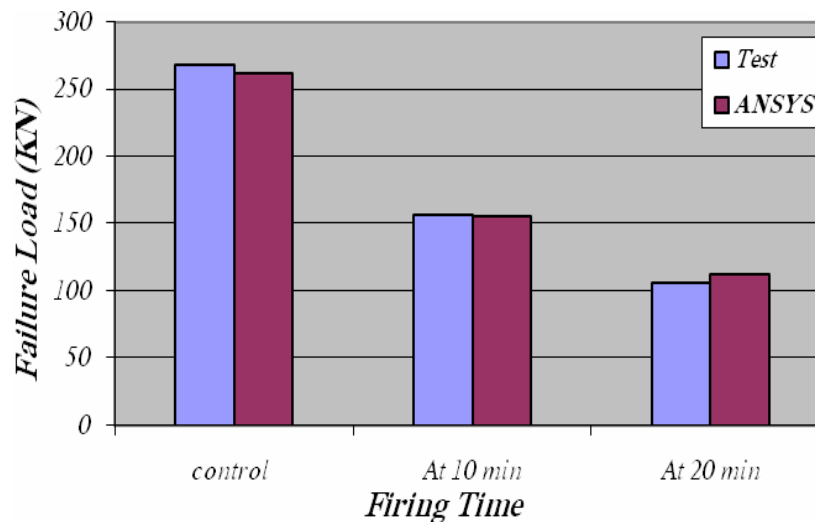


Fig. 1 : Models of Concrete and Steel Bars in the F.E. Program.

Table 2: Comparison between Experimental and Numerical Analysis.

Column No.	Fire Duration	Experimental Results (KN)	Numerical Results (ANSYS) (KN)	% Error
C1	No Temp.	268	261	-2.313
	10 Min.	157	156.05	-0.6051
	20 Min.	106	112.14	5.794
C2	No Temp.	1033	1010.98	2.132
	10 Min.	705	673.45	-0.6051
	20 Min.	469	493.768	5.281
C3	No Temp.	667	653.84	-0.002
	5 Min.	514	500.56	-2.605
	10 Min.	366	374.12	2.219
	15 Min.	349	342.14	-1.966
	20 Min.	265	248.39	-6.266
C4 (Reference)	No Temp.	705	720	2.13
	15 Min.	565	536.1	-5.12
C5	No Temp.	845	876.8	3.76
	15 Min.	580	606.3	4.53
C6	No Temp.	860	807.9	-6.06
	15 Min.	700	694.5	-0.79



Column Model (C1).

Fig. 2 : A Sample of Comparisons between Experimental Tests and ANSYS Results for Load Failure.

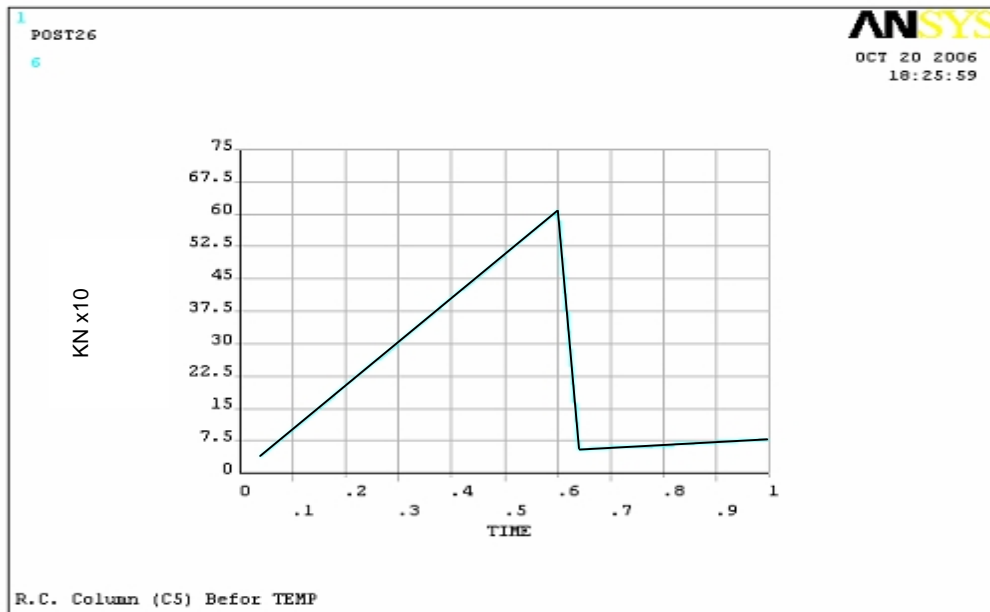


Fig. 3-a: Residual Load Capacity for Column No C5 after Firing Time 15 min.

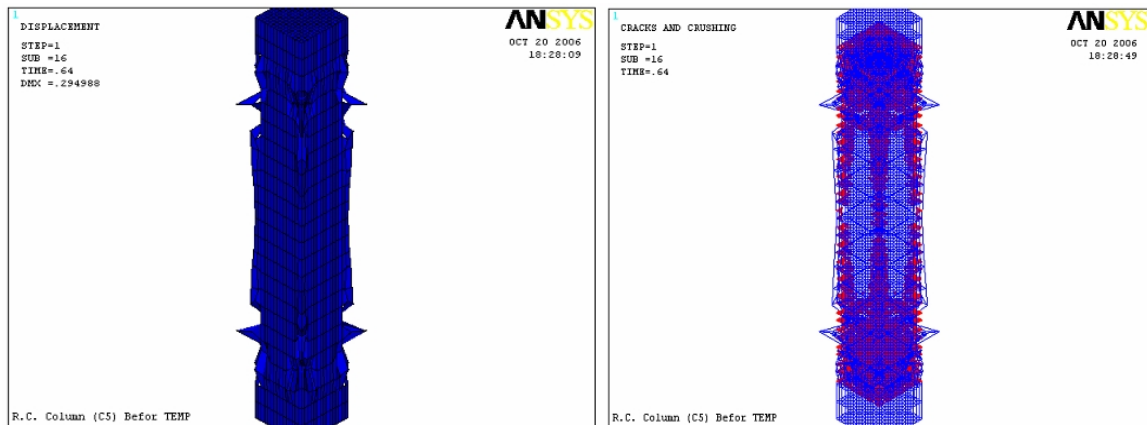


Fig. 3-b: Deformed Shape and First Crack for Column No C5 after Firing Time 15 min.

PARAMETRIC STUDY

Parameters of the Numerical Analysis

After the verification of the experimental results discussed in previous section, a parametric study of 27 columns was conducted to investigate the following variables:

1. Column dimensions (C1=100x150 mm, C2=150x150 mm, and C3=150x200 mm).
2. Fire duration (Control without temperature, at temperature 600°C and after 20 min heating).
3. Concrete characteristic strength. ($F_{cu} = 25, 30, \text{ and } 35 \text{ N/mm}^2$).

Column load and column residual load due to exposed to elevated temperature were obtained at each load step. Temperature distribution or temperature gradient, First crack loads, deformed shape and failure mode are obtained for each column at failure load. Load-time curves were obtained at mid-height of the columns.

Twenty-seven reinforced concrete columns were analyzed under the effect of axial compression load and the effect of high temperature. All columns dimensions used in experiments were modeled to be 1/3 scale of the original columns in ordinary buildings. Also firing time was scaled based on the model mentioned by Farid, et. al.,[10]. Specimens are classified to three group according to specimens cross section (Group "C1= 100x150 mm", Group "C2= 150x150 mm", Group "C3= 150x200 mm"). All specimens had a height of 90 cm as shown in Figure (4). Each group is sub- classified to three subgroups according to the following parameters study, Concrete characteristic strength and exposure firing time (in air condition, at 600°C and at 20 min exposed to temperature). Table [3] shows columns model dimensions, reinforcement and material properties for all specimens.

Table 3a: Columns Model Dimensions and properties of Group C1 (100x150 mm).

Group No.	Col. No.	Concrete Cover mm	F _{cu} (MPa)	VRL. Rft. % μ	Firing time
GROUP C1	C1-1a	10	25	1.13%	Control
	C1-1b	10	25	1.13%	At 600°C
	C1-1c	10	25	1.13%	20min
	C1-2a	10	30	1.13%	Control
	C1-2b	10	30	1.13%	At 600°C
	C1-2c	10	30	1.13%	20min
	C1-3a	10	35	1.13%	Control
	C1-3b	10	35	1.13%	At 600°C
	C1-3c	10	35	1.13%	20min

Table 3b: Columns Model Dimensions and properties of Group C2 (150x150 mm).

Group No.	Col. No.	Concrete Cover mm	F _{cu} (MPa)	VRL. ft. % μ	Firing time
GROUP C2	C2-1a	10	25	0.93%	Control
	C2-1b	10	25	0.93%	At 600°C
	C2-1c	10	25	0.93%	20min
	C2-2a	10	30	0.93%	Control
	C2-2b	10	30	0.93%	At 600°C
	C2-2c	10	30	0.93%	20min
	C2-3a	10	35	0.93%	Control
	C2-3b	10	35	0.93%	At 600°C
	C2-3c	10	35	0.93%	20min

Table 3c: Columns Model Dimensions and properties of Group C3 (150x200 mm).

Group No.	Col. No.	Concrete Cover mm	F_{cu} (MPa)	VRL. Rft. % μ	Firing time
GROUP C3	C3-1a	10	25	1.00%	Control
	C3-1b	10	25	1.00%	At 600°C
	C3-1c	10	25	1.00%	20min
	C3-2a	10	30	1.00%	Control
	C3-2b	10	30	1.00%	At 600°C
	C3-2c	10	30	1.00%	20min
	C3-3a	10	35	1.00%	Control
	C3-3b	10	35	1.00%	At 600°C
	C3-3c	10	35	1.00%	20min

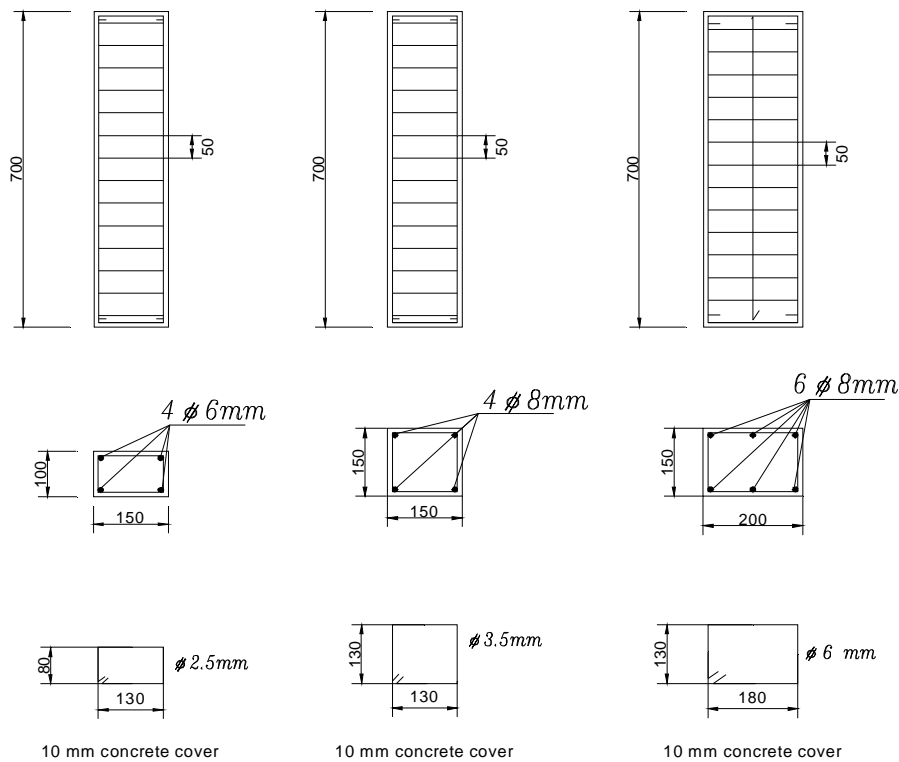


Fig. 4: Columns Cross Section and Reinforcement Details of Tested Columns.

Temperature Effect and Equivalent Model Exposure Time.

Figure (5) shows the *ISO-834 standard time-temperature curve* used in the current study. The time-temperature relationship on the boundary member is defined in equation (1).

$$T_b = 345 \times \log_{10}(8t + 1) + T_0 \tag{1}$$

Where

t is time [min].

T_0 is ambient temperature [°C] and T_b is boundary temperature [°C].

Figure (6) shows the temperature distribution at temperature 600°C and after firing time 20 min from ANSYS program for different column model.

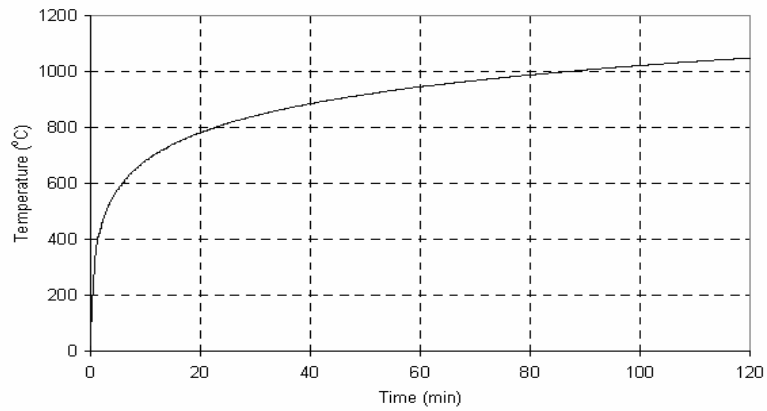
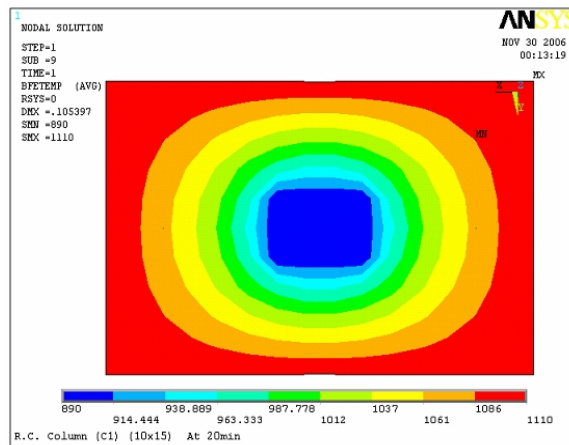
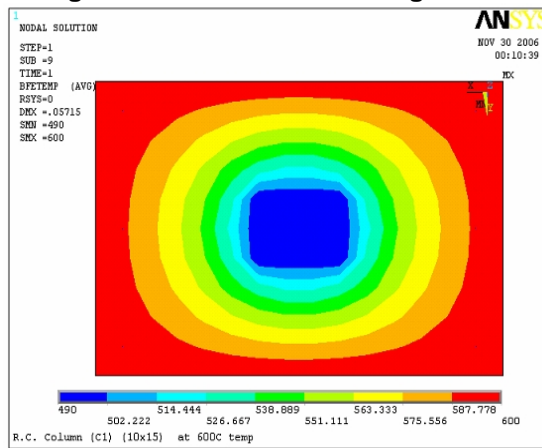
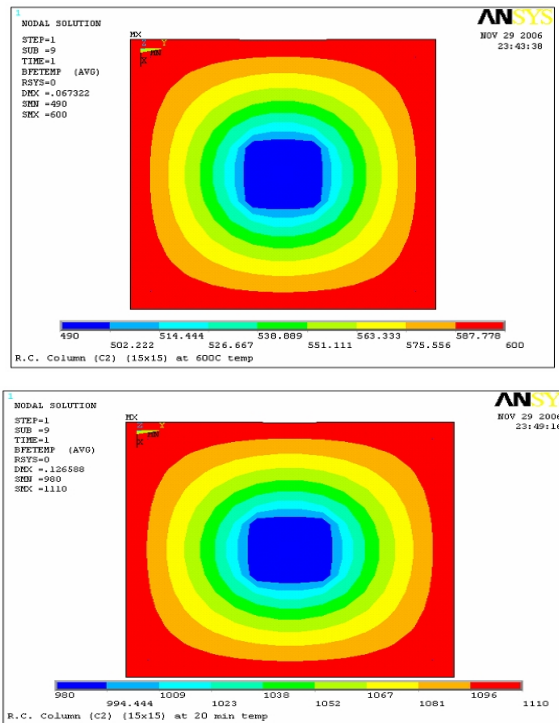


Fig. 5: Standard ISO 384 Firing Curve.



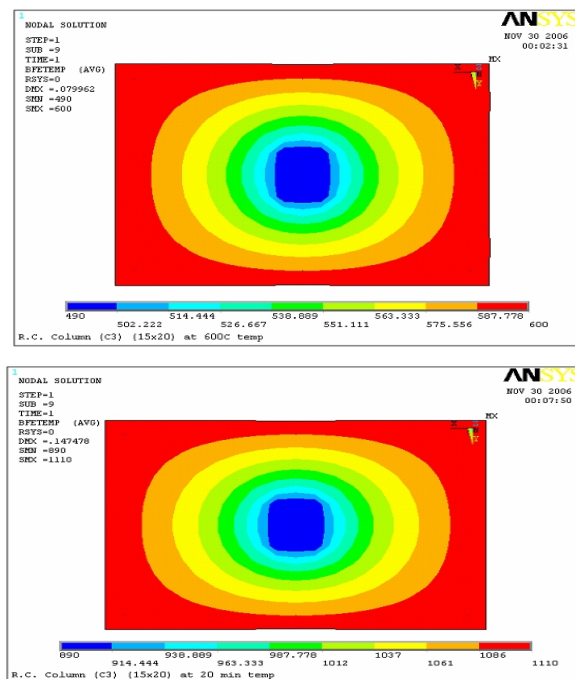
At Temperature 600°C after Firing Time 20 min
 (a) Temperature Distribution for Column C1. (100 x 150 mm).



At Temperature 600°C after Firing Time 20 min

(b) Temperature Distribution for Column C2. (150 x 150 mm).

Fig. 6: Temperature Distribution for Tested Column Groups.



At Temperature 600°C after Firing Time 20 min

(c) Temperature Distribution for Column C3. (150 x 200 mm)

Fig.(6): Temperature Distribution for Tested Column Groups(Cont.).

RESULTS OF PARAMETRIC STUDY.

Results

All the tested models were classified to three cases of firing exposure, the reference case at normal condition while second and third case are at temperature 600°C, and after firing time 20 min, as mentioned before. Tables [4a, b, and c] show the load capacity and residual load capacity percentage of studied columns before and after exposure to elevated temperature for all tested column models. It concluded that, all reference specimens' give crushing load capacity higher than specimens exposed to fire.

From Table [4] and Figure (7), it can be observed the following:

- For a high concrete characteristic strength, the column residual loads capacity was increased as concrete characteristic strength increases.
- Columns cross-section rectangularity ratio affect the residual crushing loads of different modeled columns after fire. The square cross-section model group (C2 150x150 mm) have more residual load capacity than other two groups, (C1 100x150 mm) and (C3 150x200 mm) after exposed to temperature 600. In the other hand, after 20min firing time the residual load capacity decreases with cross-section increasing.

Figure (8 & 9) shows the residual load capacity, deformed shape, and the first crack for sample of tested column models.

Table 4a: Crushing Load and Residual Load Capacities for Group C1 (100x150 mm)

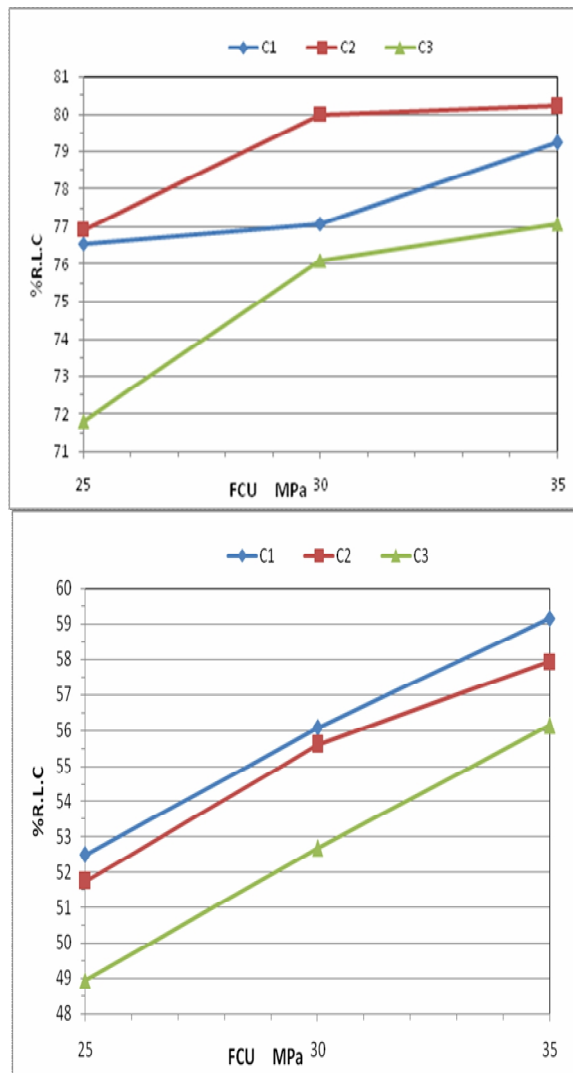
Group No.	Col. No.	R.L.C. (KN)	% R.L.C.
GROUP C1	C1-1a	393.62	100
	C1-1b	301.39	76.56
	C1-1c	206.67	52.50
	C1-2a	475.62	100
	C1-2b	366.56	77.07
	C1-2c	266.65	56.065
	C1-3a	535.53	100
	C1-3b	424. 2	79.22
	C1-3c	3316.8	59.16

Table 4b: Crushing Load and Residual Load Capacities for Group C2 (150x150 mm)

Group No.	Col. No.	R.L.C. (KN)	% R.L.C.
GROUP C2	C2-1a	589.62	100
	C2-1b	453.48	76.91
	C2-1c	305.08	51.74
	C2-2a	712.81	100
	C2-2b	570.11	79.98
	C2-2c	396.28	55.59
	C2-3a	805.46	100
	C2-3b	646.07	80.21
	C2-3c	466.67	57.94

Table 4c: Crushing Load and Residual Load Capacities for Group C3 (150x200 mm)

Group No.	Col. No.	R.L.C. (KN)	% R.L.C.
GROUP C3	C3-1a	788.15	100
	C3-1b	561.64	71.81
	C3-1c	382.79	48.94
	C3-2a	936.44	100
	C3-2b	712.59	76.09
	C3-2c	493.5	52.69
	C3-3a	1066.66	100
	C3-3b	822.39	77.09
	C3-3c	598.77	56.14



(a) At Temperature 600°C

(b) After Firing Time 20 min

Fig. 7: The Residual Loads Capacity for columns C1, C2, and C3 with Different Concrete Characteristic Strength.

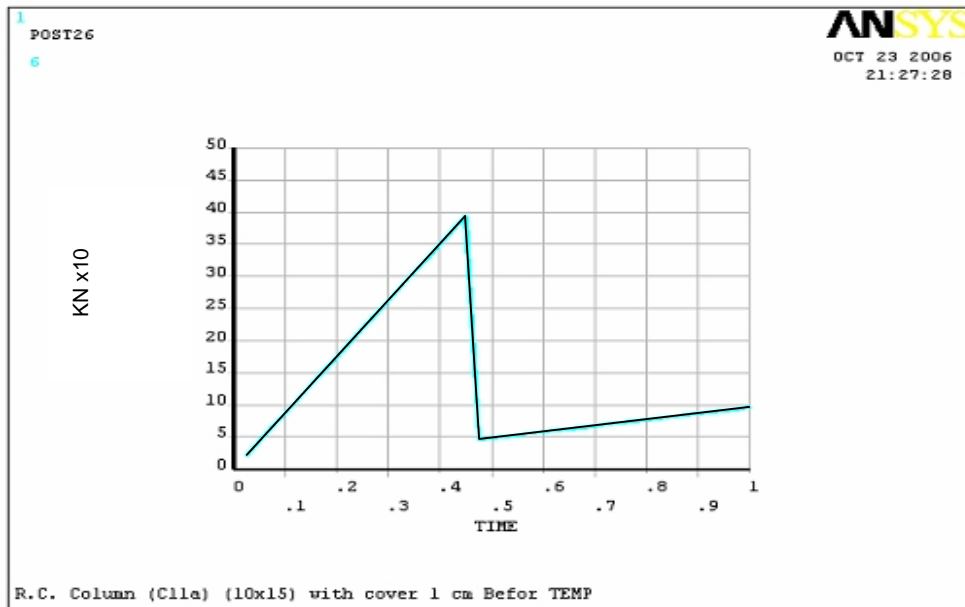


Fig. 8: Sample of Residual Load Capacity for Model (C1-1a) Before Exposed to Fire.

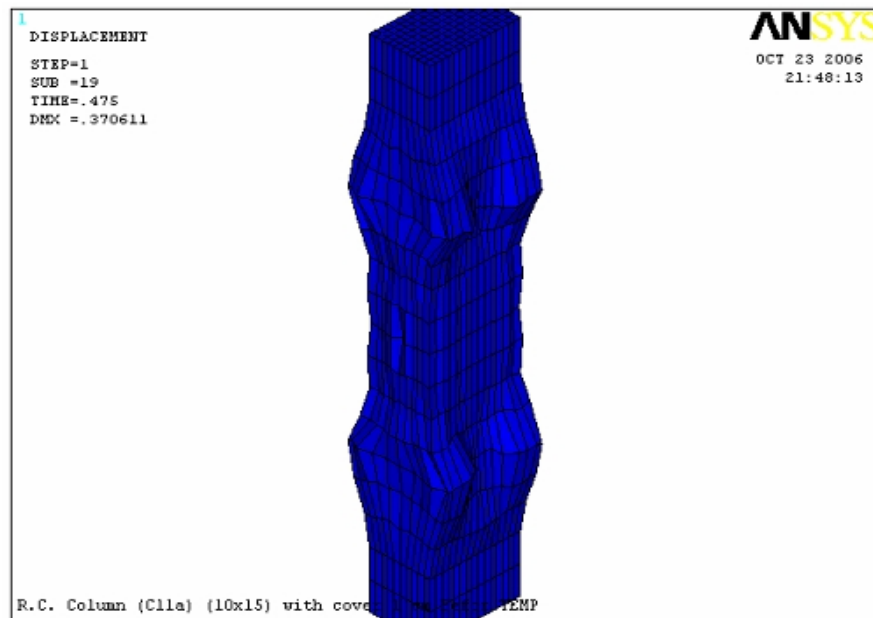


Fig. 9: Sample of Deformed Shape for Model (C1-1a) Before Exposed to Fire.

SUMMARY AND CONCLUSIONS

Based on the numerical analysis that investigated the effect of both concrete characteristic strength and fire exposure on residual load capacity of short columns, the following conclusions can be drawn:

- 1- Numerical analysis was found to be an effective method for analyzing the behavior of reinforced concrete columns subjected to fire load with different concrete characteristic strength.
- 2- Columns residual crushing loads after fire are function in exposure firing time.
- 3- For a high concrete characteristic strength, the column residual load capacity was increased as concrete characteristic strength increases.

- 4- Column cross-sectional dimensions (rectangularity ratio) affected the residual crushing loads of different modeled columns after fire. The square cross-section model group C2 (150x150 mm) had more residual load capacity than the other two groups, C1 (100x150 mm) and C3 (150x200 mm). This might be explained as the perimeter, which exposed to fire in square column cross-section is less than the rectangular column perimeter.

REFERENCE

1. James, A. M., ``Analytical Method to Evaluate Fire Resistance of Structural Members``, Journal of Structural Engineering, October 1999, pp.1179-1187.
2. Anderberg, Y., and Thelandersson, S., Division of Structural Mechanics and Concrete Construction, Bulletin 54, Lund Institute of Technology, Lund, Sweden, 1976.
3. Khoury, G.A., Grainger, B.N., and Sullivan, P.J., ``Strain of Concrete During First Heating To 600 °C Under Load``, Magazine of Concrete Research, Vol.37, No.133, December 1985, pp. 195-215.
4. Hosny, H., and Abo. Elmagd, ``fire of Reinforced Concrete Structures``, Dar Elnasher for Egyptian University, 1994.
5. Malhotra, H. L., ``the Effect of Temperature on the Compressive Strength of Concrete``, Magazine of Concrete Research, Vol. No23, August 1956, pp.85-94.
6. Castillo, Carlos, and Durrani, A. J., ``Effect of Transient High Temperature on High Strength concrete``, ACI Material Journal, V. 87, No.1, January-February, 1990, pp.47-53.
7. Khoury, G. A., Grainger B., and Sullivan, P.J.E., ``Strain of Concrete during First Time heating``, Magazine of Concrete Research, Sept. 1985, Dec. 1985, and March 1986.
8. Cruz, C. R., ``Elastic Properties of Concrete at High Temperature``, Journal, PCA Research and Development Laboratories, V.8, No.1, Jan. pp.37-45.
9. Philleo, R., ``Some Physical Properties of Concrete at High Temperatures``, American Concrete Institute, Vol.54, April 1958, pp.857-864.
10. Farid, A. S., ``Effect of Fire Exposure on Residual Load Capacity of Short Columns``, M. Sc. Thesis, Fayoum University, Faculty of Engineering, 2007.
11. ANSYS®. Manual, Version 10.
12. Khalil, U.F., "Experimental study for the residual load capacity of short modeled columns fired in a fire furnace", Ph.D. Thesis, Cairo University, Faculty of Engineering, 2002.
13. Mohamed, B.M., ``Behavior of reinforced concrete columns exposed to fire``, M. Sc. Thesis, Cairo University, Faculty of Engineering, 2004.

DYNAMIC RESPONSE OF LAMINATED POLYMER COMPOSITE PLATES WITH MATRIX CRACKS

Aly A. Emam¹, *Khaled M. Shokry¹ and E.H.Hasan²

1- Materials Research Institute, Housing & Building National Research Center,

2- National Research Institute for Standards (NIS) - Giza, Egypt.

ABSTRACT

The laminated composite materials develop extensive patterns of microstructural damage as a result of mechanical or environmental load history. The mechanical as well as the physical properties of the composite laminates get affected by the induced damage. Furthermore, the development and accumulation of such damage modes are the precursor to structural failure. An adequate understanding of the dynamic response of such materials has now become a primary design factor to insure the safety of many structural elements used in aerospace and automobile industries. Hence, the focus of this research is on the post-damage dynamic characterization of laminated composite plates containing matrix cracks type of damage. Among different damage modeling approaches, the damage mechanics approach appears to be a useful tool for predicting the global effect of matrix cracks damage modes on the constitutive response of a composite laminate. In this approach the damage is mathematically modeled using an Internal State Variables (ISV) concept. This approach is used in this study to predict the elastic parameters of laminated composites with various sizes and shapes of damage. A finite element code is developed using a consistent shear deformation theory to investigate the upper bounds of the vibration frequencies of damaged orthotropic laminates with various boundary conditions. The model is based on discrete laminate theory that allows for each ply of the composite assembly to have its own elastic properties and state of damage. Some numerical results are presented and the comparisons of these results with experimental data and other analytical models show a good agreement.

Keywords: laminated composites, damage, graphite-epoxy, continuum mechanics, matrix cracking, internal state variables, vibration.

INTRODUCTION

It is well recognized that laminated fiber reinforced polymer composite structural elements like plates exhibit matrix cracking, delamination and fiber fracture types of primary damage modes when subjected to service static as well as dynamic loads. As a result, the static as well as the dynamic characteristics of such damaged plates are affected to a lesser or greater degree depending upon the extent and kind of damage. Of particular importance are the problems dealing with impact loading situations. The studies done on these kinds of problems can broadly be categorized under two classes: (i) evolution and modeling of damage to predict the residual stiffness and strength properties, and (ii) experimental measurements of the residual static and dynamic properties. Great deal of research has been done on the problems related to the first category. A significant amount of work has been focused on investigating the free-edge delamination due to inplane static and fatigue loading.

Corresponding author
Received Date:9/4/08
Acceptance Date:3/7/08

These investigations have used different techniques to study the stress fields at the free-edge that might cause delamination as indicated by Emam [1]. Apparently, the influence of damage on the dynamic characteristics of laminated composite plates has been recognized as an area of practical importance, Gibson[2]. An overview of such area and problems that need more investigations has been presented by Rajaiah [3]. It has been recognized that damage in the form of local cracks or delaminations causes a reduction in the natural frequencies and an increase in vibration damping of composite plates, Grady and Meyn [4]. It is believed that the changes in the natural frequencies of a structural element can be an effective tool to characterize damage and residual material strength. Some attempts to this effect have been made for sheet moulding compound (SMC) composite plates, [5,6]. Chaturvedi and Zayyad [7], were probably the first to study the post-impact dynamic behavior of damaged SMC circular plates. The plate was treated as a linear elastic isotropic material in both the damaged and undamaged zones with symmetric circular damage growth due to impact. Their study shows that the vibration frequency decreases with the increase in damage zone size as well as extent of damage, and this decrease is more significant for higher modes of vibration. A comprehensive review of various kinds of problems related to impact-damage of composites can be found in publications of Abrate [8], and Cantwell and Morton [9]. The continuum damage mechanics approach has been used to study the evolution of damage and the reduction of all primary stiffnesses of laminated composite plates by Allen et al.[10], Harris et al.[11,12], and Groves et al.[13].

The primary focus of most of the early work has been on the characterization and modeling of damage in composite laminates under static loading conditions. Such investigations focused more toward finding correlations between the state of damage and the residual mechanical properties of the structural component. However, the post-impact dynamic behavior of damaged laminated composite plates has not yet been investigated. So these types of problems need immediate attention. With this in mind, Chaturvedi and Emam [14] proposed an approach to investigate the free vibration of simply supported laminated composite plates containing matrix crack type of damage. Their results show that the size and degree of damage can significantly affect the fundamental frequency. This effect becomes more pronounced for higher vibration modes.

In view of the practical importance of the above problem, the present work is aimed at investigating further the free vibration response of composite plates containing matrix crack type of damage.

DAMAGE MODES

The experimental investigations, Groves [15], indicate that the damage in laminated composites can be a combination of interply matrix cracking, interply delamination, and fiber fracture. These modes are shown schematically in Fig.(1). Generally, the early stage of damage development is dominated by matrix cracking at the interface between the fibers and matrix in the fiber directions. The crack density increases with the applied stress, the number of cycles at a constant stress, or as a result of a foreign object impact at increasing impact energy. As these cracks reach the interply surfaces, interlaminar cracks are initiated. Subsequently, these interlaminar cracks join together along the interlaminar interfaces in between the adjacent plies, which may lead to partial or total delamination, which may result in loss of integrity of the laminate. The final stage of damage development is highly localized with increased instability and large scale fiber breakage. From the above discussion, one can infer that the influence of the combined damage modes of matrix cracking and delamination are of serious concern. The complexity of modeling of such interactive modes is obviously immense. Here, an attempt is made to study the effect of matrix cracking on the frequency response of composite plates.

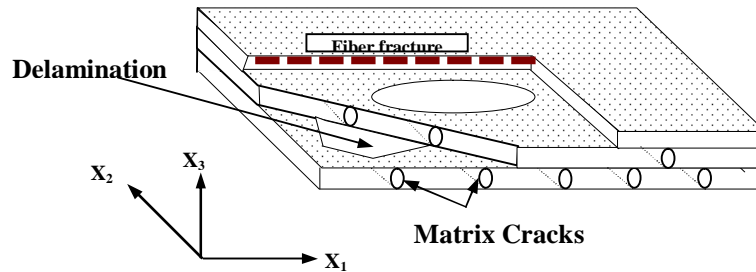


Fig. 1 Matrix cracking, delamination and fiber fracture in a continuous fiber

MATRIX CRACKS MODELING

In general there exist three primary modeling approaches [13-15] for matrix crack type of damage modes; (i)fracture mechanics, (ii)empirical correlations, and (iii)continuum damage mechanics approach. The continuum damage mechanics approach appears to be a useful tool to predict the overall behavior on the Macro-mechanics level of structural elements containing the matrix crack type of damage. In this approach, the structural component has two distinct zones: one zone is fully intact or undamaged in which the physical and mechanical properties of the material are unaffected. While the second is the damaged zone, or D-zone which is assumed to be small compared to the area of the plate. It is also assumed [14,15] that the damage is statistically homogeneous within the D-zone and the state of damage does not affect the initial boundary conditions. In this approach a set of second order tensor-valued variables, usually noted as Internal State Variables (ISV), is utilized to characterize the state of damage. As proposed by Krajcinovic [16], the internal state variables are introduced in such a way that they can account for each internal damage state. For laminated composites Allen et al. [10] developed a damage mechanics model for predicting the reduction of stiffness as a function of the state of damage. This model is expanded [14] for the study of the vibration response of some rectangular laminated composite plates with different boundary conditions.

Internal state variables

For a laminate with statistically homogenous matrix cracks in the D-zone, as shown in Fig.(2), ISV's (a_{ij}^M) are defined by [10]:

$$a_{ij}^M = \frac{1}{V} \int_S u_i n_j dS \tag{1}$$

where, u_i are the displacements on the crack faces, n_j are the components of a unit normal vector to the crack surface and V is the local volume element over which cracks are distributed and S is the surface area of matrix cracks in the volume V .

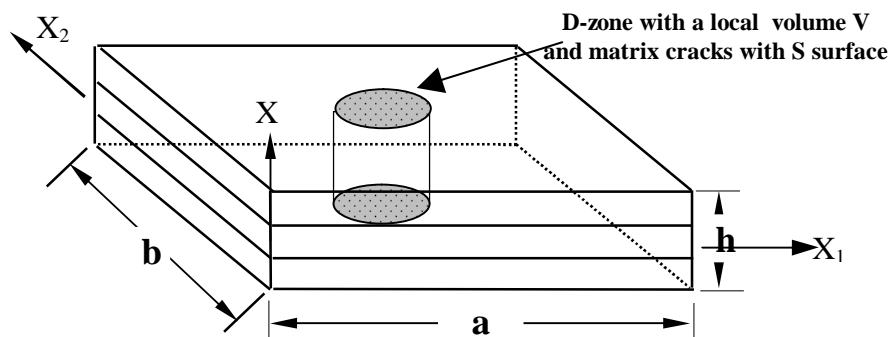


Fig. 2: A representative local volume element in D-zone of a general laminate.

For cracks normal to the laminate midplane, i.e. the case of straight vertical cracks in crossply laminate (Fig.1), the components of the unit normal \underline{n}_i are given by:

$$\underline{n} = \{0 \quad 1 \quad 0\}^T \tag{2}$$

Therefore, the only non-zero components of the damage tensor are:

$$\underline{a}^M = \begin{Bmatrix} a_{22}^M \\ a_{23}^M \\ a_{12}^M \end{Bmatrix} \tag{3}$$

Where the (ij) indices refer to (x_i) in the regular tensor notation, and we should note that the damage tensor follows the known rules of tensor transformations.

Due to inplane symmetry of each ply (a_{23}^M) is negligibly small [12]. For the case of straight vertical cracks in the 90°-plies of crossply laminates, there is no coupling between shearing and normal components and the cracking mechanism is directly related to Mode-I crack opening displacement.

Then, for a single lamina with vertical matrix cracks, the none-zero damaged stiffness (\mathcal{Q}_{ij}) and the inplane Poisson's ratio (\mathcal{N}_{12}) can be written as:

$$\mathcal{Q}_{11} = \bar{Q}_{11} \left\{ 1 - \left(\frac{\bar{Q}_{12}}{\bar{Q}_{11}} \right)^2 \frac{\mathcal{I}a_{22}^M}{\mathcal{I}e_{22}^M} \right\} \tag{4}$$

$$\mathcal{Q}_{22} = \bar{Q}_{22} \left\{ 1 - \frac{\mathcal{I}a_{22}^M}{\mathcal{I}e_{22}^M} \right\} \tag{5}$$

$$\mathcal{Q}_{66} = \bar{Q}_{66} \left\{ 1 - \frac{\mathcal{I}a_{12}^M}{\mathcal{I}e_{12}^M} \right\} \tag{6}$$

$$\mathcal{N}_{12} = n_{12} \left\{ 1 - n_{12} \frac{\mathcal{I}a_{22}^M}{\mathcal{I}e_{22}^M} \right\} \tag{7}$$

where, (\bar{Q}_{ij}) are the initial conventional lamina stiffnesses.

Equations (4) through (7) can be used to calculate the reduced elastic constants provided that expressions for the derivatives of the ISV's can be found. For $[0_q^\circ / 90_r^\circ]_s$ laminate such derivatives can be written as [14]:

$$\frac{\mathcal{I}a_{22}^M}{\mathcal{I}e_{22}^M} = \frac{n(q+r)}{2r} \frac{E_{11}}{E_{22}} \{ z_1(s) - 1 \} \tag{8}$$

$$\frac{\mathcal{I}a_{12}^M}{\mathcal{I}e_{12}^M} = 2 \left(1 - \frac{G_{12}^e}{G_{12}} \right) z_2(s) \tag{9}$$

Where, n is the number of 90°-sublayers in the 90°-ply; G_{12}^e is an experimental measure of the damaged shear modulus of $[\pm 45^\circ]_{2s}$ pure shear test specimens, and $z_i(s)$ are experimental correlation coefficients which depends upon the crack density.

Obviously, the expressions given by Eqs.(8) and (9) require some experimental work to evaluate the above parameters at different stages of damage. A task which is not always easy to achieve due to financial and time constraints. Therefore, analytical expressions, even though

they might be approximate, are desirable. Allen et al. [17] assumed that the displacement of the crack varies sinusoidally and bears a simple geometric relation for off-axis plies. The direct integration of Eq.(1) that defines the ISV's yields expressions for the damage parameters. For a thin to moderately thick crossply laminates, the cracks are mainly vertical with plane surfaces, Groves et al.[13] and Lee et al.[18]. Then, the transverse shear deformations due to matrix cracks can be neglected. A trigonometric stress field for the normal direction of the crack surface and a linear one in the plane of the crack are assumed. Then, the plane-stress effective stiffness matrix for $[0_q^o / 90_r^o]_s$ can be written as:

$$[\hat{Q}] = \frac{1}{(q+r)} \begin{bmatrix} q\bar{Q}_{11} + r(1-h_2)\bar{Q}_{22} & (r+q(1-h_1))\bar{Q}_{12} \\ (q+r(1-h_2))\bar{Q}_{12} & r(1-h_{12})\bar{Q}_{11} + q\bar{Q}_{22} \end{bmatrix} \quad (10)$$

where, η_i are functions of the crack density. In fact if the 0^o -plies are assumed to remain undamaged, which is true to great extent for crossply laminate, and neglecting the effect of the adjacent plies (i.e. $h_{12} = 0$), then for the (2r) 90^o -plies laminate Eq.(10) reduces to:

$$[\hat{Q}] = \begin{bmatrix} (1-h_2)\bar{Q}_{22} & \bar{Q}_{12} \\ (1-h_2)\bar{Q}_{12} & \bar{Q}_{11} \end{bmatrix} \quad (11)$$

where,

$$1/h_2 = 1 + m\{\mu^4/64I - 1\} \quad (12)$$

where, μ is a function of the lamina Poisson's ratios, and is given by:

$$m = (1 - n_{12}^2) / (1 - n_{22} - 2n_{12}^2)(1 + n_{22}) \quad (13)$$

and,

$$I = \sum_{m,n=1}^{\infty} 1 / \{ (2m-1)^2 (2n-1)^2 + (2n-1)^4 \frac{G_{12}(a/t)^2}{mE_{22}} \} \quad (14)$$

where, (2a) is the crack spacing, and (2t) is the crack length.

GOVERNING EQUATIONS

For the laminated composite plate with geometry and coordinate system shown in Fig.(2), we present the governing equations based on first order shear deformation theory (FSDT). Each lamina is treated as a Mindlin plate. Hence, the inplane displacements (u_a) are assumed linear and the transverse displacement (u_3) is constant across the thickness. In the expressions given below, the tensor notation are used unless it is otherwise indicated.

(a) Equations of motion in terms of stresses:

For linear small deformation theory and in the absence of body forces, the equations of motion in terms of stresses are given by:

$$S_{ij,j} = \rho_0 \ddot{u}_i \quad (15)$$

where, ρ_0 is the mass density and the superimposed dots indicate derivatives with respect to time (t).

(b) The displacement field:

For the first order shear deformation theory, the inplane displacement field can be written as:

$$u_a(x_i, t) = \bar{u}_a(x_b, t) + x_3 f_a(x_b, t) \tag{16}$$

and the transverse displacement is given by:

$$u_3(x_i, t) = u_3(x_b, t) \tag{17}$$

(c) The kinematic relations:

The components of the Euler strain tensor are related to the plate displacements through,

$$\left. \begin{aligned} e_{ab} &\equiv u_{(a,b)} = \bar{u}_{(a,b)} + x_3 f_{(a,b)} \\ e_{a3} &\equiv \frac{1}{2}(u_{a,3} + u_{3,a}) = \frac{1}{2}(f_a + u_{3,a}) \\ e_{33} &= u_{3,3} = 0 \end{aligned} \right\} \tag{18}$$

(d) The constitutive equations:

The inplane force and moment resultants are related to the plate strains and curvatures through the constitutive equations given by:

$$\begin{Bmatrix} N \\ M \end{Bmatrix} = \begin{bmatrix} A & B \\ B & D \end{bmatrix} \begin{Bmatrix} e \\ c \end{Bmatrix} \tag{19}$$

In the above expressions, the following terms are defined,

$$\{N_{ab}, M_{ab}\} = \int_{-h/2}^{h/2} \{1, x_3\} S_{ab} dx_3$$

and

$$\{A_{ij}, B_{ij}, D_{ij}\} = \int_{-h/2}^{h/2} \{1, x_3, x_3^2\} \bar{Q}_{ij} dx_3$$

where, \bar{Q}_{ij} are the conventional stiffness coefficients of the laminated plate (i,j=1,2,6) and h is the laminate thickness.

$$A_{ij} = \int_{-h/2}^{h/2} \bar{Q}_{ij} dx_3 \quad i,j=4,5$$

$$C_{ab} = \frac{1}{2}(f_{a,b} + f_{b,a})$$

(e) Transverse shear deformation

Since the focus is on the global dynamic behavior of laminated composite plates, therefore, it is reasonable to seek a solution scheme which is based on first-order-shear deformation theory (FSDT), as noted by Hong [19]. It has been concluded that the use FSDT requires a shear correction factor (k) with different values and evaluation methods. Generally, the values of the factor (k) have been derived for the analysis of homogeneous isotropic plates, and they have been used without rigorous investigation for the analysis of laminated composite plates. But recently, Hong [19] derived "a consistent shear deformation theory" or (CSDT) for the analysis of laminated composite plates. Hong's approach is based on discrete laminate theory, which adds another advantage, since the matrix cracks are generally developed in some of the layers and not in all of them in a given laminate.

The theoretical basis for the development of CSDT is a generalization of Reissner's variational mixed principle of linear elastic orthotropic plates to the case of laminated composites.

By separating the inplane equilibrium equations from the transverse ones, and ignoring the inertia terms, for the kth layer, Eqns.(15) can be written as:

$$S_{ab,b}^{(k)} + S_{a3,3}^{(k)} = 0 \tag{20}$$

$$S_{3a,a}^{(k)} + S_{33,3}^{(k)} = 0 \tag{21}$$

The inplane stresses which satisfy the static equilibrium equations are assumed linear function of the normal coordinate (x_3^k), then:

$$S_{ab}^k = A_{ab}^k + B_{ab}^k x_3^k \tag{22}$$

where, A_{ab}^k and B_{ab}^k are independent of (x_3^k).

By using the definition of the force resultants and neglecting the body forces and surface tractions, with some calculus and algebraic manipulation, the transverse shear constitutive relations are written as[19]:

$$Q_a^k = \sum_{i=1}^n C_{ab}^{ki} (j_b^i + u_{3,b}^i) \tag{23}$$

where, C_{ab}^{ki} are the coefficients of a symmetric matrix defined by the material properties, thickness of layers and the stacking sequence of a laminate.

Equations (23) represent the shear constitutive equations without the need for a shear correction factor. It also indicates that the shear force in a layer is a linear combination of the transverse shear strains of all the other layers for a given laminate.

(f) The Boundary Conditions

A set of consistent boundary conditions associated with the governing equations are given by:

$$\left. \begin{aligned}
 \bar{u}_n &= \hat{\mathcal{S}}_n & \text{or,} & & N_n &= \hat{N}_n \\
 \bar{u}_s &= \hat{\mathcal{S}}_s & \text{or,} & & N_{ns} &= \hat{N}_{ns} \\
 \hat{f}_n &= \hat{\mathcal{F}}_n & \text{or,} & & M_n &= \hat{M}_n \\
 \hat{f}_s &= \hat{\mathcal{F}}_s & \text{or,} & & M_s &= \hat{M}_{ns} \\
 u_3 &= \hat{\mathcal{S}}_3 & \text{or,} & & Q_n &= \hat{\mathcal{Q}}_3
 \end{aligned} \right\} \quad (24)$$

where, n and s refer to the normal and tangential directions at an edge respectively, and the quantities with “hat” represent a specified quantity at the boundary.

These boundary conditions given by Eqn.(24) can be written explicitly for the well-known edge conditions as follows:

(i) Simply supported edge

$$N_n = N_{ns} = M_n = \hat{f}_s = u_3 = 0 \quad (25)$$

(ii) Clamped edge

$$\bar{u}_n = \bar{u}_s = \hat{f}_n = \hat{f}_s = u_3 = 0 \quad (26)$$

(iii) Free edge

$$N_n = N_{ns} = M_n = M_{ns} = Q_n = 0 \quad (27)$$

(g) The continuity Conditions

The domain of the problem consists of two regions, the damaged and undamaged zones. However, the plate is assumed to be intact and its integrity is well-maintained. Hence, it is essential to enforce the continuity conditions at the common boundary of the two zones. The general form of these continuity conditions can be written as:

$$\left\{ \begin{array}{l} \bar{u}_i \\ \hat{f}_a \\ M_{ab} \\ N_a \\ Q_a \end{array} \right\} \text{ at the outer boundary of the damaged zone} = \left\{ \begin{array}{l} \bar{u}_i \\ \hat{f}_a \\ M_{ab} \\ N_a \\ Q_a \end{array} \right\} \text{ at the inner boundary of the undamaged zone} \quad (28)$$

When considering the continuity conditions, it must be understood that in general not all the conditions given by Eqn.(28) can be satisfied simultaneously. This usually depends on the geometry and the approximate solution technique used. For instance, in displacement-based finite element solutions only the continuity of displacements and slopes can be enforced. While, for stress-based solutions, only the continuity of the internal force resultants can be achieved.

SOLUTION PROCEDURE

Since our main focus is on the dynamical aspect, the energy formulation of the problem should take into account the time dependent applied forces and geometrical constraints. The extension of the principles of virtual work, which are limited to the static equilibrium, to the

time domain yields the well-known Hamilton's Principle for dynamical problems. For conservative systems, i.e. the sum of the potential and kinetic energies is conserved, the Hamilton's Principle can be written as follows:

$$d \int_{t_1}^{t_2} L dt = 0 \tag{29}$$

where, L is called the Lagrangian function and is given by:

$$L = T - \Pi \tag{30}$$

For a body with a volume V and if the mass density is independent of time, then the kinetic energy T is given by,

$$T = \frac{1}{2} \int_V \rho_0 u_i u_i dV \tag{31}$$

And in the absence of body forces and surface tractions, the total potential energy is the same as the strain energy in this case and can be written as,

$$\Pi = \frac{1}{2} \int_V s_{ij} e_{ij} dV \tag{32}$$

In general, the governing differential equation resulting from the minimization of the total energy functional given by Eqn.(30) is complicated with no exact solution except for a very limited class of problems after ignoring many effects like for instance the transverse shear deformation. Hence, it becomes necessary to seek approximate solutions for such class of problems. In the area of vibration of plates two approximate numerical techniques are widely used which are the finite element method and the Ritz method. In the Ritz method, it is relatively difficult to enforce the continuity conditions on the outer boundaries of the damaged zone since these conditions have to be part of the governing equations. Also, for some shapes of the damaged zone points of singularities might occur. On the other hand, the finite element method is much easier to satisfy the continuity conditions for any shape of the damaged zone. Hence, in this work the finite element method is used.

For the free vibration analysis and neglecting the effect of damping, the governing equations can be written as:

$$[M]\{\ddot{U}\} + [K]\{U\} = 0 \tag{33}$$

Assuming harmonic motion of the system into which the solution can be written as:

$$U(x_i, t) = u(x_i) e^{i\omega t} \tag{34}$$

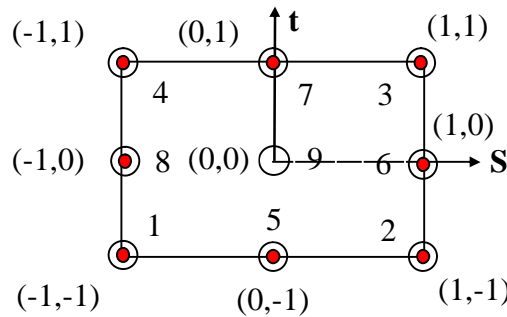
Equations (33) and (34) yield the generalized eigenvalue problem given as:

$$[K - \omega^2 M]\{u\} = 0 \tag{35}$$

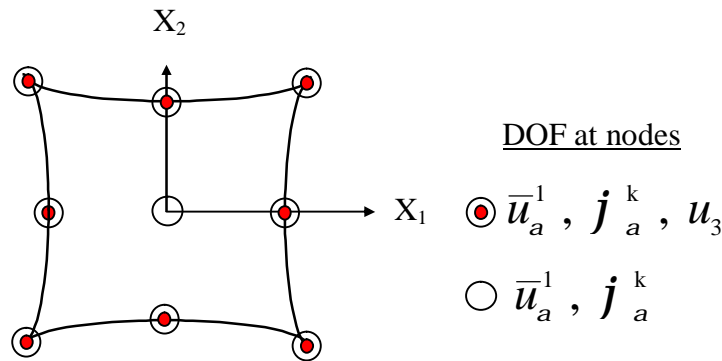
where M and K are mass and stiffness matrices resulting from Eqns.(31) and (32) respectively, (ω) is the frequency parameter and {u} is the amplitude vector.

The finite element formulation is based on the use of "Heterosis Element" which is a 9-node quadrilateral that uses serendipity shape functions for the transverse displacements and Lagrange shape function for the rotational degrees of freedom. Also, a selective/ reduced integration scheme is used to evaluate the element stiffness. The local and global coordinate systems as well as element degrees of freedom are depicted in Fig.(3). For initial value problems, the first variation of the Lagrangian, i.e. Hamilton's principle, of the energy

expression gives the variational form of the equations of motion of the laminated plate. The solution of the eigen-value system is a standard mathematical problem which yields the vibration frequencies and mode shapes. For this purpose, a finite element code that was originally developed by Hong [19] was modified to accommodate vibration and damage modeling.



(a) local



(b) global

Fig. 3: Local and global coordinate systems and DOF for "Heterosis" element

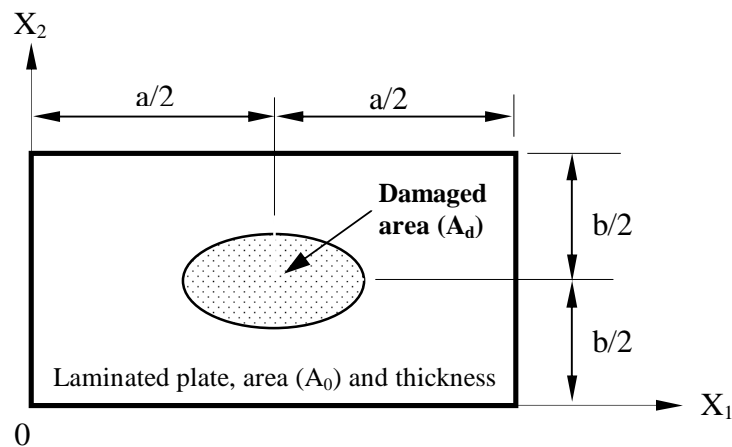


Fig. 4: Plate geometry global coordinate system and the location of damage (edges are either clamped or simply supported).

RESULTS AND DISCUSSION

Elastic constants

Equations (11) through (14) form the basis for the calculation of the change in the axial stiffness, measured by the ratio of the modified axial stiffness (E_{11}) and the original value (E_{11}^0). Similarly, the change in the inplane Poisson's ratio is measured by the ratio of the modified value (n_{11}) and the original value (n_{11}^0). The values shown in Table(1) reflect these changes for a symmetric crossply laminate with different crack density. Comparison of the normalized axial stiffness at 46 cracks per in. with the experimental investigation [20] and analytical model [12] as depicted in Table (2) shows the conformability of the present results with both.

Table 1: Changes in E_{11}^0 and n_{11} due matrix cracking in the 90°-plies of $[0^\circ/90^\circ]_s$ laminate.

N*	λ	ζ_2	E_{11}/E_{11}^0	n_{11}/n_{11}^0
0	0	0	1	1.0
10	0.0899	0.034	0.9979	0.9440
20	0.2550	0.1014	0.99377	0.8969
30	0.4182	0.1752	0.98923	0.8595
40	0.5648	0.2485	0.98463	0.8510

*N=number of cracks per in.

Table 2: Comparison of normalized axial stiffness(E_{11}/E_{11}^0) due to cracks in the 90°-plies.

Laminate	N*	Experm.[20]	Analytical [12]	Present
$[0^\circ/90^\circ]_s$	46	0.969	0.962	0.975
$[0_2^\circ/90_2^\circ]_s$	46	0.958	0.953	0.960

*N=number of cracks per in.

Vibration frequencies

The effect of transverse shear deformation on the frequency response is investigated for sandwich square plate with a known elasticity solution [21]. The plate geometry is depicted in and elastic constants are given in Table (3). For the sake of comparing current results with those in literature, a frequency parameter $\{\Omega = w \sqrt{rh^2 / E_{11}^{(2)}}\}$ is used. Which is expressed in terms of the vibration frequency (ω), plate density (ρ), thickness (h) and Young's modulus in the secondary material direction ($E_{11}^{(2)}$). The effect of the thickness aspect ratio (h/a) on vibration frequencies (first and second modes) is depicted in Table (4). The variation of the fundamental frequency mode with the degree of orthotropy of the composite laminate represented by ($E_{11}^{(1)} / E_{11}^{(2)}$) is shown in Table (5). These results serve as batch test for the

finite element code. Using only 16 elements the deviation from the exact value of the fundamental frequency is 8.31% compared to 76.52% for the thin plate theory for a very thick plate ($h/a = 0.5$). It is worthy to note that the classical plate theory erroneously predicts vibration frequencies of thick plate due to neglecting the influence of shear deformation (Srinivas and Rao [21]). The results also confirm the fact that the thin plate theory overestimates the vibration frequencies and that the error increases rapidly for larger values of the thickness aspect ratio and/or degree of orthotropy.

Table 3: Material properties using local coordinate system as a reference, [21]

E_{11}	18.5×10^6 psi
E_{22}	10×10^6 psi
ν_{12}	0.23
G_{12}	4.86×10^6 psi
ρ_k	0.055 lb/in ³

Table 4: Effect of (h/a) on the frequency parameter (Ω)* for a square simply supported specially orthotropic plate

h/a	First mode			Second mode	
	Exact [21]	Thin Plate [21]	FEM	Exact [19]	FEM
0.1	0.04742	0.04967 (4.74) [†]	0.047656 (0.5)	0.21697	0.22244 (2.52) [†]
0.3	0.33200	0.44699 (34.64)	0.352584 (6.2)	0.65043	0.71053 (9.24)
0.5	0.70338	1.24160 (76.52)	0.771831 (8.31)	1.08240	1.21683 (12.42)

$$*\Omega = (w \sqrt{rh^2 / E_{11}^{(2)}})$$

[†] % error from the exact values

Table 5: Effect of ($E_{11}^{(1)} / E_{11}^{(2)}$) on the frequency parameter (Ω) for a square simply supported specially orthotropic plate (First mode)

$E_{11}^{(1)} / E_{11}^{(2)}$	Exact [21]	Thin Plate [21]	FEM
1	0.04742	0.04967 (4.74) [†]	0.047656 (0.5)
5	0.077148	0.08533 (10.61)	0.078267 (1.45)
15	0.70338	0.13899 (24.06)	0.114835 (2.51)

[†] % error from the exact values

Comparison of the first and second free vibration modes of two Graphite-Epoxy[AS4/3501-6] plates without damage and with stacking sequence of $[\pm 18^\circ/90^\circ]_S$ with the experimental work [20] shows good agreement, as shown in Table (6). For the same test specimens, Table (7) shows that the present finite element results compare reasonably well with those of ABAQUS, [22]. These numerical results and the presented specific examples illustrate that the proposed procedure as well as the finite element implementation can accurately predict the vibration

frequencies for undamaged composite laminates. Next, we use the preceding damage mechanics model to investigate some typical composite plates with various boundary conditions.

The effect of the size and shape of damage area on the frequency response of simply supported crossply laminated square plates were investigated. The plate geometry, coordinates and the location of damage is shown in Fig.(4). Three different shapes the D-zone having the same area were considered; rectangular, elliptical and circular. For a damage level of 40 cracks per in. in the 90°-plies, there is no significant difference in the vibration frequency between the three shapes as shown in Table (8) and graphically in Fig.(5). Hence, the results presented hereafter are for rectangular damage zones which is easier to handle in regards to data input and mesh generation. The size of damage is measured as the percentage of the D-zone with respect to the total area of the plate. Figure (6) shows the variation of the first five frequency modes of a simply supported crossply laminate with the percentage of damage. The graph reflects a decrease in the fundamental frequency of about 5% when 50% of 90°-plies are saturated with 40 cracks per inch. It also shows that this effect becomes more pronounced for higher vibration modes.

Using the material properties in Table (9), the frequency parameters were investigated for three composite laminates with different boundary conditions with and without damage. Centrally located damage zone which represents 30% of the total plate area is considered for all cases. In the damaged zone the 90°-plies are saturated with 40 cracks per inch. Tables (10) and (11) show the lowest five frequency parameters for specially orthotropic simply supported and clamped plates, respectively. The results for the undamaged plates show very good agreement with the exact and other numerical solutions. The results indicate a reduction in the vibration frequencies up to 10% in the 5th mode due to damage. The first (4) mode shapes for undamaged and damaged clamped crossply plates are depicted in Fig.(7), which shows no significant change due to matrix cracking in the 90°-plies. Table (12) presents the frequencies for graphite-epoxy 8-angle-ply [0₂/±30] _s cantilever plate. The predicted frequencies for the undamaged plate compare reasonably well with the experimental investigation [24].

CONCLUDING REMARKS

The current investigation present an analysis for the free vibration response of moderately thick laminated composite plates containing matrix cracks type of damage. The damage mechanics approach was used for the modeling of these cracks in the global macro level of analysis. The analysis shows that this approach can be very effective tool to predict the global dynamic response of damaged plates. This study has incorporated the effect of shear deformation in a consistent manner into a finite element solution algorithm. The presented results for different plate boundary conditions show that the matrix cracks type of damage reduces the vibration frequencies. This reduction is more pronounced for higher frequency modes. Moreover, the study show that for the same damage level, the shape of the damaged zone has a very little influence on the frequency response.

With more investigations on the same track, we believe that it should be possible to use the change in the frequency as a measure to develop a suitable non-destructive evaluation technique for monitoring the integrity of laminated composite structural components.

Table 6: Comparison of Finite Element results with experimental work, [20].

Case	Stacking Sequence	Dimensions (in)	FE (ω_1) (hz)	Exp. (ω_1) (hz)	FE (ω_2) (hz)	Exp. (ω_2) (hz)
1	[±18 3/90 6] _s	6x6	589.657	588	1168.576	1180
2	[±18 5/90 10] _s	10x10	353.789	343	700.983	790

Table (7): Comparison of Finite Element results with ABAQUS, [22].

Case	Stacking Sequence	Dimensions (in)	FE (ω_1) (hz)	Abaqus (ω_1) (hz)	FE (ω_2) (hz)	Abaqus (ω_2) (hz)
1	$[\pm 18 \ 3/90 \ 6]_s$	6x6	589.657	588.345	1168.576	1167.974
2	$[\pm 18 \ 5/90 \ 10]_s$	10x10	353.789	372.015	700.983	722.732

Table 8: Effect of the damaged zone shape on the fundamental frequency of crossply laminate.

$\% \frac{A_d}{A_0}$	Normalized frequencies for damage at the center of the plate (area A_0), the damage area (A_d) with the shape of:		
	Rectangular	Circular	Elliptical
0	1	1	1
10	0.9948	0.9932	0.994
20	0.988	0.9851	0.9869
30	0.9772	0.9735	0.9753
40	0.964	0.9609	0.9628
50	0.9512	0.946	0.9491

Table 9: Material properties using local coordinate system as a reference, [23].

E_{11}	18.5×10^6 psi
E_{22}	1.6×10^6 psi
ν_{12}	0.25
G_{12}	0.65×10^6 psi
ρ_k	0.055 lb/in ³
t_k	0.0052 in

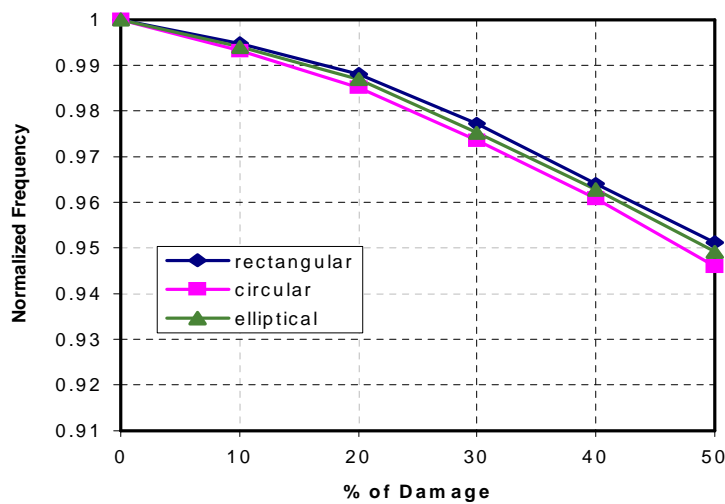


Fig. 5: Effect of the damaged zone shape on the fundamental frequency of crossply laminate

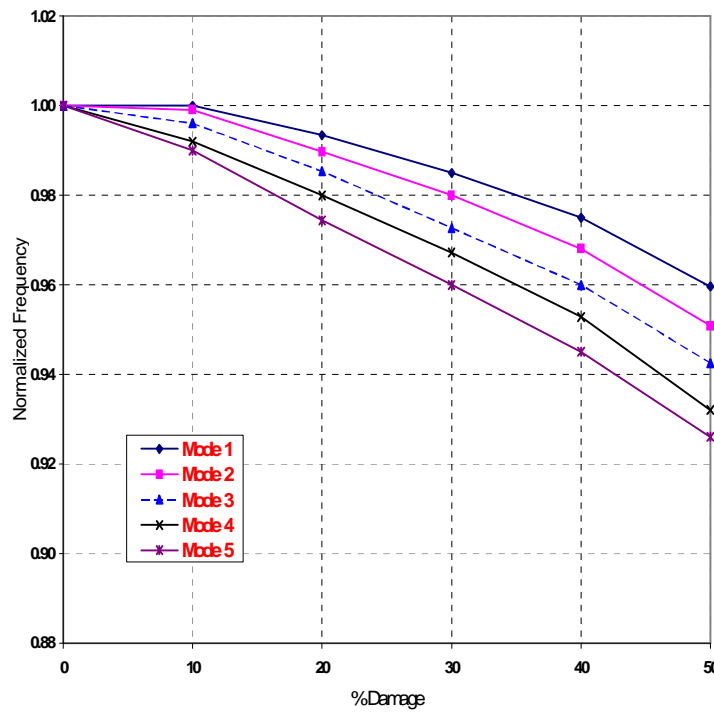


Fig. 6: Effect of the damage size on the first five frequencies of crossply laminate

Table 10: Frequency parameter ($\bar{\Omega}$)* for a square simply supported orthotropic plate.

Mode	Exact	FEM undamaged	FEM damaged**
1	3.60555	3.60555	3.54782
2	5.83095	5.83104	5.69226
3	10.4403	10.4416	10.0667
4	13.0000	13.0024	12.2352
5	14.4220	14.4229	13.1825

* $\bar{\Omega} = (w a^2 \sqrt{r / D_{22}}) / p^2$

** 30% at the center of the plate

Table 11: Frequency parameter ($\bar{\Omega}$) for a square orthotropic clamped plate.

Mode	Ritz Method[23]	FEM undamaged	FEM damaged*
1	7.719	7.712	7.433
2	10.100	10.095	9.584
3	15.060	14.873	14.091
4	20.180	20.412	18.951
5	21.740	22.475	20.165

* 30% at the center of the plate

Table 12: Frequencies (hz) of a cantilever 8-ply graphite-epoxy 6x3 in. $[0_2/\pm 30]_s$ plate

Mode	Experiment[24]	FEM undamaged	FEM damaged*
1	58.3	64.235	56.326
2	148	136.546	131.443
3	362.7	407.204	392.065
4	508	525.557	515.128
5	546	587.025	566.982

* 30% at the center of the plate

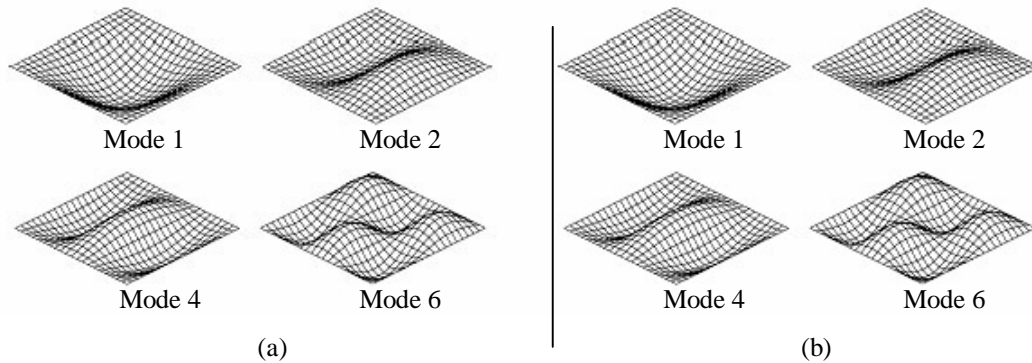


Fig. 7: Mode shapes for clamped crossply laminated plate: (a) undamaged; (b) damaged.

REFERENCES

1. Emam, Aly "One-dimensional hermit polynomials finite element model for predicting interlaminar stress fields in laminated composites," 10th Annual International Conference on Composites/Nano Engineering, New Orleans, Louisiana, USA, July 20-26, 2003.
2. Gibson, R.F. "Recent research on dynamic mechanical properties of fiber reinforced composite materials and structures", The Shock and Vibration Digest, Vol. 15, No.2, pp.3-15, 1983.
3. Rajaiiah, K. and Rao, M.R. " Damage assessment in composites through NDE: Some recent studies in India," Theor. and Applied Fracture Mech., Vol. 13, pp.125-135, 1990.
4. Grady, J.E. and Meyn, E.H. "Vibration testing of impact damaged composite laminates, 30th Structures, Struct. Dynamics & Materials Conference, pp.2186-93, April 3-5, 1989.
5. Sun, C.T., Sankar, B.V. and Tan, T.M."Dynamic response of SMC to impact of a steel ball, " Advances in Aerospace Structures & Materials, AD-01, pp. 99-107, 1981.
6. Chaturvedi, S.K. and Sierakowski, R.L. "Residual strength assessment of SMC subject to dynamic impact, Composite Structures, Vol.3, pp. 137-162, 1983.
7. Chaturvedi, S.K. and Zayyad, N.A. "Free vibration of impact damaged short-fiber composite plates," Achievement in Composites in Japan and United States, Proc. Japan-U.S. CCM-V, Tokyo, pp. 671-78, 1990.
8. Abrate, S." Impact on laminated composite materials," Applied Mech. Rev., Vol.44, No.4, pp.155-87,1991.
9. Cantwell, W.J. and Morton, J. "The impact resistance of composite materials -- a review," Composites, Vo.22, No.5, pp.347-62, 1991.
10. Allen, D.H., Groves, S.E. and Harris, C.E. "A cumulative damage model for continuous fiber composite laminate matrix cracking and interply delaminations," Composite Materials Testing & Design, ASME STP-972, pp.57-80, 1987.
11. Harris, C.E., Allen, D.H. and Nottorf, E.W. " Damage-induced changes in the Poisson's ratio of cross-ply laminates," Winter Meeting, Damage Mechanics in Composites, pp.17-23, Dec. 1987.

12. Harris, C.E., Allen, D.H., Nottorf, E.G. and Groves, S.E. "Modeling stiffness loss in quasi-isotropic laminates: application of a continuum damage mechanics model for laminated composites," ASME Microstructural damage, J.of Enging. Materials and Technology, Vol.110, pp.128-132, April 1988.
13. Groves, S.E., Harris, C.E., Allen, D.H. and Norvell, R.G. "An experimental and analytical treatment of matrix cracking in crossply laminates," Experimental Mechanics, pp.73-9, March 1987.
14. Chaturvedi, S.K. and Emam, A." Effect of matrix cracks on the free vibration of laminated composite plate," proceedings of the 7th International Colloquium on Structural and Geotechnical Engineering, Ain-Shams Univ., Egypt, Dec. 1996.
15. Groves, S.E."A study of damage mechanics in continuous fiber composite laminates with matrix cracking and internal delaminations," PhD dissertation, University of Texas A&M, 1986.
16. Krajcinovic, D. "Continuum damage mechanics," Applied Mechanics Reviews, Vol.37, pp.1-6, Jan.1984.
17. Allen, D.H., Nottorf, E.W. and Harris, C.E."Effect of microstructural damage on ply stresses in laminated composites," Recent advances in Macro- and Micro-Mechanics of Composite Matl. Struct., AD-Vol.13, ASME 1988.
18. Lee, J.W. and Allen, D.H. "Internal state variable approach for predicting stiffness reductions in fibrous laminated composites with matrix cracks," J. of Composite Materials, Vol.23, pp.1273-91, Dec.1989.
19. Hong, S.J. " A consistent shear deformable theory for the vibration of laminated plates," PhD. Dissertation, The Ohio State University, 1988.
20. Duggan, M.B. and Ochoa, O.O. "Natural frequency behavior of damaged composite materials," J. of Sound and Vibration," Vol.158, No.3, pp.545-51, 1992.
21. Srinivas, S. and Rao, A.K. "Bending, vibration and buckling of simply supported thick orthotropic rectangular plates and laminates." Intl. J. of Solids & Structures, Vol.6, pp.1463-81, 1970.
22. Hibbitt, H.D., Karlson, B.I. and Sorenson, E.P. 2006. ABAQUS, version 6.5, Finite Element Program. Providence, R.I., USA: Hibbitt, Karlson & Sorenson, Inc.
23. Baharlou, B. " Vibration and buckling of laminated composite plates with arbitrary boundary conditions," PhD Dissertation, The Ohio State University, 1985.
24. Crawley, E.F." The natural modes of graphite/epoxy cantilever plates and shells", J. Composite Materials, Vol. 13, No.3, July 1979.

NUMERICAL MODEL TO PREDICT THE SETTLEMENT RESPONSE OF TWO NEARBY FOUNDATIONS DUE TO GEOTEXTILE SLIPPAGE

*AQEEL SH. AI-ADILI

Assistant Prof., University of Technology, Department of Building and Construction Engineering, Baghdad , IRAQ. Tel. +9647901766126, E-mail; aqeeladili@hotmail.com

ABSTRACT:

In this paper, a numerical study is undertaken to investigate the settlement response of two dependent flexible loads resting on a reinforced granular bed underlain by a soft soil, considering the plain strain loading conditions. The finite element code PLAXIS-8 has been used. The granular fill, soft soil and geosynthetic reinforcements are considered as linear elastic materials. The geosynthetic reinforcement is modeled with interface elements for allowing slip between the soil and reinforcement. When no interface elements were used, the geosynthetic reinforcement was modeled as if there is no slip. It appears that allowing slip has a negligible effect on the settlement predicted.

The results obtained from the present investigation showed that as the number of reinforcement layers increase up to three layers, the vertical stresses in the loaded region decreases causing maximum settlement reduction at a decreasing rate of 16% and 20% for 3-layers without and with slippage respectively. Parametric study has been carried out to bring out the effect of slippage of the reinforcement layer on the settlement response in dry and saturated soils. The increase in the settlement is not significant when the slippage of the reinforcement is considered. An interesting conclusion in this study, for both one and three layers of geotextile, one particular load induces about 10% more settlement than in case of two adjacent loads.

Key words: Geosynthetic reinforcements, dependence foundations , PLAXIS, multi layer, interface slippage.

INTRODUCTION

Reinforced granular beds with single or multiple layers of geosynthetics are very common in use over soft soil beds to increase the overall load bearing capacity of soft soils and improve their settlement performances. The lumped parameter modeling is very often adopted to analyze such problems due to its simplicity. Most of the studies reported in the literature are only with single layer of geosynthetics (7),(2),(10),(11), but, recently some work in the area with multi layer of reinforcements has also been reported (8),(3) using lumped parameter modeling. Some studies on single layer reinforced system with finite element modeling to solve such problems are also reported in the literature (6),(9),(10). Though some qualitative comparison with respect to the settlement profile obtained with these two methods could be made, there is always a need for quantitative comparison.

Improvement of soft soils with geosynthetics (Geogrid) is becoming increasingly common practice in the construction industry. The soil reinforcement method is well established and suited for a wide range of soils. The design methods for geosynthetics are mainly semi-empirical.

* Corresponding author
Received Date:10/2/08
Acceptance Date:13/7/08

Deb et al., (2007)(4) reported the results of a numerical study conducted for multi layer geosynthetic-reinforced granular fill on soft soil and compared the finite element study and lumped parameter modeling results. It was assumed there was no slip between the reinforcement and the granular soil. However, most of the researches reported in the literature are limited to single loads with no interferences from any adjacent ones. Nevertheless, in reality, there are situations where there is interference of the influence zones of two adjacent loaded areas

In the present study the slippage between the reinforcement and the granular layer is considered and its effect on the settlement response is investigated. Moreover, the second aim of this paper is to investigate the effect of interaction of dependant loads on settlements in case of soil reinforcement in saturated and dry conditions.

STATEMENT OF THE PROBLEM

Figure-1 shows a two meter thick granular fill reinforced with geosynthetic layers placed over a 12 m thick soft soil underlain by a very stiff layer, such as hard bedrock. The number of reinforcement layers is varied from one to three enmeshed within the sand bed such that it is equally divided. Two different footing loads of nonuniform intensities q_1 and q_2 are applied over a width of foundation ($B=4\text{m}$ and 6m) on the reinforced granular fill and the reinforcements are chosen to be extending beyond the edge of the footing on both sides, by a distance equal to twice of footing width.

In this study there are three problems analyzed; in problem 1 only a single layer of reinforcement is considered with the water table (level) being present at 3m below the ground surface . In problem-2, three layers of reinforcement are taken with the water table being present. Aat 3m depth as in problem--1 . In problem-3, one and three layers of reinforcement are considered and the fill is taken to be dry

The main objectives of the present study are to predict the settlement of two adjacent interfering foundations and the bending moments along the footing using PLAXIS. The results when slip of the reinforcement is considered are compared with the results when the slip is not considered for 1-layer (problem-1) and 3-layers (problem-3) of reinforcement for an assessment of the difference in the response due to slippage, as well as , the effect of phreatic surface on the settlement behavior of the reinforced soil is assessed.

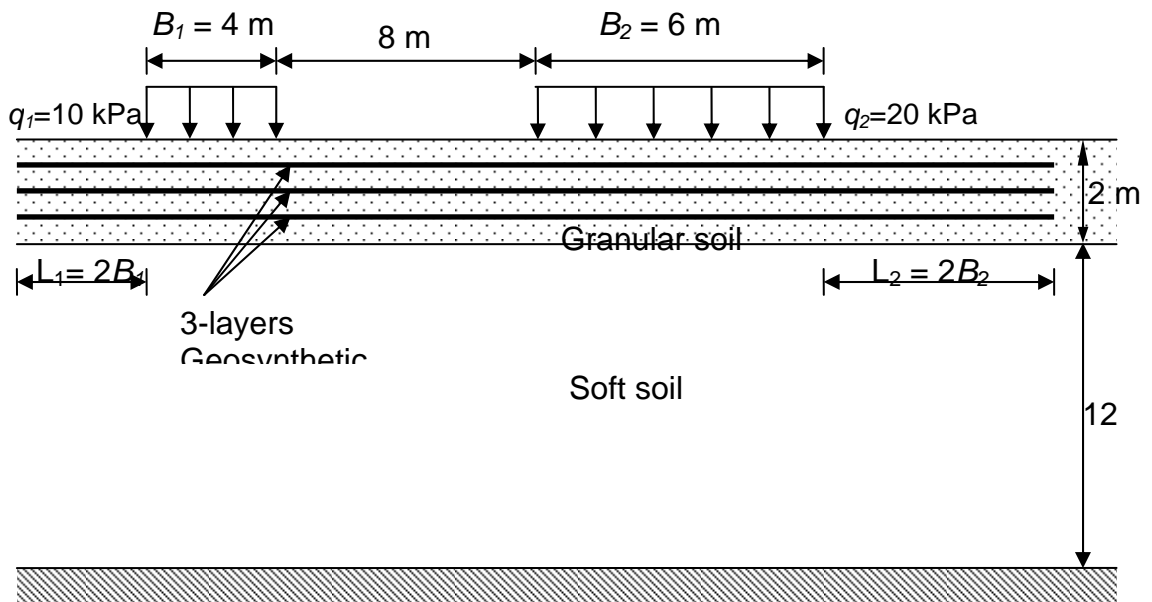


Fig. 1: Multi layer geosynthetic-reinforced granular fill over soft soil

NUMERICAL MODELING

The numerical approach used in this research is the 2-D finite element special purpose computer package PLAXIS-8 (1) to determine the settlements of surface soils with and without slippage (interface) of the geosynthetic reinforcement and the bending moment distribution. To minimize the boundary effect, the vertical boundary at the far ends, on both sides is set as 2B away from the end of each loading ; the boundary is assumed to be free in the vertical direction and restricted in horizontal direction. The bottom horizontal boundary is restricted in both the vertical and horizontal directions against displacements.

The analysis is based on plane strain with Mohr Coulomb material model to simulate the behavior of soil and continua, with drained conditions for problems-1 and 2, to simulate the soil conditions and to assess the settlements, as well as , the elastic plastic deformation, not taking the decay of excess pore pressures with time into account.

Furthermore, ground water flow in this porous medium could be described by Darcy’s law, considering steady flow in applying models on soil strata. Also, the interface elements are treated specially in ground water calculations in PLAXIS Ver-8. When the element is activated there is full coupling of the pore pressure degrees of freedom.

Three different materials are involved in the analysis: soft soil, granular fill, and geosynthetic reinforcements. However, all the materials are assumed to be non linear. For simplification, creep of geosynthetic reinforcements is not considered while allowing for slippage at the interface between geotextile and soil.

Realistic values of different parameters representing the physical properties of the materials used in the analysis are chosen based on previous studies (10),(12),(4) and are presented in Table-1. In the present study high Poisson ratio values of the soft soil and granular fill have been chosen ($\mu = 0.45$) to simulate the undrained condition in problem-3.

The discretization of the medium for modeling is shown in Figures 2, 3 and 4 for the problems. A convergence study was done on Problem-1 for the particular value of the loads intensity ($q_1=10$ and $q_2=20$ kN/m²) and the results are presented in Table-2. As the results for coarse mesh are not significantly different from the results obtained for fine meshes, it was decided to adopt coarse meshes for all three cases considered in this study.

Table 1: Physical properties of soil and geosynthetics

Material	Parameters
Soft soil	$E_s = 800$ kPa, $\mu_s = 0.3$
Granular bed	$E_{gb} = 10$ MPa, $\mu_{gb} = 0.33$
Geosynthetic layers	$E_g =$ varies, $\mu_g = 0.49$, $L = 4$ m

Note: L = half length of the geosynthetic layers E_s = Elastic modulus of soft soil; μ_s = Poisson’s ratio of the soft soil; E_{gb} = Elastic modulus of granular fill; μ_{gb} = Poisson’s ratio of the granular fill; E_g = Elastic modulus of geosynthetic layer; μ_g = Poisson’s ratio of the geosynthetic layers .

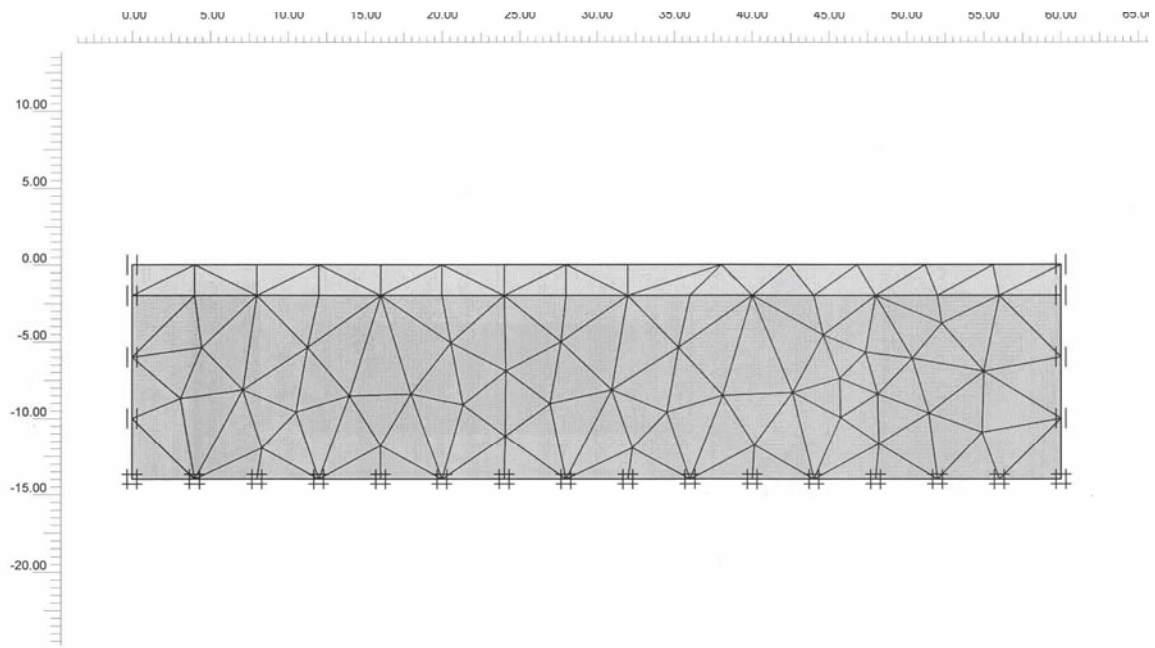


Fig. 2 Discretization of two loads only

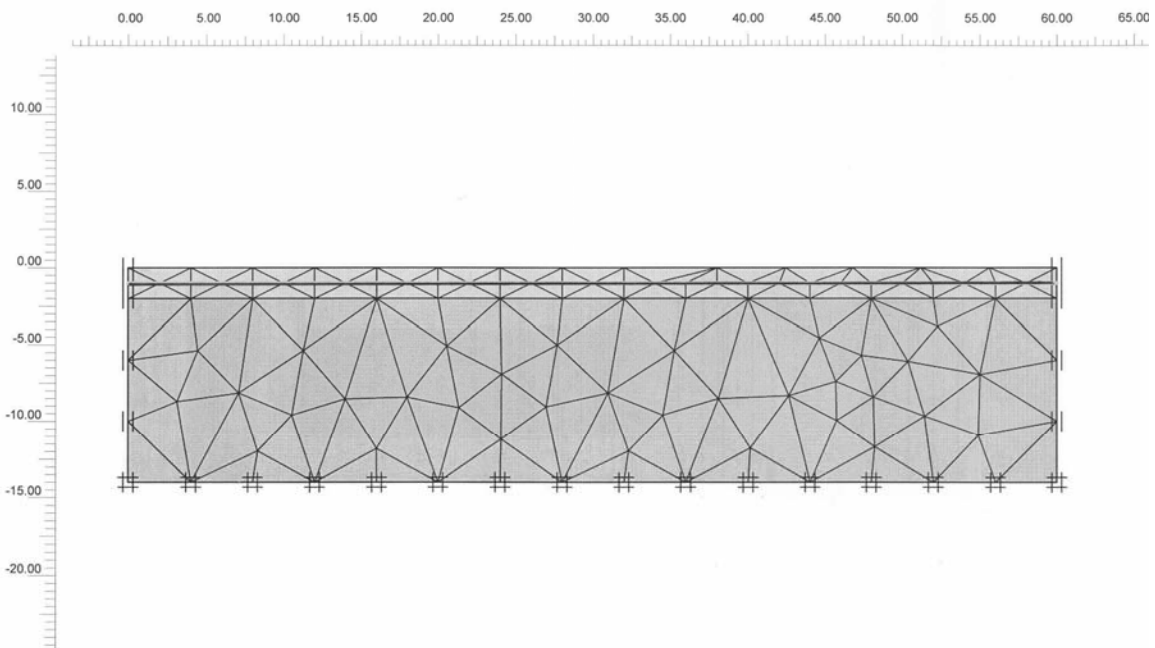


Fig. 3: Discretization of one-Layer geotextile (Problem-1).

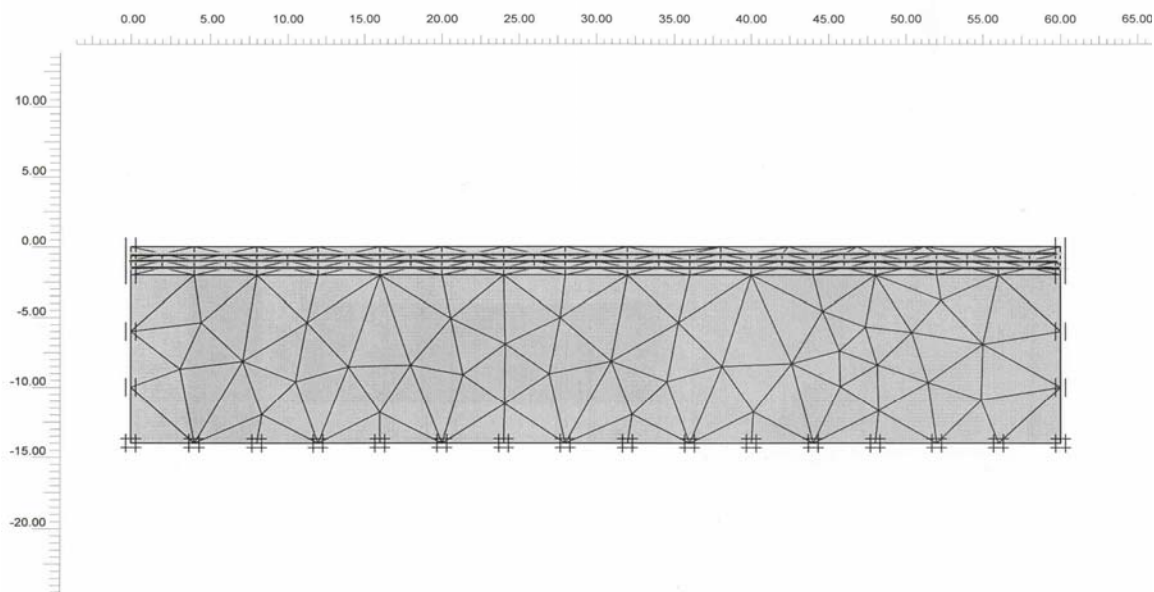


Fig. 4: Discretization of Three-layers geotextile (Problem-2).

Table-2 Convergence study

Mesh type	No. of elements	Maximum Displacement (mm)
Coarse	134	199.8
Refine 1	257	201.3
Refine 2	560	203.4

COMPARISON OF SLIPPAGE RESULTS

The results obtained from the present numerical analysis using PLAXIS-8 for a single layer of geosynthetic reinforcement is presented in Figure-5. Here, X and W are dimensionless parameters defined as ;

$$W = w/B \quad \text{and} \quad X = x/B$$

where x is the distance from the centerline, and being the settlement (w) is normalized with respect to half width of the loading ($B=1/2L$). Here, the soft soil is idealized by a series of springs (Yin, 1997a). In this approach the reinforced granular soil bed is treated to be elastic. The elastic parameters used for granular fill are: $E_{gb} = 1.0$ MPa and $\mu_{gb} = 0.45$ (Table-3), and for the geosynthetic layer are: $E_g = 0.5$ MPa, $\mu_g = 0.49$, $L = 2B$ (these values are the same as the values chosen by Yin (1997a)⁽¹⁰⁾. It can be seen from Figure-5 that the reinforcement have comparable trend for both of the slippage and no slippage cases. However, the settlements are understandably greater for the case without reinforcement. It could be noticed that the reduction in settlements with the geotextile is slightly greater when the slippage is neglected at the interface.

To improve the settlement reduction by using geogrid, three layers of geotextile have been used in Problem-2. The effect of tensile stiffness of the geosynthetic on the settlement response and the mobilized tension in the geosynthetic layers have also been studied for multi layer reinforced soil. This improvement of settlement can be noticed obviously in case of three layers of geotextile especially beneath the centre of loading (Figure-6), which matches the expected results.

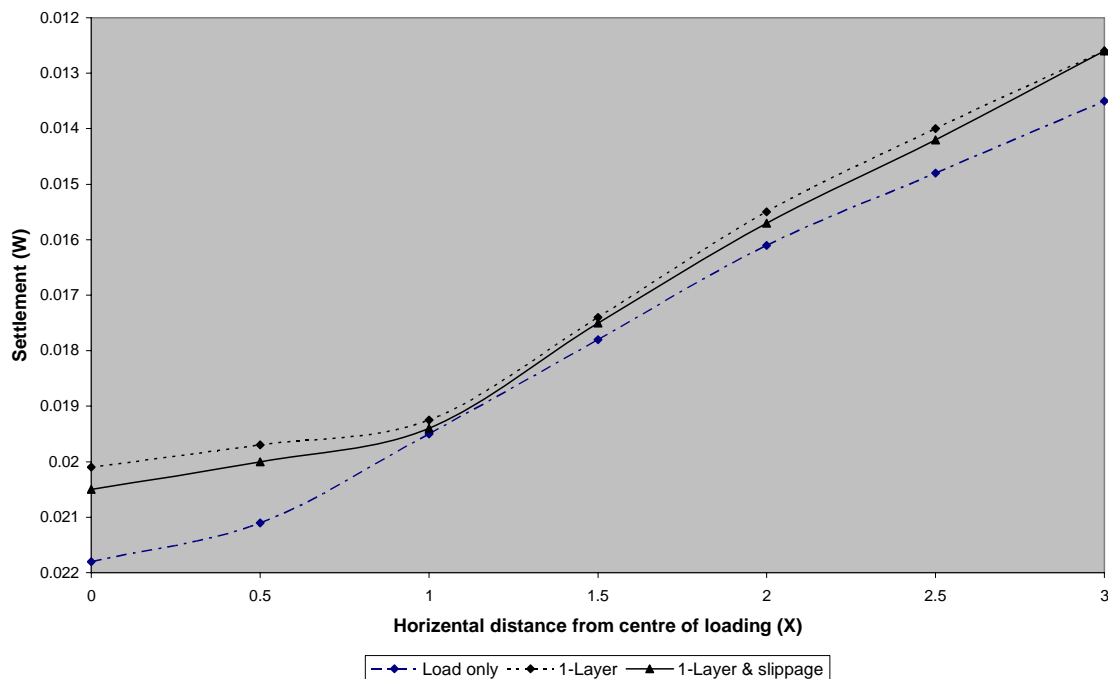


Fig. 5: Problem-1 settlement dimensionless profile .

Table-3: Properties assumed in the model

Parameters	Granular soil	Soft soil
Dry Unit weight (kN/m ³)	18	16
Saturated Unit weight (kN/m ³)	20	18
Horizontal Permeability (m/day)	0.5	0.0001
Vertical Permeability (m/day)	0.5	0.0001
Young modulus(kN/m ²)	10000	800
Poisson's ratio (μ)	0.33	0.3
Cohesion (kN/m ²)	1	5
Friction angle	30	25

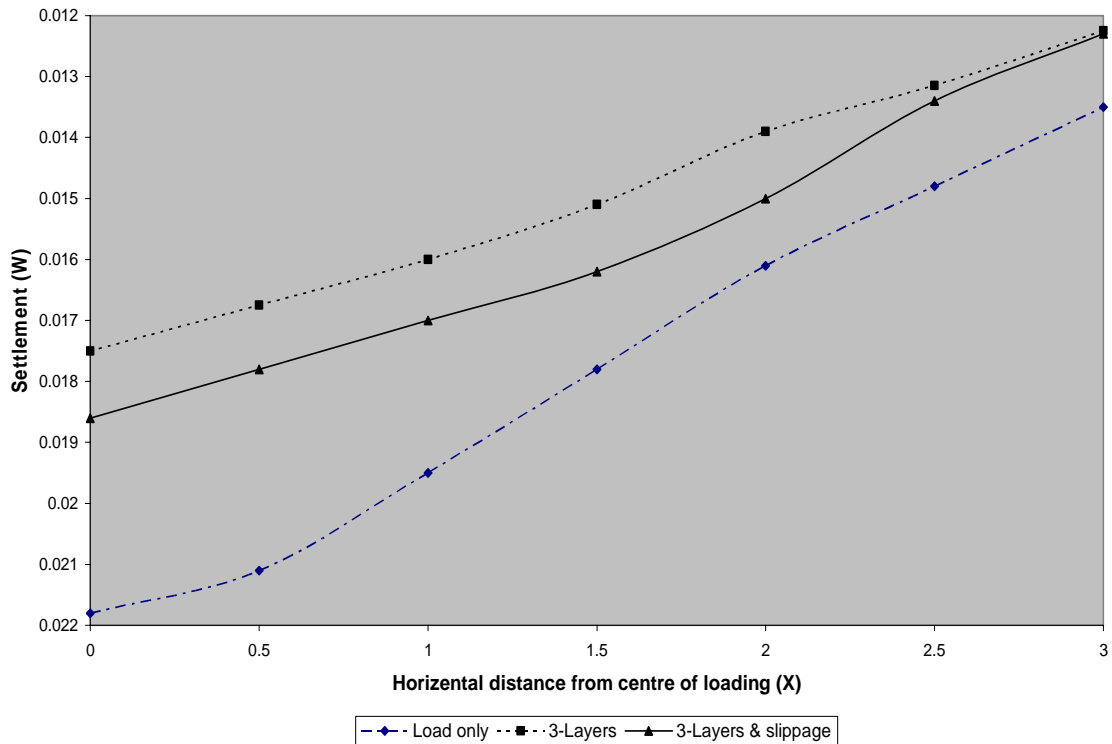


Fig. 6: Problem-2 settlement dimensionless profile

RESULTS AND DISCUSSION

The results obtained from the present numerical analysis using PLAXIS-8 are discussed in this section. The soil reinforcement with geotextile has reduced the settlement in present study with 7.5% and 6% of the original settlement in case of slippage and without slippage respectively for one layer geotextile (Fig.-7). In the presence of reinforcement, major parts of the shear stresses are taken up by the geosynthetic layers. Thus, the presence of the reinforcement causes a reduction in the outward acting shear stresses leading to better performance of the foundation under the superimposed loads. This fact could be revealed when three layers of geotextile have been used (Problem-2). Here, Figure-8 presents the load-displacement curves, which shows the reductions of settlement are 15% and 20% respectively for slippage and without slippage of geotextile. The load is applied in increments, which (loads) reached 100% (final situation of loading). The corresponding maximum settlements are calculated, and the load-settlement curves are plotted. It is very clear that at all stages of loading, the geosynthetic reinforcement reduced the settlement and these settlements were slightly larger when slip is allowed.

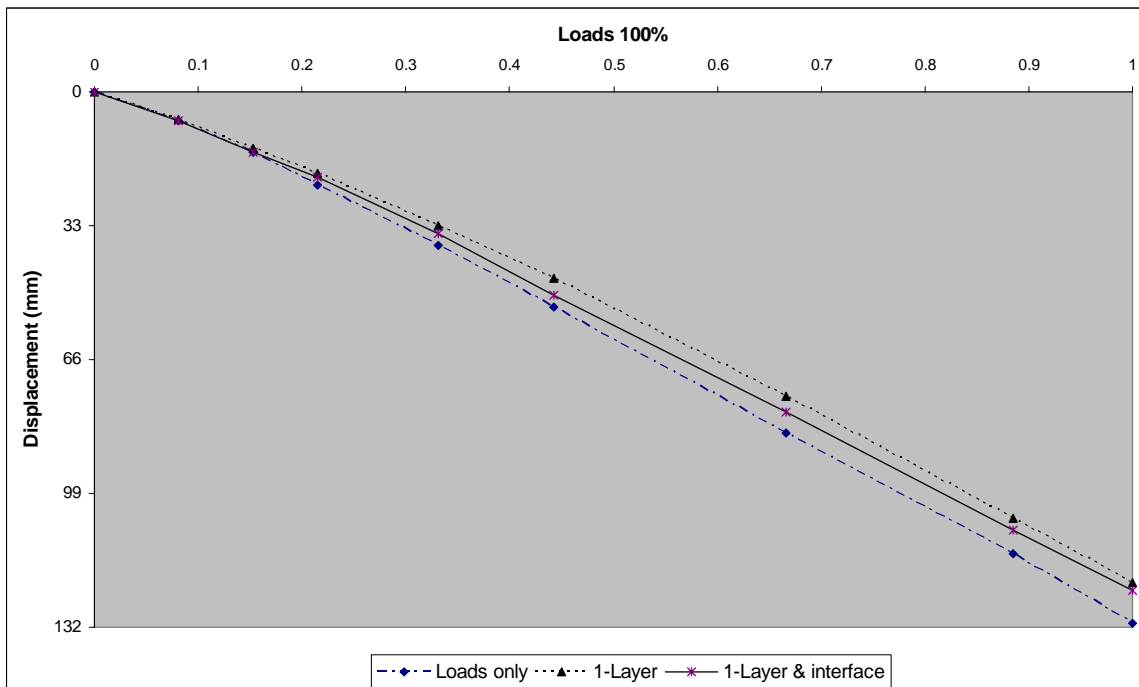


Fig. 7: Load – settlement curve for one-layer geotextile, Problem-1.

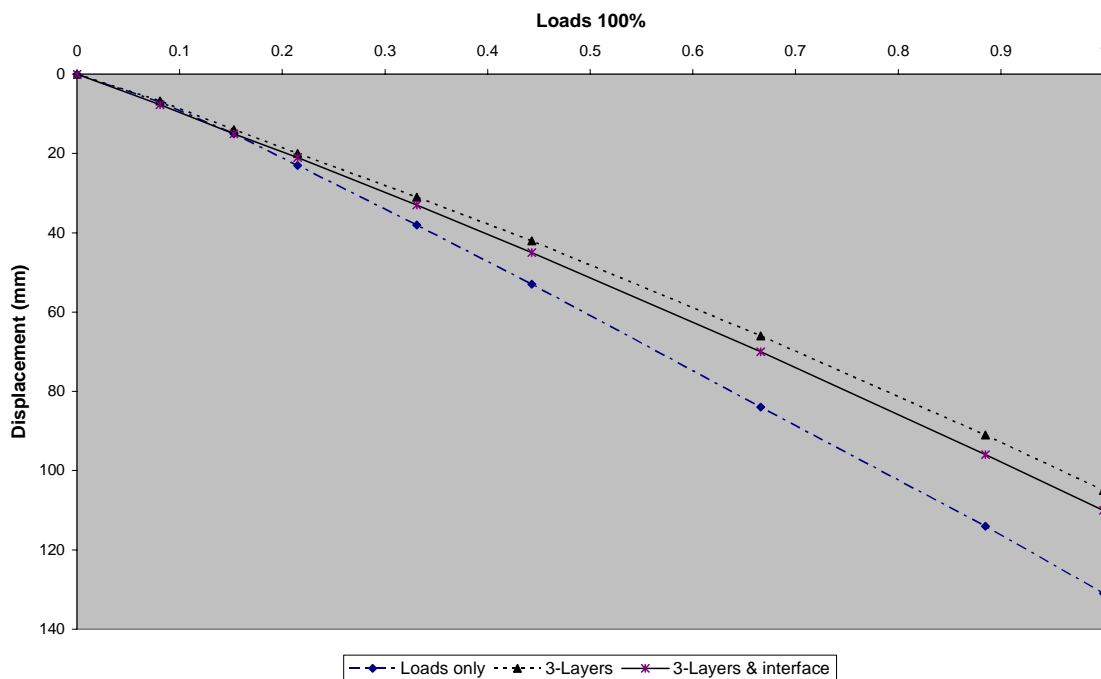


Fig. 8: Load – settlement curve for three-Layers geotextile, Problem-2.

In Figure 9, the plot of settlement versus distance is presented for problem-1. The plot for the unreinforced case is also presented and the results are compared with the response with reinforcement when the slip is permitted and when it is not permitted. When slip is allowed, the settlement is slightly greater than when it is assumed that there is no slip, especially at the centre of loading. Figure-10 is clearly indicates that if the slippage of the reinforcement is considered there is a variation of about 4 to 5% percentage in the settlement response.

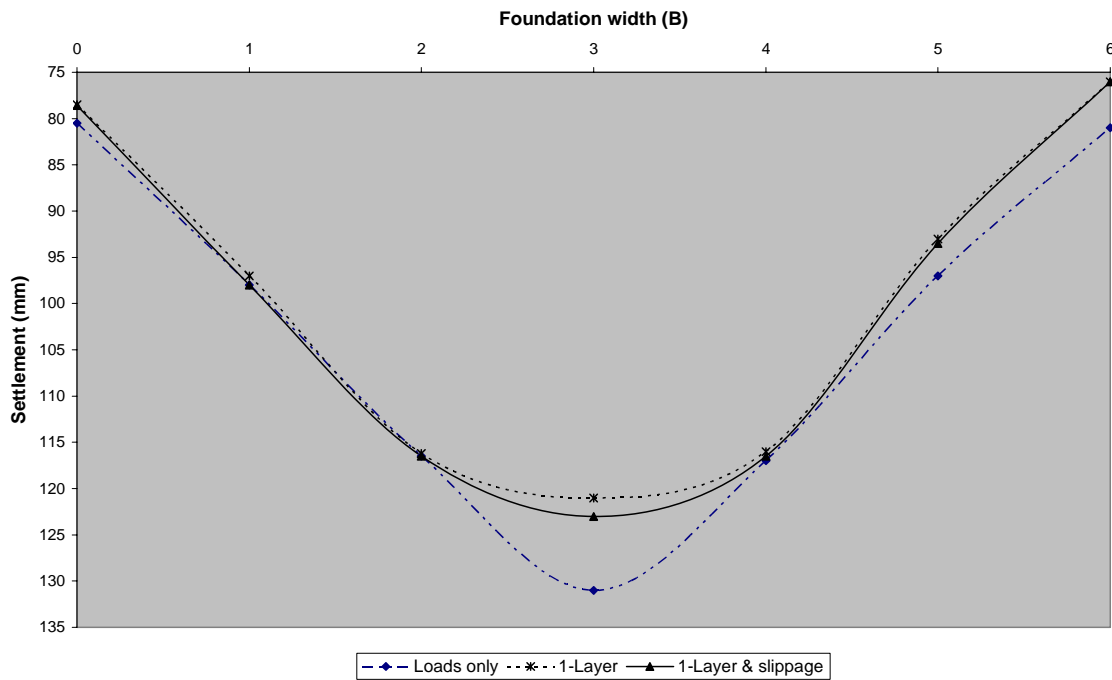


Fig. 9: Settlement profile along foundation width for Problem-1.

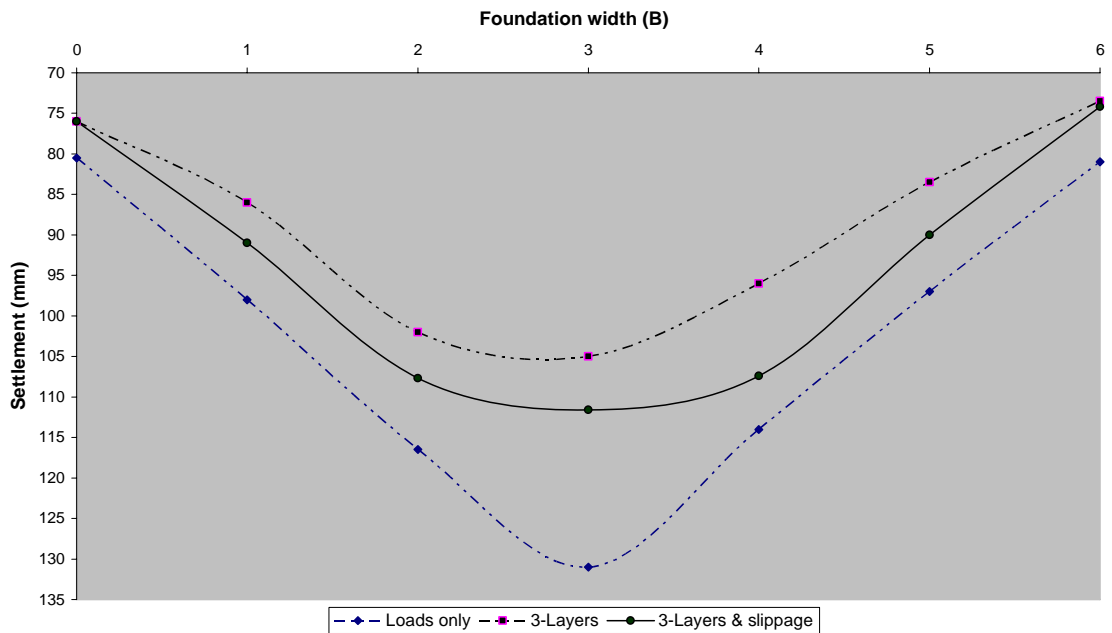


Fig. 10: Settlement profile along foundation width for Problem-2.

The variation of Bendingbending moment within the footing along the horizontal distance from the centre line is shown in Figure-11. As expected at both edges of the footing ($x= 0$ and $x = 6m$), the bending moment is zero, and it is maximum at $x = 3m$ (centre of foundation). The bending moments are smaller when geosynthetic is applied. The maximum bending moment which is close to the centre of the footing is observed to be less in the case where slip of the reinforcement is allowed than the one where slip is not allowed

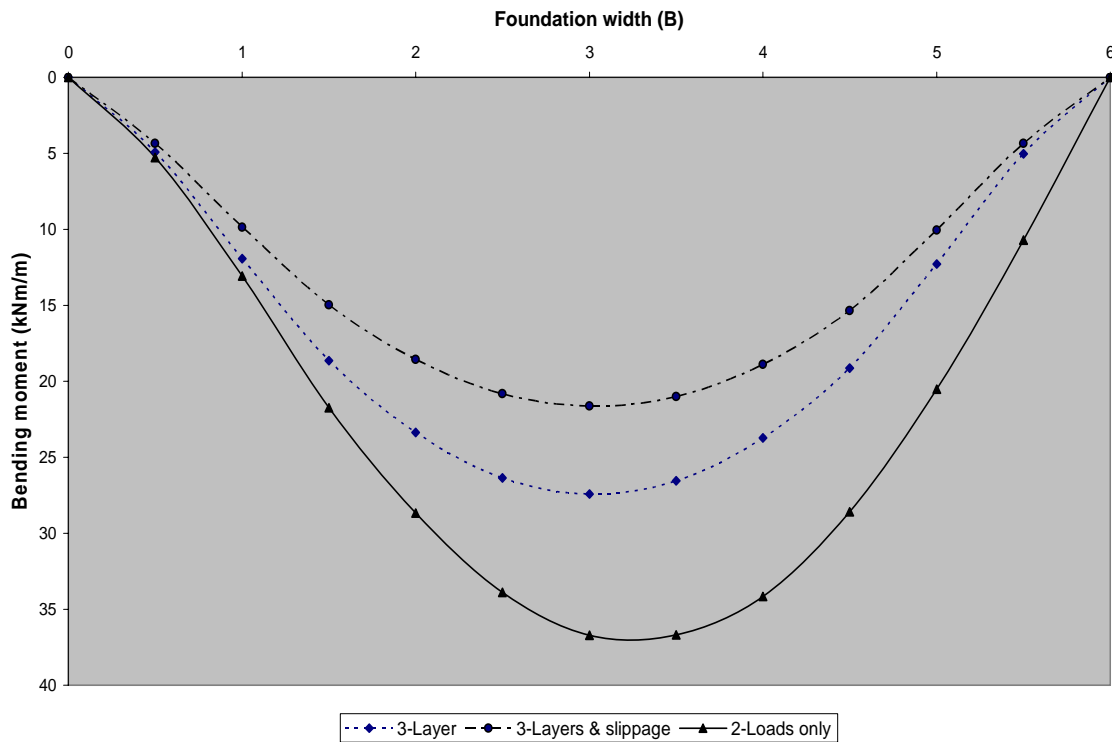


Fig. 11: Bending moment of large foundation with 3-layer geotextile (Problem-2).

Adjacent Foundations Interaction:

To find out the interaction between the two dependent loads and the effect of such adjacent foundations, this analysis has been carried out by considering *one* load ($q = 20 \text{ kN/m}^2$) under the same conditions of one and three geotextile layers. Figure -12 shows the results of settlement profile along foundation width with one and three layers geotextiles (Problems 1&2). The results are much similar regarding reducing the settlement when two loads are applied. The reduction percentages here are 7% and 18.6% for one and three layers respectively. But the interesting phenomenon is that the rate of settlement with *one* load is *higher* than two loads case. The settlement under one load was 145.5 mm while under two loads is 131.3 mm. These results could be attributed to the interaction between the two groups of soil particles beneath the loads. They act like pushing soil particles in the interaction area of granular soil and reduce the pores and voids (interlocking), due to lateral displacements (Lamb and Whitman, 1979). The soil under one load has more ability on granular strata for mobility (as the actual conditions are saturated granular sand).

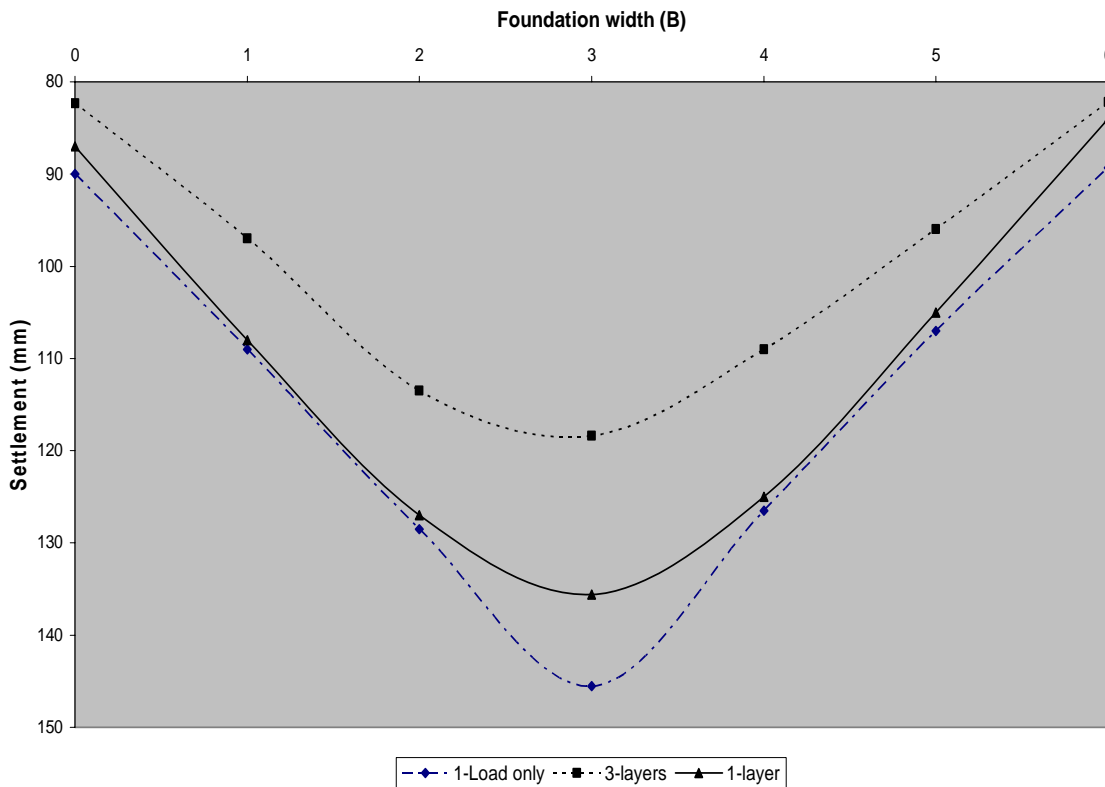


Fig. 12: Settlement profile along foundation width for one load (20kN/m²) only with one and three layers of geotextiles.(Problem 1&2).

Effect of Phreatic Level

Problem-3 deals with dry soil where there is no phreatic surface. Figure-13 shows the settlement profile along foundation width for dry soil. This figure presents the settlement trend which is quite similar to the settlement profile of saturated soil strata, and the reduction of settlement also close to settlement percentage of one and three layers in saturated soil (Problem-1 & 2). These results indicate that the effective stress is the dominant stress in such conditions, as well as the dissipation of pore water pressure is a minimal (Figures 14 & 15). So, this fact obviously could be seen from Figures 16 and 17 for total stresses, which indicate that there is no significant difference between the effective stresses for dry and saturated soils. However, the settlement variation could occur with fluctuations of phreatic level .

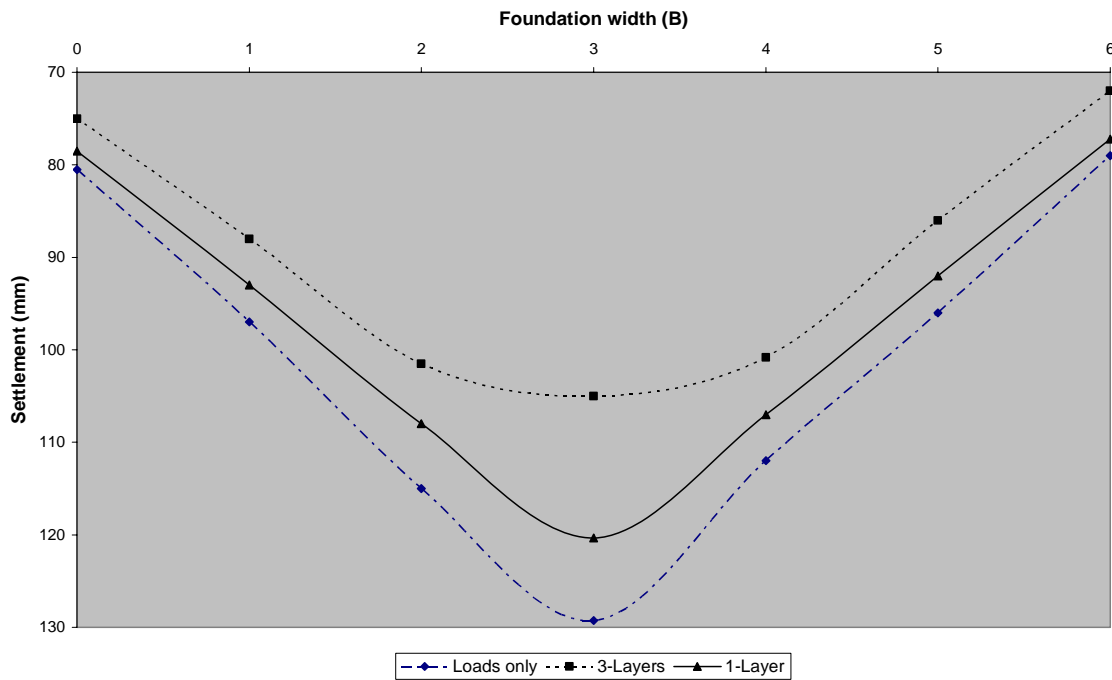


Fig. 13: Settlement profile along foundation width for dry soil (Problem-3)

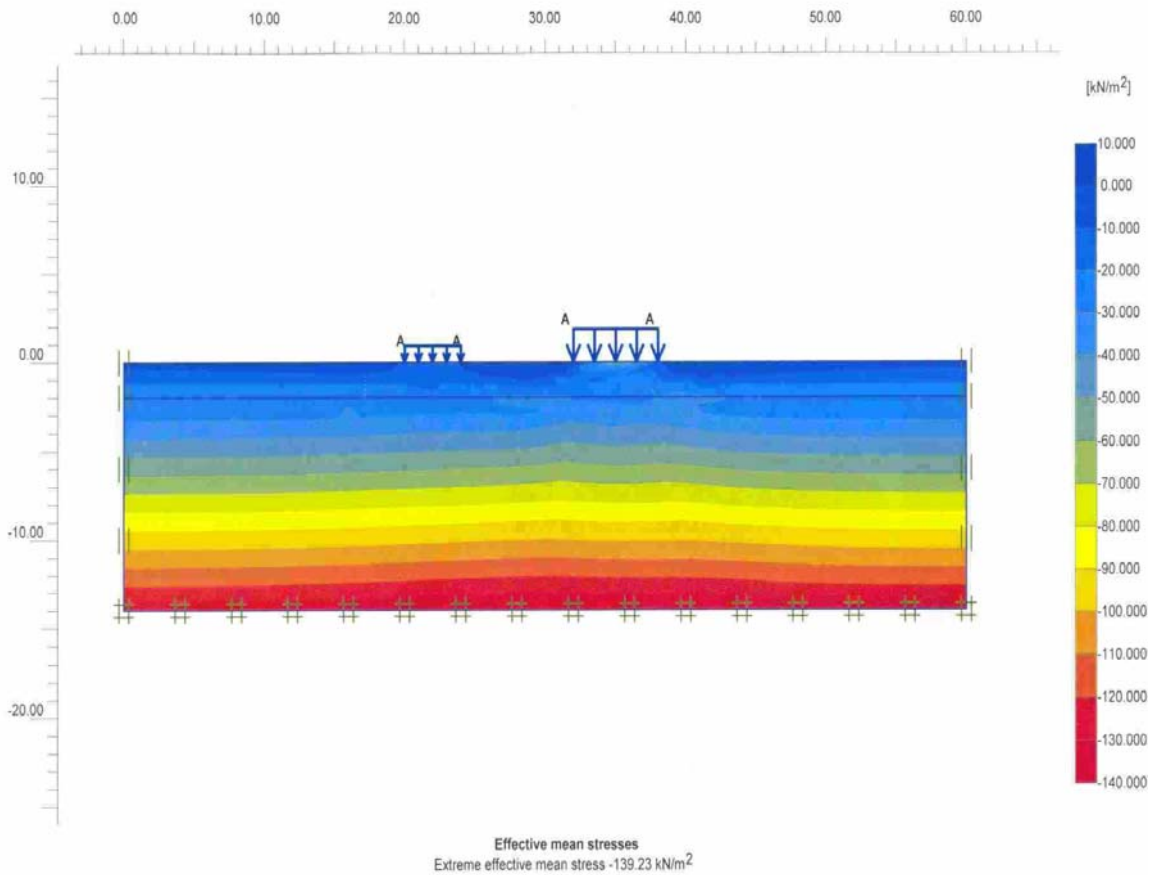


Fig. 14: Effective stress for dry soil (Problem-3).

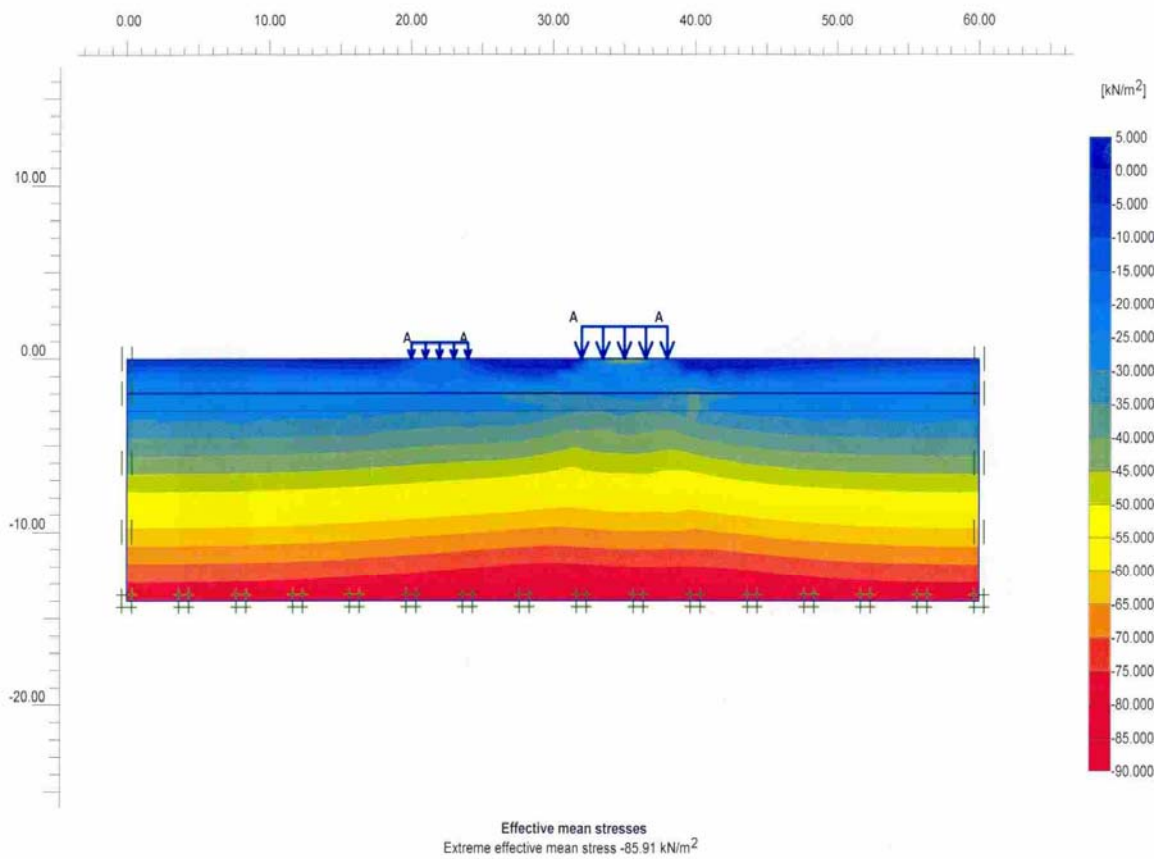


Fig. 15: Effective stress for saturated soils (Problem-1).

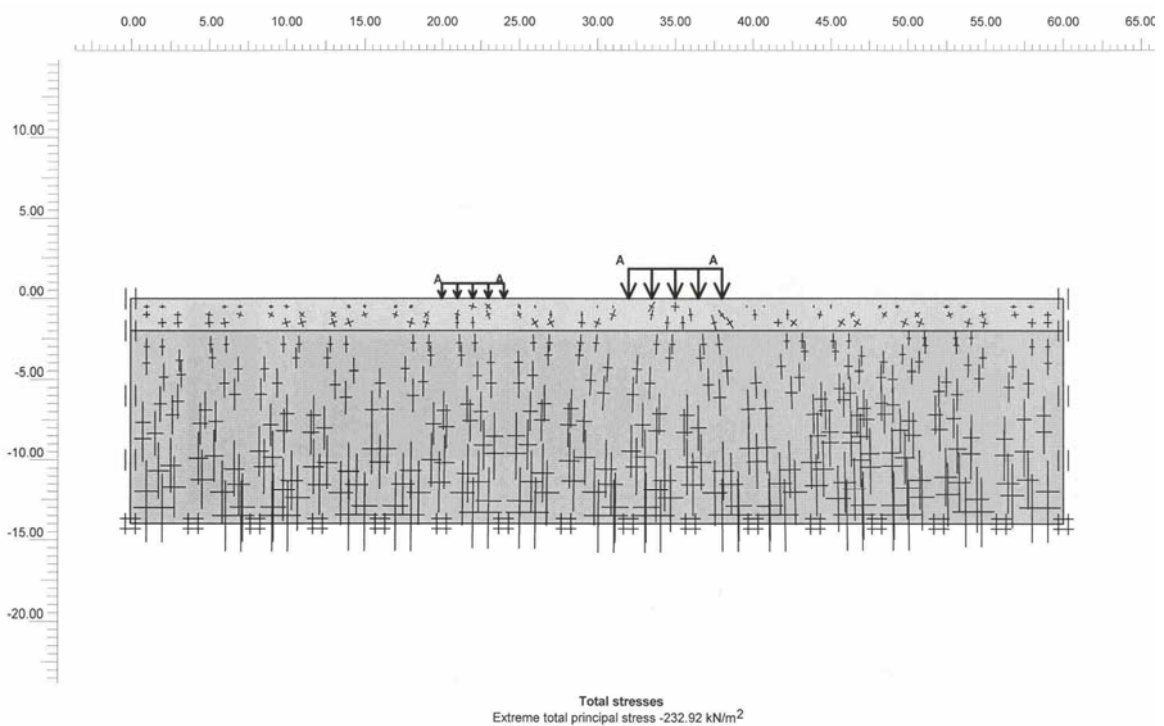


Fig. 16: Total stress for dry soils (Problem-3).

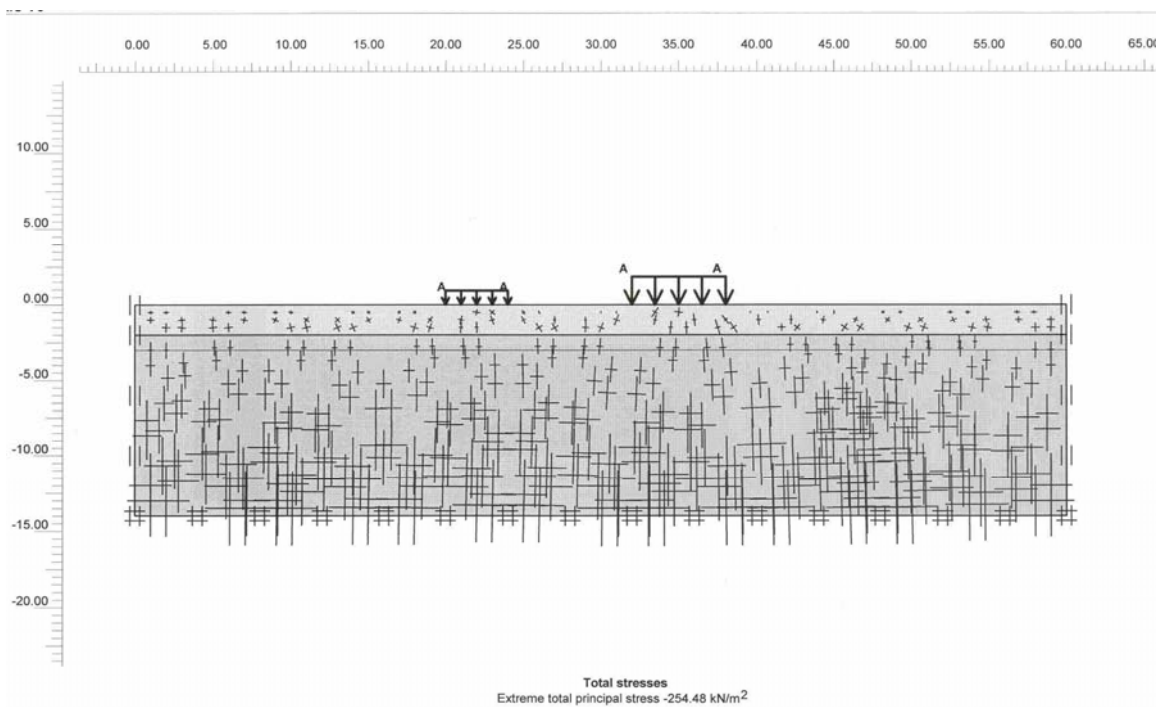


Fig. 17: Total stress for dry soil (Problem-1).

Geotextile Stiffness

The settlement versus geotextile stiffness was also examined in this study to find out the effect of increasing geotextile stiffness effect and the suitable stiffness for designing soil reinforcement (Fig.18). This analysis indicates that increasing stiffness will decrease settlement especially when the stiffness of geotextiles increases from 5 kN/m up to 50000 kN/m (which can be the preferred stiffness), while increasing stiffness more than 5000 kN/m will not be very effective in reducing settlement in such soil conditions. The relation appears to be not linear.

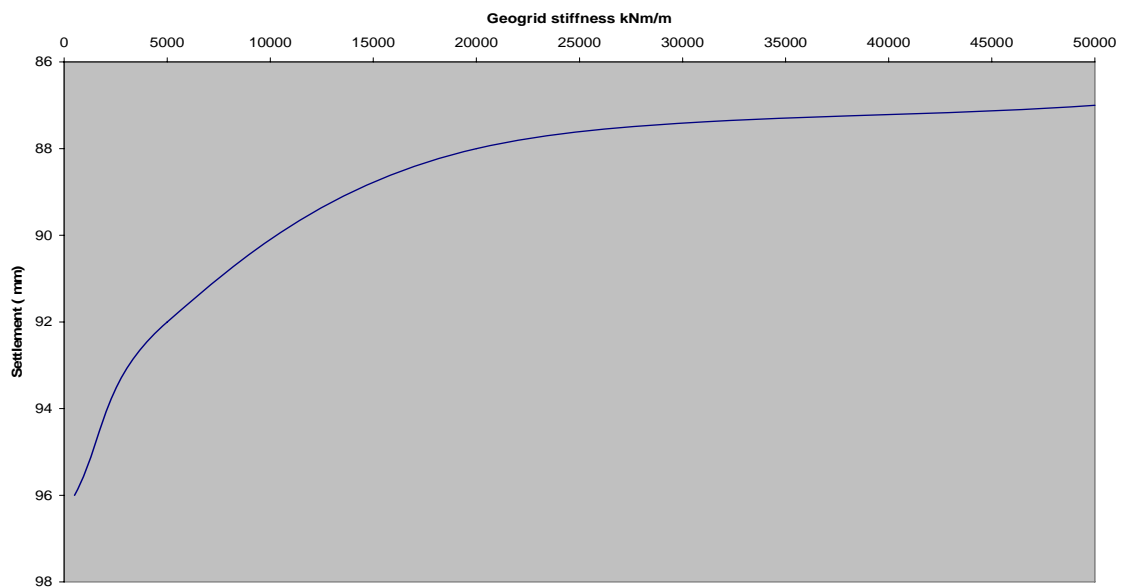


Fig. 18: Settlement – Geogrid stiffness curve .

CONCLUSIONS

This research has revealed noticeable conclusion aspects, as follows;

1. The present study demonstrates a successful application of PLAXIS in analyzing the response of one as well as, multi-layer geosynthetic-reinforced granular fill placed over a soft soil deposit. The results obtained are found to be compatible and in close agreement with the results of finite element for soil reinforcement studies reported in literature.
2. As the number of reinforcement layers increase, the vertical stresses in the loaded region decrease causing maximum settlement reduction at a decreasing rate. Beyond the loaded region a reversal in the trend occurs.
3. The slippage of the reinforcement at the interface of reinforcement and granular soil shows less reduction of settlement than reinforced of soil in both one-layer and three-layer cases. The difference is about 4% to 5% in case of three layers of geosynthetic reinforcement.
4. The presence of phreatic surface does not reduce the settlement rate compared to the dry soil strata.
5. Bending moments in foundations on reinforced soils are less in case of slippage than in case of no slippage between geotextiles and soil.
6. For both one and three layers geotextile, one particular load induces more settlement than in case of two adjacent loads in the same soil strata types.
7. Geotextile stiffness increase leads to a decrease in settlement up to 5000 kN/m, while increasing stiffness more than 5000 kN/m will not be very effective in reducing settlement.

REFERENCES

1. Brinkgreve, R. B. T., Vermeer, P. A. (1998), 'PLAXIS- finite element code for `soil and rocks analysis'. *Version 7 and 8*, A. A. Balkema-Rotterdam-Brookfield .
2. Ghosh, C. and Madhav, M. R. (1994). Settlement response of a reinforced shallow earth bed, *Geotextile and Geomembranes*, 13(9), 643-656.
3. Deb, K., Chandra, S. and Basudhar, P. K. (2005). Settlement response of a multi layer geosynthetic-reinforced granular fill-soft soil system, *Geosynthetics International*, 12(6), 288-298
4. Deb, K., Sivakugan, N., Chandra, S., and Basudhar, P. K. (2007). Numerical analysis of multi layer geosynthetic-reinforced granular bed over soft fill, *Geotechnical and Geological Engineering* , Springer ,The Netherlands,(in press).
5. Lambe, W. and Witman, R. (1979) , *Soil Mechanics* , John Wiley & sons inc., New york, 553 p .
6. Love, J.P., Burd, H.J., Milligan, G.W.E. and Houslyby, G.T. (1987). Analytical and model studies of reinforcement of a layer of granular fill on soft clay subgrade, *Canadian Geotechnical Journal*, 24, 611-622.
7. Madhav, M. R. and Poorooshasb, H. B. (1988). A new model for geosynthetic-reinforced soil., *Computers and Geotechnics*, 6(4), 277-290.
8. Nogami, T. and Yong, T.Y. (2003). Load-settlement analysis of geosynthetic-reinforced soil with a simplified model, *Soils and Foundations*, 43(3), 33-42.
9. Poran, C.J., Herrmann, L.R. and Romstad, K.M. (1989). Finite element analysis of footing on geogrid-reinforced soil. *Proceeding of geosynthetics*, San Diego, USA, 231-242.
10. Yin, J. H. (1997a). Modeling geosynthetic-reinforced granular fills over soft soil, *Geosynthetics International*, 4(2), 165-185.
11. Yin, J. H. (1997b). A non-linear model for geosynthetic-reinforced granular fill over soft soil, *Geosynthetics International*, 4(5), 523-537.
12. Zhan, C. and Yin, J.H. (2001). Elastic analysis of soil-geosynthetic interaction, *Geosynthetics International*, 8(1), 27-48.

A KNOWLEDGE-BASE SYSTEM FACILITATING THE QUANTITATIVE EVALUATION OF SWOT AND CPR IN ALL KINDS OF FIRMS

*A. El-Sharkawy¹, M.Bakry² and M. El Said³

1-Lecturer of Constr. Engrg. and Mgmt, Faculty of Eng., Cairo University, Egypt

2- Head, Planning Dept. of Social Fund Development, Egypt

3- Professor of Constr. Engrg. and Mgmt, Faculty of Eng., Cairo University, Egypt

ABSTRACT

A knowledge base acting as an expert system has been prepared to enable the strategist to calculate easily all parameters of a mathematical model developed by the author. This model was developed to evaluate mathematically the components of Strengths, Weaknesses, Opportunities, Threats, the (SWOT) and the Competitive Position Rating (CPR) of a firm. This knowledge-base system presents the implementation process of the evaluation method developed in that model. However, the system allows the strategic questions to be answered based on the positive percentage value (P) and then computes automatically different aspects of the quantitative evaluation process. The application of this system is implemented by using the Microsoft Access 2000 and Microsoft visual basic 6 codes. The system has a very friendly operating environment, allowing the user to get started quickly. The user will be capable to perform a productive work after spending only a little time.

Keywords: knowledge base, strategist, quantitative evaluation, SWOT, CPR.

INTRODUCTION

The quantitative evaluation of a firm's (SWOT) and (CPR) now depends on the work [1] presented a developed mathematical model. Based on this model, the SWOT's environmental factors of very wide-range numbers can be mathematically evaluated, however each internal or external factor has many subfactors, while each of these subfactors has numerous related aspects. These great numbers of SWOT's elements became ready to be evaluated according to mathematical equations developed in that work. These equations evaluate each factor separately as well as all factors simultaneously. The manual application of these equations is available, but this will cause a very exhaustive personal effort. The main objective of this present knowledge-base system is to enable the strategist to apply easily the applications of these mathematical equations to access the strategic information and the required accurate results relating to the evaluation process. All these benefits will be gained in a form of friendly user interface, however data base generally has a good use for organizing and managing data to achieve a good extraction of queries, results and strategic reports based on that data. Therefore this present knowledge-base system provides a computerized technique aids to evaluate mathematically any unlimited numbers of the SWOT's elements. This system presents the implementation of the (SWOT) evaluation model, however the system components are: 1 - Input data module; which allows the strategic questions to be answered, based on the positive percentage value (P). 2 - The database module; that contains physical files, tables and reports. 3 - The computing module; to compute different aspects of the developed evaluation process. This present system has the following advantages: 1 - Database of any firm can be used. 2 - The system is applied to a local or a global firm. 3 - The system is used for guidance a firm to determine their strategic vision, mission, and goals.

* Corresponding author
Received Date:4/10/07
Acceptance Date:8/6/08

BACKGROUND

A mathematical model [1], has structured to provide a quantitative evaluation method for the firm's SWOT, [2,3,4,5,11]. This model follows the tree method in which the firm environment contains several keyfactors (branches), while each branch carrying many sub-branches called subfactors. Each subfactor has numerous leaves (aspects). The developed method aids to determine mathematically both of the factor's rating (R) and weight (W), however these two parameters are calculated from both of the positive and negative percentages relating to each factor respectively.

The positive percentage (P) of a factor indicates the response degree of a firm's current strategies to that factor, while the negative percentage (N) indicates the relative importance of the factor for being successful in a firm's industry, however (N=1-P). The developed technique interprets mathematically the meaning of factor's rating and weight, however, the factor's rating (R) is interpreted by the first mathematical equation:

$$R = P \times 4 \dots\dots\dots (1)$$

Where:

R : Factor's Rating

P : The positive percentage of a factor indicating the response degree of a firm's current strategies to that factor

4 : Maximum value of the response degree means the (superior response)

While the factor's weight (W)) is interpreted by the second mathematical equation:

$$W_F = W_{Fi} \times C_{ir} \dots\dots\dots (2)$$

Where:

W_F : Factor's weight indicating the relative importance of that factor.

W_{Fi}: The initial Factor's weight.

C_{ir} : The Coefficient of Factor's relative importance.

However this equation tends to the simplified one:

$$W_F = \frac{1 + N_i}{(1+N_1) + (1+N_2) + \dots\dots\dots + (1+N_n)} \dots\dots\dots (2S)$$

Applying both of equations (1) and (2S) to tree leaves (aspects) will drive the strategist to find both rating and weight of each branch (subfactor). In turn applying such equations to the branches leads to determine rating and weight of each big branch (keyfactor). Consequently, the rating and weight of the firm's environment can be calculated by applying both equations to the keyfactors. This application of these two main mathematical equations and their derived equations will be solved automatically by using the present knowledge-base system as will be shown in this paper.

THE KNOWLEDGE-BASE METHODOLOGY

Capabilities of Software Applications

The system contains a database to store widely the information related a firm's (SWOT) components. It is used to force the strategists to answer the strategic questions with the value of (P). Based on physical database design, the system is capable to implement different aspects of the quantitative evaluation of (SWOT) components as will be illustrated in the following:

1- Factor's Rating (R)

By feeding the developed derived-equations {R_i = P_s X 4 ... (4-2-a)} in case of internal environment , and {R_E = P_o X 4 ... (4-2-b)} in case of external environment , in the database design code, the value of factor's Rating (R) can be calculated and will appear as an output when calling it by the strategist.

2- Factor's Weight (WF)

When applying the developed equation (2S) and feeding its applications in the database design code, the factor's weight (WF) can be computed separately and will appear as an output when calling it. Also, this value can be determined when it is involved in a group containing numerous numbers of factors by applying the same equation and feeding it in the design code to be ready for calling.

3- Factor's Weighted Score (Wsc)

The derived equation (4-3), which shows that: $(Wsc) = (WF) \times (R)$, is fed in the database design code, to determine the value of weighted score (Wsc). Once calling this value, it will appear as an output. The same is done to determine and feed value of (Wsci) or (Wsce). Such values can be calculated from equations $\{Wsci = Wif \times Ri \dots (4-3-a)\}$ and $\{Wsce = Wef \times Re \dots (4-3-b)\}$, however values of $\{Wsci, Wif, Ri \text{ and } Wsce, Wef, Re\}$ represent weighted score, weight and rating of internal and external factor respectively.

4- Factor's Total Weighted Score (WTSC)

The value of total weighted score (WTsci) or (WTsce) of internal or external firm's environment can be calculated by adding all weighted scores of internal or external factors respectively, and by feeding this summation in the design code, such value will be determined and will appear if the strategist calls it. The same is done in case of the total weighted score of the firm's environment (WTSC). This value can be calculated by adding the two previous values as seen in the equation $\{WTSC = WTsci + WTsce \dots (4-4)\}$, which will be ready for calling after feeding it. This final total weighted score (WTSC) determines "the firm's Competitive Position Rating (CPR)".

5- Overall Factors Evaluation

The environmental factors can be evaluated totally to represent the evaluation of firm's environment as a whole taking into consideration that, "the summation of the weights of all key and subfactors of internal and external environments finally equal to 1.0". In this case, four steps of calculations are applied: equation (1) to determine each keyfactor's rating, equation (2S) to determine each keyfactor's weight, equation (4-3) to calculate each keyfactor's weighted score and summation of weighted scores of all keyfactors. However, feeding such equations in database design code, the total weighted score (WTSC) of the firm can be calculated and will be ready for calling.

6- Separate Factor Evaluation

Also, any factor, subfactor or aspect can be evaluated separately, taking into consideration that; when evaluating any of them, the basic condition must be achieved to such examined element which is; "the summation of weights of all related (components) must equal to 1.0". By applying the four previous steps (as illustrated in case of overall evaluation), the (Wsc) of any examined factor can be determined and called as an output.

7- Firm's Competitive Position Rating (CPR)

As seen from the equation $\{CPR = WTSC \dots (4-5)\}$, the value of competitive position rating (CPR) of a firm is calculated, however it equals the total weighted score (WTSC) of the firm. According to the CPR-Scale involved in the mathematical model, the recommendations related to the value of (CPR) are exposed. These previous information (The CPR and its related recommendations) are fed in the design code, therefore determining this value can extract the related recommendations from the database and to be called when required.

8- Firm's Cross-Competitive Position Rating (C-CPR)

The Cross-Competitive Position Rating (C-CPR) of any firm's environmental factor is calculated separately, however it equals the weighted score (Wsc) of that factor as shown in equation $\{C-CPR = Wsc \dots (4-6)\}$. Also, the value and recommendations related to the (C-CPR) are stored in database code for calling them when needed.

9- Internal Cross-Competitive Position Rating (C-CPRI)

The Internal Cross-Competitive Position Rating (C-CPRI) of any internal factor can be calculated separately however its value equals the weighted score ($WSCI$) of that factor as illustrated in equation $\{C-CPRI = WSCI \dots (4-7)\}$. As mentioned before in case of (C-CPR), the value of (C-CPRI) and its related recommendations will appear when they are calling.

10- External Cross-Competitive Position Rating (C-CPRE)

From equation $\{(C-CPRE = WSCE \dots (4-8)\}$, the value of (C-CPRE) of any external factor is equal to the weighted score ($WSCE$) of such factor. However the recommendations related to the external cross-competitive positions are determined and stored in the developed module. Therefore at request the value of (C-CPRE) and its recommendations can be determined and will appear when the strategist calls them as outputs.

11- Identification of strategic issues

The developed technique aids to identify the firm's internal and external strategic issues, however values of (Ps), (Nw), (Po), and (Nt) represent degrees of strength, weakness, opportunity and threat of any environmental factor respectively. These degrees are determined according to the developed SWOT's evaluation scale involved in the mathematical model. The previous values and their related recommendations are stored in the design code, to call them when they are required.

The Software Structure

The integration of multi-components and functions (software modules) forms the proposed system. This is under one stand-alone environment (Access 2000 and Visual Basic Code 6). Each of these modules has multi-functions to support all processes of the system.

These system modules are: 1- Interface module designed for user's questions answers input, different aspects of evaluation process, the output reports and recommendations. 2- Knowledge-base module stores and presets the required data related to aspects of evaluation process. 3- Expert system module contains knowledge base of strategic questions, and relating elements of evaluation technique to determine finally different aspects of evaluation process and reports to be outputs in friendly screens.

The System Design

The system design introduces both of the Visual design showing a friendly user interface and the Event-driven programming as illustrated in the following:

1- The Main Screen

Once the program is activated the welcome screen appears for short time displaying the function and objective of the system. Then the main interface window appears. This main window consists of some guides, and buttons to enter data that answer the system questions, definitely the strategist should enter the positive percentage (P). New set of screens will appear, every one contains a header, some buttons commands, each of these buttons provides to access to one of the application command.

2- The physical database design

The physical database design considers the final step in database design process, however in this step the logical database structure is transferred into physical storage structure forming physical files, tables and reports.

2-1 The logical tables into physical tables

In this area logical tables in the developed technique are turned into the physical tables as shown in (table1)

2-2 Creating Queries

These queries can be created by using Structured Query Language (SQL), which is a specialized set of programming commands (sample-table.2).

These programming commands enable the developer to do the following tasks [12]:

1-Review data from one or more table. 2-Manipulate data in tables by inserting, deleting or updating records. 3-Obtain summary information about data in tables. 4-Create, modify or delete tables in database. 5-Create or delete indices for a table.

2-3 Database Input Screens

These screens are designed to be used as a user–interface between the strategist and database, these screens are: 1-Feeding (P) screen. 2-Factors Evaluation screen. 3-Competitive Position Rating (CPR) screen. 4- Cross-Competitive Position Rating (C-CPR) screen. 5- Identification of strategic issues screen.

Table1: Physical table screen

Strategic Audit Question	post	ff
Does firm's management know government's requirements relating its business?	1	GOVERNMENT EF1-1
Does firm's management aware of government's regulations controlling its business?	1	GOVERNMENT EF1-1
Does firm's management aware government's laws narrowing its business?	1	GOVERNMENT EF1-1
Does firm's management determine laws increasing social responsibilities?	1	GOVERNMENT EF1-1
Does firm's management aware of government's regulatory agencies controlling business?	0.9	GOVERNMENT EF1-1
Does firm's management assess influence of the court's rulings through their:	1	GOVERNMENT EF1-1
insecticide acts?	1	GOVERNMENT EF1-1
rodenticide acts?	1	GOVERNMENT EF1-1
water pollution control acts?	1	GOVERNMENT EF1-1
acts of solid wastes disposal quality?	1	GOVERNMENT EF1-1
acts of resource conservation?	1	GOVERNMENT EF1-1
of the court's rulings through their: equal pay acts?	1	GOVERNMENT EF1-1
influence of the court's rulings through their: civil rights acts?	1	GOVERNMENT EF1-1
veterans' employment acts?	1	GOVERNMENT EF1-1
pregnancy acts?	1	GOVERNMENT EF1-1
national traffic safety?	0.9	GOVERNMENT EF1-1
motor vehicle safety?	0.9	GOVERNMENT EF1-1
product safety?	1	GOVERNMENT EF1-1
product warranties?	1	GOVERNMENT EF1-1
consumer goods pricing acts?	1	GOVERNMENT EF1-1
energy administration laws?	1	GOVERNMENT EF1-1
energy reorganization laws?	1	GOVERNMENT EF1-1
energy supply laws?	1	GOVERNMENT EF1-1
energy environmental coordination laws?	56	GOVERNMENT EF1-1

Table 2: Sample query

```

Private Sub 27أمر_Click()
If (A.Value >= 0.85 And A.Value <= 1) Then CRT.Caption = "This opportunity of positiv
'
If (A.Value >= 0.75 And A.Value < 0.85) Then CRT.Caption = "This opportunity of posit
'
If (A.Value > 0.6 And A.Value < 0.75) Then CRT.Caption = "This opportunity of positiv
' "
If (A.Value > 0.501 And A.Value < 0.6) Then CRT.Caption = "This opportunity of positi
' "
If (A.Value < 0.501 And A.Value > 0.495) Then CRT.Caption = "This opportunity of posi
' "
If (A.Value >= 0.25 And A.Value < 0.5) Then CRT.Caption = "This opportunity of positi
' "
If (A.Value < 0.25) Then CRT.Caption = "This opportunity of positive percentage (P <
|
End Sub

Private Sub 31أمر_Click()
On Error GoTo Err_31أمر_Click

Dim stDocName As String
Dim stLinkCriteria As String

stDocName = "EF1AVOID"
DoCmd.OpenForm stDocName, , , stLinkCriteria

Exit_31أمر_Click:
Exit Sub
    
```

2-3-1 Feeding (P) screen

The screen of feeding the positive percentage (P) has two divisions, the first one as illustrated in the screen (fig.1), is structured to act its function by three buttons. The first button (Feeding Positive Percentage value-P) is to contact the strategist with the screen of external and internal environments (fig.2), and the second button (After Feeding P Click here) to enable the strategist to approach following stage of the evaluation process. While the function of the third or lower button is to go back to the former stage.

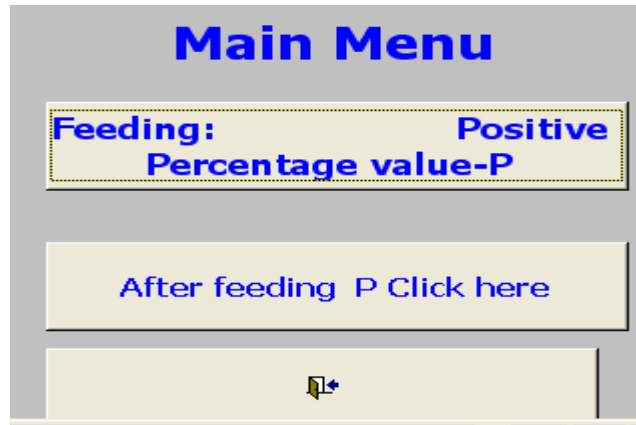


Fig.1: Feeding (P) Screen

The second division represents the screen (fig.2), which consists of seven buttons. Six of these buttons indicate the names of external and internal environmental keyfactors. In order to select any of them, the related button must be pressed and then the screen of the selected factor will be displayed. Then the strategist can feed his reply with the positive percentage (P) in the specific screen as illustrated in (fig..3). When feeding process for all environmental factors is completed by the strategist, automatically all aspects of the evaluation process will be determined. The seventh button to go back.



Fig. 2: Screen of feeding (P) for Ext./ Int. keyfactors.

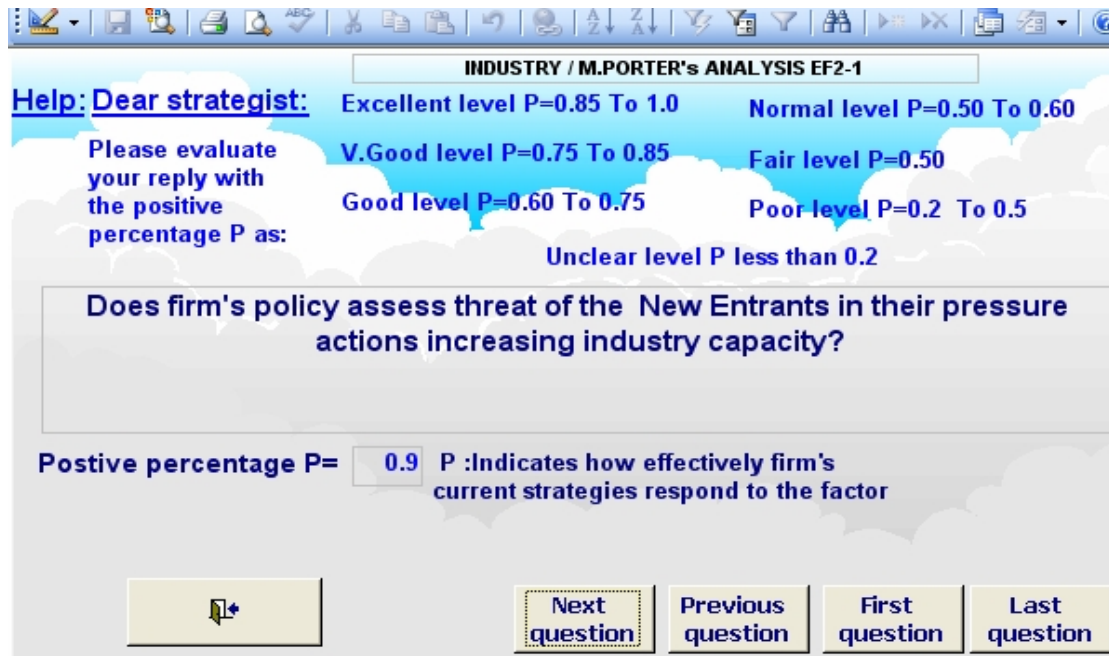


Fig.3: The specific screens for feeding (P)

2-3-2 Factors Evaluation screen

The opening screen of factor evaluation (Fig.4) has four main functions. These functions are expressed by four buttons. The first button is to open the screen of the external environmental keyfactors, the second to display the screen of the internal environmental keyfactors, while the third button is responsible to display the screen of the firm's environment as a whole, whereas the last button is to help the strategist to return to the former stage. For example, when the strategist selects the overall evaluation for the firm he should press the related button (Overall Evaluation of Firm's Environment) to display the specific screen(Fig..5), of the overall factor evaluation, which is designed to have two main parts. The upper part shows the weight, rating and weighted score for each environmental keyfactor concerns the examined firm. While the lower part of the screen exposes the total weighted score belongs to the firm as well as the total weight of all weights of such keyfactors. However the total of weights must be equal to 1.0.



Fig. 4: Opening screen of factor evaluation

Weight	Rating	Weighted Score	KEY FACTOR
0.1647	3.6553	0.6020	General Environment EF1
0.1603	3.7706	0.6046	Competitive Environment EF2
0.1955	2.8419	0.5557	Global Environment EF3
0.1585	3.8202	0.6053	Management Capabilities IF1
0.1592	3.8000	0.6050	Programming Capabilities IF2
0.1617	3.7333	0.6039	Financing Capabilities IF3
TOTAL WEIGHT		TOTAL WEIGHTED SCORE	
1		3.5765	

Fig. 5: Specific screen of overall factor evaluation

Also, if the strategist requires to evaluate only any of internal or external environment, then pressing the related button in the above screen (Fig.4) gives the required results as shown in their specific screens. For example the specific screen (Fig.6), displays the evaluation results of the internal key factors, one can note that the upper part of the screen illustrates the weight, rating and weighted score for each keyfactor belongs to the internal environment of the firm, while the lower part of the screen exposes the total weight of all weights of such internal keyfactors (must be equal to 1.0) and the total weighted score belongs to this internal environment. Similarly the specific screen (Fig.7), displays the evaluation results of the external keyfactors.

Weight	Rating	Weighted Score	KEY FACTOR
0.3305	3.8202	1.2626	Management Capabilities IF1
0.3321	3.8000	1.2620	Programming Capabilities IF2
0.3374	3.7333	1.2596	Financing Capabilities IF3
TOTAL WEIGHT		TOTAL WEIGHTED SCORE	
1		3.7842	

Fig. 6: Specific screen of internal factor evaluation

Weight	Rating	Weighted Score	KEY FACTOR
0.3164	3.6553	1.1565	General Environment EF1
0.3080	3.7706	1.1613	Competitive Environment EF2
0.3756	2.8419	1.0675	Global Environment EF3
TOTAL WEIGHT		TOTAL WEIGHTED SCORE	
1		3.3853	

Fig. 7: Specific screen of external factor evaluation

2-3-3 Competitive Position Rating (CPR) screen

Figure.8 represents the opening (CPR) screen. When selecting the upper button the specific screen (Fig.9) will be displayed. The specific screen of (CPR) contains two main areas. The above area exposes the weighted scores relating to each keyfactor, while the bottom area displays the total weighted score which represents the required competitive position rating (CPR) for the firm.



Fig.8: Opening (CPR) screen

	Weighted Score	KEY FACTOR	EVALUATION
	0.6020	General Environment EF1	
	0.6046	Competitive Environment EF2	
	0.5557	Global Environment EF3	
	0.6053	Management Capabilities IF1	
	0.6050	Programming Capabilities IF2	
	0.6039	Financing Capabilities IF3	
EVALUATION: The firm's competitive position rating (firm's CPR) is :			TOTAL WEIGHTED SCORE 3.5765

Fig.9: The specific (CPR) screen

2-3-4 Cross-Competitive Position Rating (C-CPR) screen

The cross-competitive position rating (C-CPR) screen is responsible to open the related three interior screens. The screen illustrated in fig.10, is structured to present its function by three buttons. The upper button is for conducting the strategist with the related specific screens with which the evaluation results of the external and internal environmental keyfactors are exposed. The second button helps in approaching to another stage of the evaluation process. While the third or lower button is to go back to a former stage.

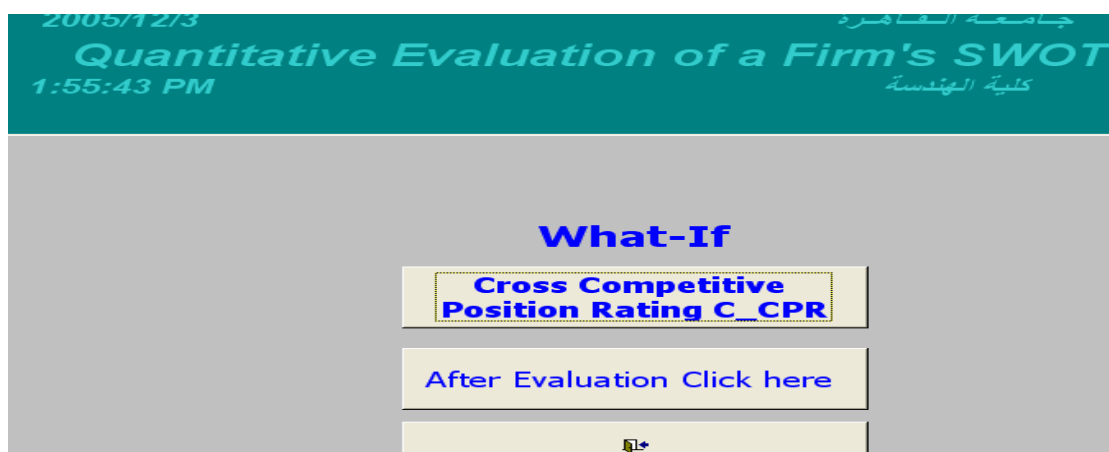


Fig. 10: Opening (C-CPR) screen

The first interior screen (fig.11) consists of seven buttons; six of them belong to the six keyfactors of the firm's environment. Each of these buttons matching one of such keyfactors, for

displaying the second or third screen which exposes the cross-competitive position rating (C-CPR) of the selected factor, as illustrated in the screens (figs.12, 13). IF the strategist needs to go back he should select the seventh button.



Fig. 11: (C-CPR) screen of keyfactors

The (C-CPRE) specific screen (fig.12) is designed to have two main areas. The above area displays the weighted score for each subfactor belongs to the examined external keyfactor, also it displays the functional button of the evaluation. Once pressing this button the result of the evaluation of such keyfactor will appear in the bottom area, which contains the competitive position rating for the firm and the total weighted score. Similarly the specific screen (fig.13) of (C-CPRi), presents the result of the evaluation of an examined internal keyfactor.

2-3-5 Identification of strategic issues screen

This screen has three subscreens; the first screen (fig.14) is considered as the opening screen and it has three buttons. The upper button is for matching the strategist with the second screen (fig.15), The second button helps to end the evaluation process as it is indicated by (STOP). While the third or lower button is to go back to the former stage.

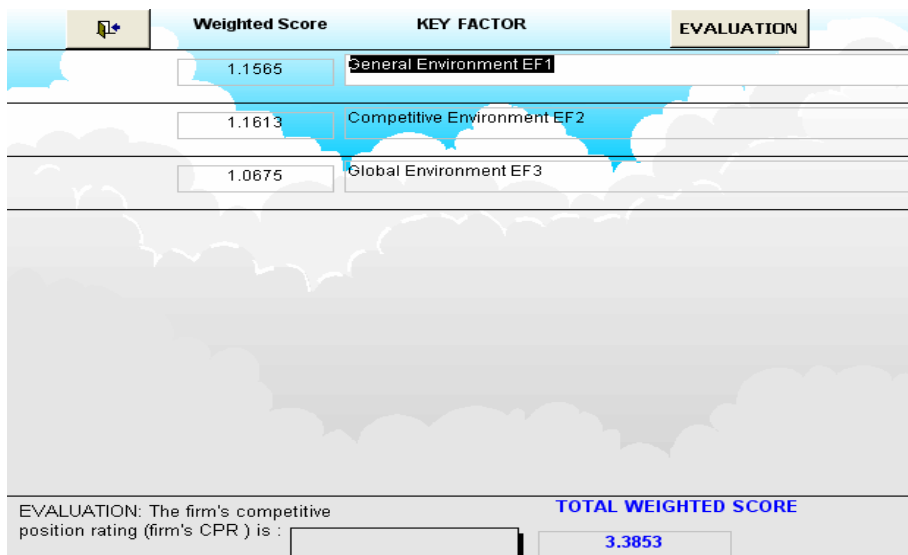


Fig. 12: The (C-CPRE) specific screen

Weighted Score	KEY FACTOR	EVALUATION
1.2626	Management Capabilities IF1	
1.2620	Programming Capabilities IF2	
1.2596	Financing Capabilities IF3	
EVALUATION: The firm's competitive position rating (firm's CPR) is :		TOTAL WEIGHTED SCORE
SUPERIOR CPRs		3.7842

Fig. 13: The specific screen of (C-CPRI)

3-2-3-5 Identification of strategic issues screen

This screen has three subscreens; the first screen (fig.14) is considered as the opening screen and it has three buttons. The upper button is for matching the strategist with the second screen (fig.15), The second button helps to end the evaluation process as it is indicated by (STOP). While the third or lower button is to go back to the former stage.

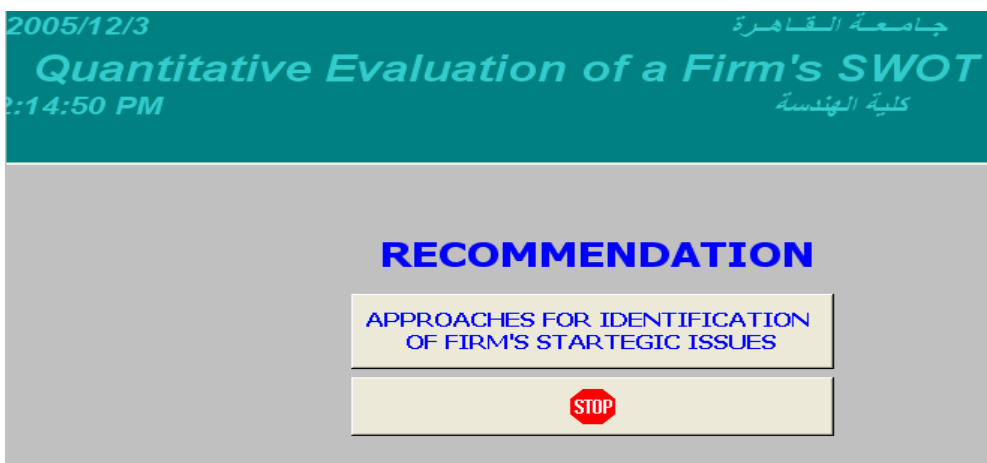


Fig. 14: Opening screen of strategic issues identification

The second screen (fig.15) helps the strategist to conduct with any of the keyfactors for both the external and internal environments. However each of the upper six buttons in the screen indicates the evaluation of one from these keyfactors, and the lowest button is for going back to the former stage. When selecting any one of the upper six buttons, the related evaluation of opportunity and threat for external keyfactor are exposed in the third or specific screens (figs.16, 17), as well as strength and weakness for the internal keyfactor. This evaluation will be revealed through its related alarm and recommendation.

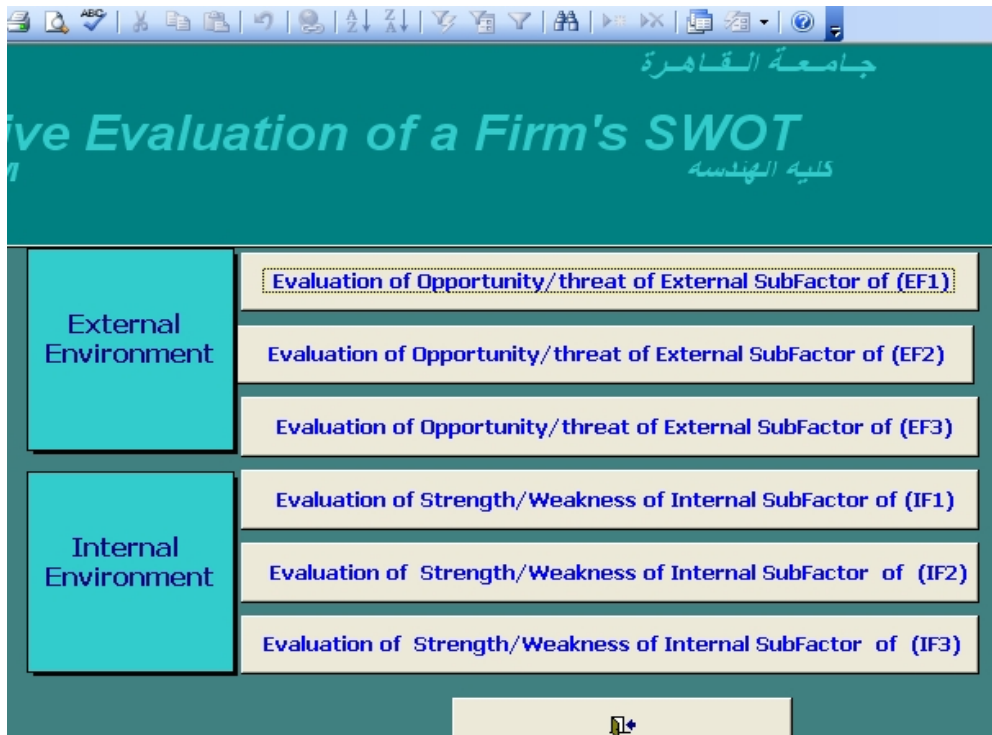


Fig. 15: Strategic issues screen

The third screen is the specific screen, which involves two main functional buttons, the alarm and recommendation buttons.

3-2-3-5-1 Alarm screen

The alarm screen (Fig.16) is structured to have two main areas. The above area contains the factor's name and presents in brief the results of evaluation of the SWOT's factors to be as alarm for the firm management, however it exposes the degree of opportunity or threat in case of the external environment or the degree of strength or weakness in case of the internal environment. While the lower area contains the functional buttons such as the two main buttons for the alarm and recommendation and four buttons for approaching the alarms for different factors (the first, next, last or previous factor) in addition to the button of going to another screen.

3-2-3-5-2 Recommendation screen

The recommendation screen (Fig.17) is designed also to have two main zones. The above zone introduces the strategic advices to be considered when formulating the adopting strategy. While the lower area contains the factor's name and the functional buttons such as recommendation button which is activated when pressing on it to display the recommendation of the examined factor and four buttons for approaching the recommendations for different factors (the first, next, last or previous factor) and with the button for going to another screen.



Fig. 16: Alarm screens

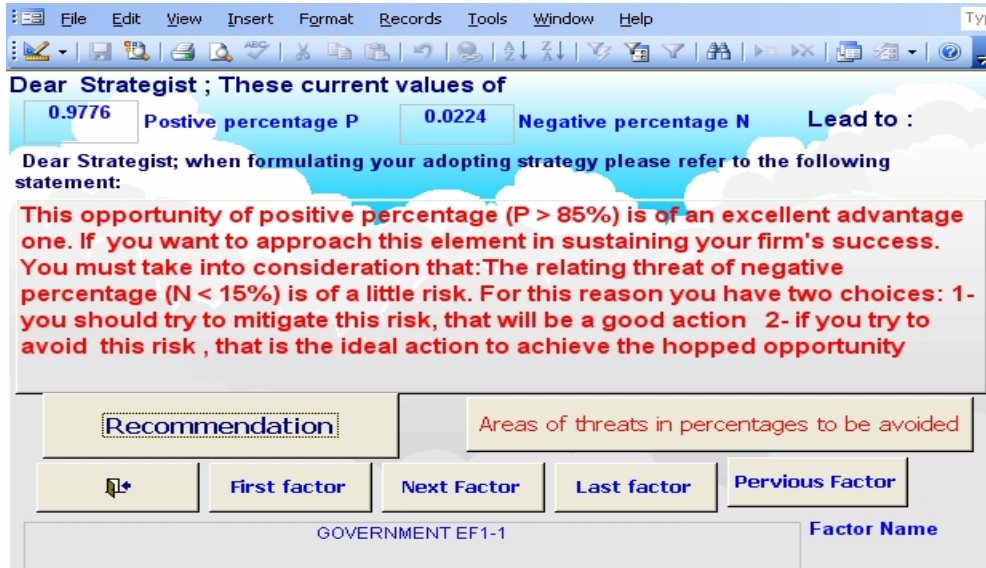


Fig. 17: Recommendation screens

CONCLUSIONS

- 1- This paper has explained the implementation system for (SWOT) and (CPR) evaluation model to enable the strategist to apply easily the applications of the mathematical model developed by the authors.
- 2-The system contains three components which are:
 - 2-1 Input data module.
 - 2-2 The database module.
 - 2-3 The module of computation.
- 3- This implementation is based on the Microsoft Access 2000 and Microsoft visual basic 6 codes.
- 4- In this paper, the system's objective, advantages, capabilities of the software applications, the software structure and the system design are introduced.

ACKNOWLEDGEMENTS

The authors gratefully acknowledge the experts in the department of computer science, Institute of Statistical Studies and Research (ISSR), Egypt, for their valuable advices and assistance to support the effort of this present computer programming system.

REFERENCES

1. El-Sharkawy A.. & El-Said, M. (2004), "*Adopting a long-term strategy enhancing competitive performance in construction firms*". HBRC, conference on "future vision and challenges for urban development" Cairo, 20-22 December, 2004.
2. Gary Hackbarth & William J. Kettinger (1996) working Paper, "*E-commerce strategy breakout*". Internet.
3. Terry C. Carson (1997), "*Organizational Change and Strategies for Turbulent Environments*" , Microsft Internet explorer, pp.1-23.
4. Stefani K.. (1998), "*Tools for Market Strategy*", Microsoft Internet, September ,pp.1-5.
5. Chuckill's College Resources (1998-2000), "*Netscape Operation Strategic Audit*". Internet.
- 6- MSH-Unicef (1998), "*SWOT Analysis : Internal Analysis*". Present sites (Erc. Home) (Unicef). erc@msh.org.
- 7- MSH-Uncef (1998), "*SWOT Analysis*". Present sites (Erc. Home) (Unicef). erc@msh.org.

8. Cyril Levicki (1999), " *The Strategy Workout* ", Second Edition, P. Education Limited, London.
- 9- Higgins M. & Vincze W. (1993), "*Strategic Management-Text and Cases*", (pp. 5-193, pp. 324-354).
10. Bryson M. (1995), " *Strategic Planning for Public and Nonprofit Organizations* ". , San Francisco.
- 11- Clive Reading (1993), "*Strategic Business Planning* ", Kogan Page Ltd., London,. (pp. 132-134).
- 12- Maher A. (2003), "*Integration of Simulation and Expert Systems for Optimal Selection of Asphalt Paving Equipment*", Ph.D., Cairo University

CHEMICAL MODIFICATION OF THE CELLULOSE FOR AN APPLICATION IN THE WASTE WATERS TREATMENT

*Lamia Timhadjelt , Aicha Serier and M. Serier

Laboratory LRME- University UMBB, Independence Avenue, Boumerdes-35000, Algeria

Email: serier_ac@yahoo.fr

ABSTRACT

The shortage of the water resources and the pollution which is growing these last years, constitute the prime motivation for searching any alternative resources.

This study consists to modify the cellulose by grafting of the amidoxime groups in order to use it for the adsorption of the Cu(II), Cr(III) and sulphide ions which exist in the industrial effluents. The cellulose is an abundant biodegradable polymer; the amidoxime groups have a strong complexation power towards heavy metal ions. The grafting is achieved in two steps: cyanoethylation and amidoximation which are confirmed by FT-IR. The optimum conditions of the two reactions are determined by the kjeldahl's method and by FT-IR. The amidoxime quantity is determined by measuring the quantity of the amine functions by HCl. The application of the modified cellulose is intended for the adsorption of the metal ions Cu(II) and Cr(III) and sulphide ions 'S²⁻' in a double adsorption.

The FT-IR analysis reveals that the fixing of metal cations is based on the complexation of the latter with the ligands of the adsorbent. The optimum adsorption was recorded at pH = 6 for a contact time of 5 hours and an initial concentration of 10⁻¹M in metals. Desorption of fixed metals is possible by the EDTA, and the reuse of the adsorbent confirms the effectiveness of regeneration of the adsorbent.

Keywords: Cellulose, modification, sorption, heavy metals, waste water treatment.

INTRODUCTION

The treatment of the waste waters represents at the same time a solution to cure the lacks of water and on another side takes part in the decrease of the pollution generated by the industrial effluents. The economic limits of the traditional techniques of metal processing liquid waste resulted in developing new processes. The latter implement properties of adsorption and complexation of biomaterials particularly those based on cellulose, most abundant of natural polymers [1]. The aim of our study consists of the introduction of the amidoximes groups into cellulose in order to improve its surface quality for an application in the field of the treatments of waters charged with heavy metals Cu(II) and Cr(III) and with sulphide ions. The latter are eliminated by fixing in the second adsorption on the metals already trapped on amidoximated cellulose.

MATERIALS AND METHODS

Materials:

Pure cellulose powders some (60-65% crystalline) (Sigma-Aldrich), Acrylonitrile (Aldrich), hydroxylamine (Fluka Chimie). The metal ions (Cu²⁺ and Cr³⁺) were obtained starting from the metal salts (CuCl₂, 2H₂O) and (CrCl₃, 6H₂O) adjusted with pH between 3 and 6 using the solutions of Clarck-Lubs [1], by using the hydrogenophthalate potassium (table 1).

* Corresponding author
Received Date:12/9/07
Acceptance Date:9/6/08

Table 1: Clarck-Labs buffer solutions [1].

PH	metals Solution (ml)	Potassium Hydrogeno-Phthalate 0.2 M (ml)	HCl 0.2 M (ml)	NaOH 0.2 M (ml)	Deionized water
3	250	250	101.6	2	Dilute for 1000 ml
4	250	250	/	119.25	Dilute for 1000 ml
5	250	250	/	227.25	Dilute for 1000 ml
6	250	250	/	/	Dilute for 1000 ml

Techniques:

- ✓ The products are characterized by a spectrometer FT-IR of Thermo-Nicolet Nexus series at ambient temperature. After drying under 40°C during 48h, 3mg of the sample is crushed with 150mg of KBr then pressed. The pastille of Ø=6mm is analyzed.
- ✓ The influence of the various parameters on the reactions was expressed by the degree of substitution (DS) determined by the Kjeldahl's method (equation 1) and by FT-IR.
- ✓ The proportioning of the metal ions in solution is carried out by an Atomic Adsorption spectrometer, SOLAAR M6, after acidification, dilution and filtration of the solutions.
- ✓ The spectrometer UV, JASCO 3200, is used to highlight the effectiveness of the regeneration of Amidoxime Cellulose (Am-Cel). The solutions are introduced into a basin of optical way of 1cm.
- ✓ The quantity of the sulphide ions fixed is determined by iodine proportioning.

Modification of cellulose:**1. Preparation of the cyanoethyl cellulose:**

For obtaining the Am-Cel, we must pass through the cyanoethyl cellulose (CE-Cel) like first stage. The latter is obtained by the action of the acrylonitrile (AN) on the cellulose (Cel) in alkaline medium (NaOH) with 36% in weight in the presence of tetramethylammonium chloride (TMAC) [1, 2]. The Degree of substitution (DS) of the CE-Cel is obtained from the ultimate analysis of nitrogen rate N (%) using the following relation [1]:

$$DS = \frac{M_{\text{Cel}} \text{ N (\%)}}{100M_{\text{N}} - M_{\text{AN}} \text{ N (\%)}}$$

2. Preparation of the amidoxime cellulose:

The CE-Cel prepared is then treated by an aqueous hydroxylamine hydrochloride solution [1] at constant temperature (60 - 80°C) for variant time (90 - 180min). The modified cellulose obtained is washed with deionized H₂O and filtered under vacuum. The results are expressed by the quantity of amidoxime Q_A obtained by the absorption of HCl by the amidoxime groups [1].

Adsorption and desorption of the metal ions:

The experiments of adsorption were carried out in batch for a ratio of mass of adsorbent/volume of solution of 1/100 (g/ml), with variation successively the pH of the solution between 3 and 6, the contact time from 0 to 48 hours and the initial heavy metal (Cu²⁺ and Cr³⁺) concentrations from 0 to 10⁻¹ M.

Selectivity of the ions of copper and chromium by the adsorbent:

For the same ratio of mass of adsorbent/volume of solution, a well defined mass of Am-Cel was immersed in an adequate volume of solution containing Cu^{2+} and Cr^{3+} ions for 24 hours at ambient temperature under continuous agitation. The suspension is then filtered. The quantities of the Cu^{2+} and Cr^{3+} ions were determined by Atomic Absorption spectroscopy.

Regeneration of the adsorbent:

The Am-Cel was regenerated by desorption of the metal ions adsorbed by a solution of EDTA at 0,1N. A quantity of 0,1g of Am-Cel is immersed in this last solution at ambient temperature during 24 hours. The suspension is then washed by deionized H_2O , filtered and finally analyzed by UV spectroscopy.

Fixing of the sulphide ions:

After the adsorption of the metal ions on the Am-Cel, the sulphide ions are eliminated in the second adsorption by immersing 0,005g of the powder not regenerated in a sulphide solution with various concentrations: $2 \cdot 10^{-2}$, $4 \cdot 10^{-2}$ and $8 \cdot 10^{-2}\text{M}$ in closed bottles with continuous agitation.

RESULTS AND DISCUSSIONS**Characterization:**

The CE-Cel and the Am-Cel are characterized by FT-IR. The comparison of the respective spectra (figure 1) shows the appearance of a characteristic peak of the $\text{C}\equiv\text{N}$ groups to 2254 cm^{-1} on the spectrum of the CE-Cel (b), while on that of the Am-Cel (c), we observe a considerable reduction in the peak characteristic of the $\text{C}\equiv\text{N}$ groups and the appearance of a characteristic peak of the double bond $\text{C}=\text{N}$ to 1666 cm^{-1} thus indicating the formation of the CE-Cel and the Am-Cel respectively.

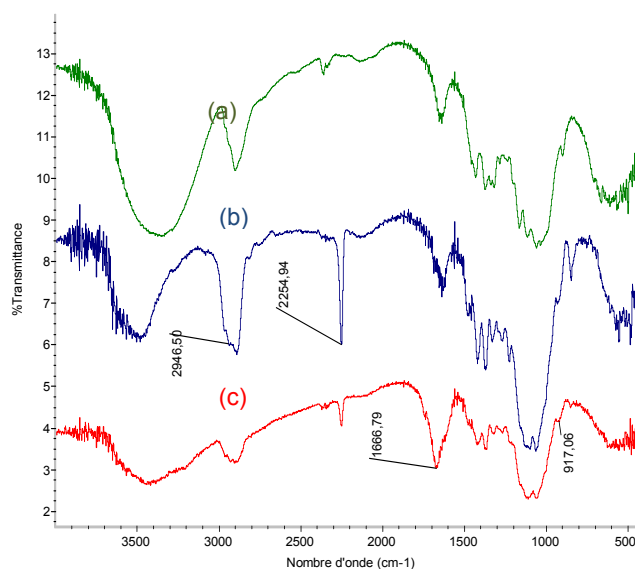


Fig. 1: Cel pure (a), CE-Cel (b) and Am-Cel (c) infrared spectrum

Parameters affecting the reactions:

Table 2 indicates the effect of the operating conditions of cyanoethylation and amidoximation reactions on DS and quantity of amidoxime (Q_A). We note that the DS of the CE-Cel increases with the presence of chloride of tetramethylammonium (TMAC) and with the time of reaction. It increases too with the NaOH concentration up to an optimal value when this latter concentration reaches 20%. Q_A contained in the Am-Cel, increases with the temperature and time until this latter reaches 180min. According to authors [1, 3, 4], obtaining a stage beyond 180min indicates a maximum of conversion. The amidoximation is privileged by a concentration in NH_2OH of 10%. These results agree with works of the literature [1-4].

Table 2: Evolution of the DS of CE-Cel and Q_A of the Am-Cel with the reactions conditions.

cyanoethylation				amidoximation				
TMAC	Time (min)	[NaOH] (%)	DS	Temp. (°C)	Time (min)	[NH_2OH] (%)	DS of CE-Cel	Q_A (mmol/g)
Without	90	36	1,510	80	90	5	2,297	3,80
With	90	36	2,297	80	90	10	2,297	4,27
With	45	36	0,847	80	60	10	3,385	3,73
With	150	36	2,385	80	90	10	3,385	4,10
With	90	10	0,391	80	150	10	3,385	4,40
With	90	20	0,739	80	180	10	3.385	5.00
				60	90	10	3.385	3.37
				75	90	10	3.385	4.03

Adsorption of heavy metals (Cu^{2+} and Cr^{3+}) ions:

Contrary to the Cel and the CE-Cel, the Am-Cel showed a great affinity for heavy metals (Cu^{2+} and Cr^{3+}). An octahedral compound tends to be formed between the latter and the Am-Cel in the presence of the phthalates anions [5] at ambient temperature.

Factors affecting the adsorption of the metal (Cu^{2+} and Cr^{3+}) ions:

Effect of the initial concentration of the heavy metal ions:

The results (figure 2) show that the quantity of (Cu^{2+} and Cr^{3+}) ions adsorbed increases with their initial concentration.

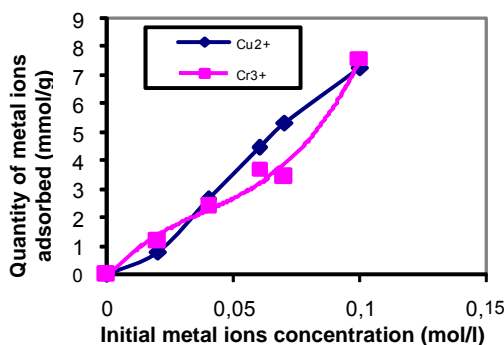


Fig. 2: Variation of the quantity of Cu^{2+} and Cr^{3+} ions adsorbed with their initial concentration.

Effect of the contact time:

Figure 3 shows that the quantity of (Cu^{2+} and Cr^{3+}) ions increases with the time of contact, the equilibrium time is 5 hours, the curves tend then towards a stage in accordance with the theory, indicating the saturation of the adsorption sites. The reduction recorded after 24 hours can be explained by a light desorption due to the molecular collisions.

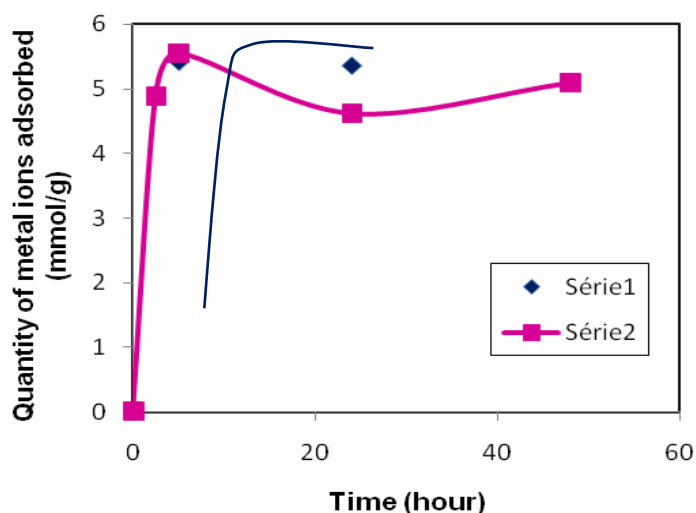


Fig. 3: Variation of the quantity of Cu^{2+} and Cr^{3+} ions adsorbed with the contact time.

Effect of the solution pH:

The results represented on figure 4 shows, in the case of chromium, that the quantity of the Cr^{3+} ions adsorbed increases with the solution pH. A small quantity was recorded towards $\text{pH}=3$, this is due to the inhibiting effect. On another side, with $\text{pH}=6$, we observe the precipitation of the metal ions with the OH^- ions.

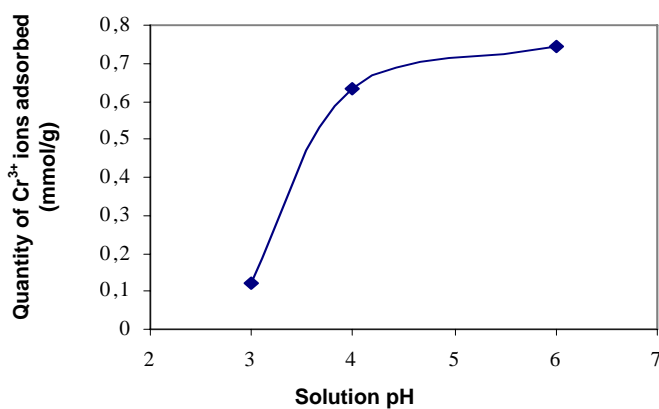


Fig. 4: Variation of the quantity of Cu^{2+} and Cr^{3+} ions adsorbed with solution's pH.

Effect of the quantity of amidoxime:

Figure 5 shows an increase in the quantity of Cu^{2+} ions adsorbed with Q_A contained in the adsorbent. This is foreseeable because the amidoxime groups represent the sites of adsorption.

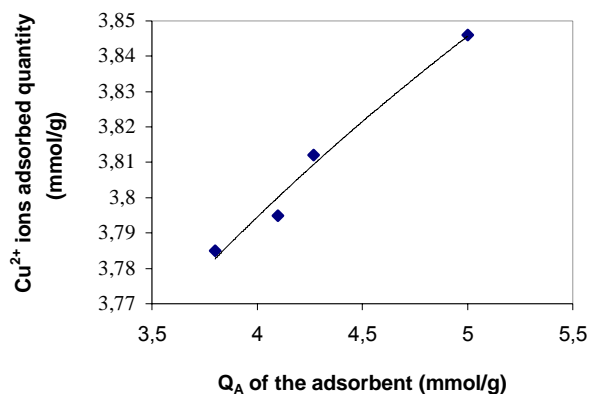


Fig. 5: Variation of the quantity of Cu^{2+} ions adsorbed with the quantity of the amidoxime.

Selectivity of the amidoxime cellulose towards the Cu^{2+} and Cr^{3+} ions:

The results deferred on table 3, shows that the Cu^{2+} ions is selectively adsorbed on the amidoxime cellulose. This result agrees with works of Gauthier and al. [1] and EL-Wakil and al. [3].

Table 3: Determination of the quantity of Cu^{2+} and Cr^{3+} ions adsorbed for evaluation of their selectivity.

Sample	Initial Concentration (mol/l)	Metal ion non adsorbed content (mol/l)	Metal ion adsorbed quantity (mmol/0,01g)	Metal ion adsorbed quantity (mmol/g)
Cu^{2+}	$7 \cdot 10^{-2}$	$0,885 \cdot 10^{-2}$	$6,114 \cdot 10^{-2}$	6,11(4)
Cr^{3+}	$7 \cdot 10^{-2}$	$3,782 \cdot 10^{-2}$	$3,218 \cdot 10^{-2}$	3,21(8)

Regeneration of the amidoxime cellulose:

It is carried out by desorption of the Cu^{2+} and Cr^{3+} ions by a solution of EDTA 0,1N. In the presence of the latter, the Am-Cel doe's n't shows any affinity towards the metal ions. The effectiveness of regeneration is proven by the reuse of the treated powder.

Fixing of the sulphide ions:

It is highlighted by the change of color (green \rightarrow yellow) obtained by immersion of the powder in a sulphide solution during $t = 30 - 60$ min. Figure 6 shows that the quantity of the sulphide ions fixed increases with their initial concentration.

CONCLUSION

The cellulose was modified in Am-Cel passing by the CE-Cel. The amidoxime groups can form with heavy metal ions an octahedral compound metal-Am-Cel that makes them useful for the treatment of waste waters. The operating conditions of preparation are simple. The adsorption of heavy metals is influenced by several parameters. It increases with their initial concentration, the time of contact and the solution pH. The sulphide ions are fixed on the heavy metals adsorbed beforehand on the Am-Cel. The regeneration of the Am-Cel is possible using a solution of EDTA at 0,1N.

REFERENCES

1. Saliba R., Gauthier H., Gauthier R., Petit-Ramel M. (2000); "Adsorption of copper (II) and chromium (III) ions onto Amidoximated cellulose»; Inc. J. Appl. polym. Sci., 75, pp 1624-1631.
2. Hassan M. L., EL-Wakil N. A., Sefain M. Z. (2001); "Thermoplasticization of Bagasse by cyanoethylation"; Inc. J. Appl. polym. Sci., 79, pp 1965-1978.
3. Hassan M. L., EL-Wakil N. A. (2003); "Heavy metal ion removal by amidoximated bagasse"; Wiley Periodicals, Inc. J. Appl. Polym. Sci., 87, pp 666-670.
4. Kubota H., Shigehisa Y. (1995); "Introduction of Amidoxime Groups into cellulose and its Ability to Adsorb Metal Ions"; Inc., J. Appl. Polym. Sci., vol.56, Issue 2, pp 147-151.
5. Seko N., Tamada M., Yoshii F. (2004); "Current status of adsorbent for metal ions with radiation grafting and crosslinking techniques»; 6th International Symposium on Ionising Radiation and Polymers, IRAP 2004.

INVESTIGATION OF AIR FLOW INSIDE A MECHANICALLY-VENTILATED ROOM MODEL

*Nabil M. Guirguis¹, Amr Ibrahim² and Mahmoud A. Hassan¹

1 Housing & Building Research Center, Cairo, Egypt, Email: nabilmilad@yahoo.com

2 Faculty of Industrial Education, Helwan University, Egypt

ABSTRACT

It is known that indoor air quality has a great impact on health and behavior and therefore becomes an economic issue regarding especially health cost and productivity. The traditional approach to create good indoor air quality involves removing pollution load and addressing thermal comfort by means of standards. The indoor air is perceived as positive or negative depending on whether the room occupants feel that air is artificial or whether they accept the air as natural, most by a perception of artificial indoor air. As discussed from the previous work [5] "the efficiency of the ventilation systems depends, in turn, on the location of the supply outlets and extraction ports". Most mechanical engineers face the common problem "where can we locate the supply outlets and extraction ports and what is the proper direction of the airflow inside the space". To overcome the problem of ineffective ventilation, guidelines of proper location selection of the supply outlets and extraction intakes should be established. Ventilation accordance with ASHRAE standards [1], ventilation for acceptable indoor air quality (AIAQ) should be used for areas where specific standards are not given. Design of a ventilation system must as much as possible, provide air movement from clean to less clean areas. Building an effective ventilation system to achieve the optimum-hygiene conditions needs more careful and collaborative work. Making indoor air quality (IAQ) a top priority in the healthcare facilities starts with the building design [7]. The air flow patterns are a very important factor in obtaining good indoor air quality.

This paper discusses an experimental and theoretical study of test room models to investigate the most suitable and effective location of the supply and return grills for better air flow distribution inside the conditioned space.

Keywords: Airflow, Supply, Return, Grills, Extraction, Smoke Generator, ANSYS, CFD

INTRODUCTION

Egypt is located in the tropical region which is characterized as a hot and humid climate where a large number of buildings are served by air-conditioning systems. Air-conditioning is a means to achieve a controlled atmospheric condition in an enclosed space at all seasons of the years, using air as the medium of circulation. Since most people spend most of their time indoors, thermal comfort and indoor air quality is a major concern in designing air-conditioning systems of buildings. Energy use related to IAQ (which requires airing or ventilation) is a fraction of the total energy use, which may be very small in naturally-ventilated buildings in warm climates or rather important in fully air conditioned buildings [5].

Mechanical ventilation is often used where natural ventilation cannot fulfill the requirements, either because of poor outdoor conditions (noise, pollution, climate) or in locations that cannot be naturally ventilated. It has the following advantages: a)

* Corresponding author
Received Date:27/12/07
Acceptance Date:21/7/08

it allows ventilating deep spaces with low ceilings and rooms that are not accessible to natural ventilation, b) where well-designed and built airtight building, it ensures a total and continuous control of air flows and also allows a better control of the indoor climate, c) it can protect from outdoor noise and pollution, d) heat recovery from exhaust air is relatively easy. Kameel and Khalil [4] present the balance between the energy efficient thermal comfort and indoor air quality. It was found that the design of the HVAC airside systems plays important role for the energy consumption optimization and achieving the optimum IAQ. The results recommended that, the factors that affect the IAQ in healthcare application in two main groups, namely; architectural design group and airside system design group. Kempinski [3] discuss a new approach for evaluating the environment of building, which is called Olfactory Comfort average (OCA) which is determining the perception of the hedonic value of the indoor air taking into account the state of mood of the occupant. Roulet [5] presents of energy uses in building and in particular of energy needed for ventilation, and presents the relationships between indoor air quality and ventilation, ending by general guidelines on how to improve both IAQ, comfort, well being and energy performance of buildings. Gong et al [2] explores the thermal and air movement perception of a group of tropically acclimatized subjects (24 people) after 90 minutes of facial exposure to local air movement.

This paper divided into an experimental work using a smoke generator test facility to visualize the air flow patterns inside the tested room and theoretical work using a CFD program to investigate the air velocity distribution inside the test models in contour and vector lines for different supply and return grills locations. The efficiency of the ventilation systems depends mainly on the efficiency of the airside design. The efficiency of the airside design depends, in turn, on the locations of the supply outlets and extraction ports. Most of mechanical engineering face the common problem "where can we locate the supply outlets and extraction ports" and "what is the proper airflow direction inside conditioning space".

Experimental work

The objective of air distribution in forced air heating, ventilating, and air conditioning systems is to create the proper combination of temperature, air velocity, and air-contaminant concentrations in the occupied zone of the conditioned space. Airflow patterns and current that are created from the locations of supply diffuser and return grills in the occupied space affect the thermal comfort.

In order to show and photograph the air flow pattern inside the test model a smoke generator was connected to the supply outlet of the test room. A schematic diagram and a photo of the smoke generator are shown in figure 1 which consists of a kerosene container attached to the evaporator. An electrical heater was wound around evaporator stem. As the smoke generator is switched on, the kerosene reaches its boiling point and evaporates in the glass evaporator, then the blower pushing the white smoke kerosene vapor out through a rubber tubing which connected to the supply outlet of the test room. Therefore, the air flow pattern can be viewed and photographed inside the test room. Different experimental tests were conducted for different supply outlets and extraction locations.

Test Models

To evaluate the air flow pattern inside an air conditioning room, experimental and numerical investigations are conducted on a model with different supply outlet and extraction port locations. Different scaled-up test models with different supply outlets and extraction ports are used using the smoke technique to study the airflow pattern inside the conditioned room. The test models have a cubic shape of dimension 0.25 m and are fabricated from a plastic sheet of 2 mm thickness (Plexiglas). On the front wall and the roof a rectangular opening 0.06 m x 0.03 m was made at different locations as shown in Figure 2. The outlet (supply) of the test model was connected to the smoke generator through a rubber tube. The test model has a scale 1: 20 of the prototype.

COMPUTATIONAL TECHNIQUE (“ANSYS” SOFTWARE PACKAGE)

To investigate the air velocity distribution inside the test model with different supply outlet and extraction locations, a CFD (ANSYS) program was used. This program is based on the solution of Navier-Stokes equations, the energy equation, the momentum and concentration equations as well as the transport equations for the turbulent velocity and its scale. A mathematical $k-\epsilon$ turbulence model is needed for numerical simulation. The $k-\epsilon$ turbulence model in which k is the turbulence energy and ϵ is its dissipation, is one of the most popular turbulence models. The $k-\epsilon$ turbulence model is usually known as an implicit scale and currently it is most widely used due to of its applicability to the wide-range flow problems.

In the present work, an investigation was carried out using ANSYS which is based on the finite element approach to examine the best combination of supply outlets on the roof and extraction grills at the front wall of a conditioned room. The results of ANSYS which are the velocity-contours and streamline vectors will be discussed and compared with visualization findings (smoke-tunnel visualization). The test room is of dimension 0.25 m and has three openings on the ceiling (R1, R2, and R3) and three openings on the front facade at different locations (W1, W2, and W3), as shown in Figure 2.

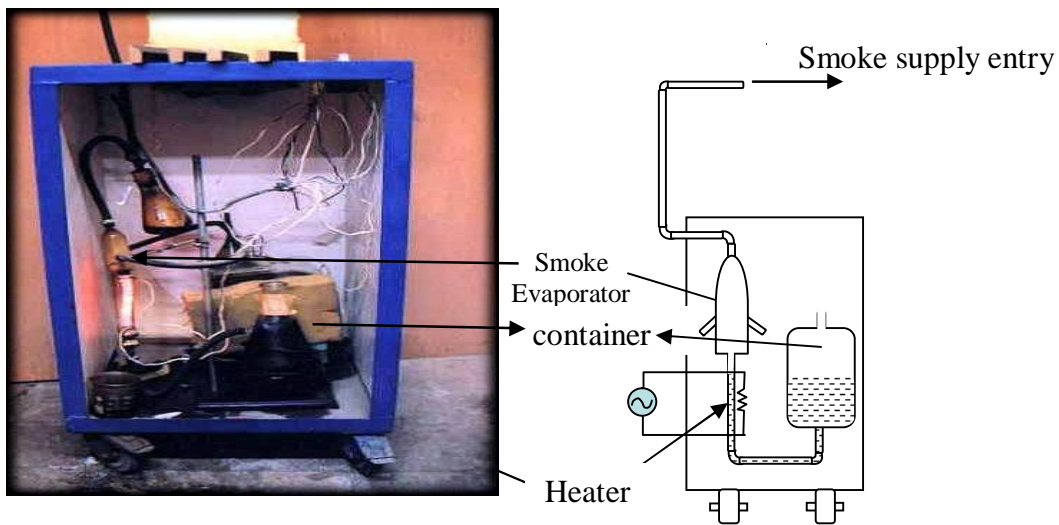


Fig. 1: Schematic diagrams and photo of smoke generator.

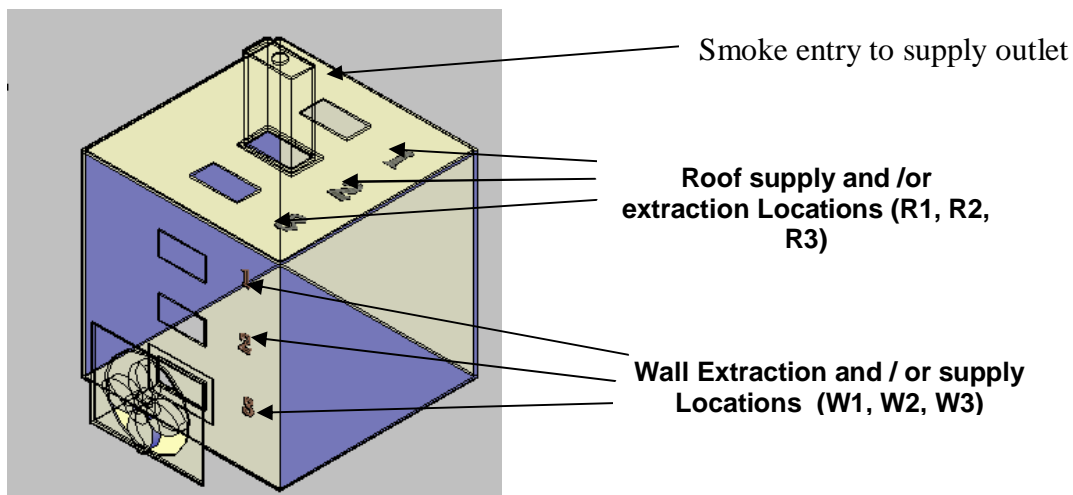
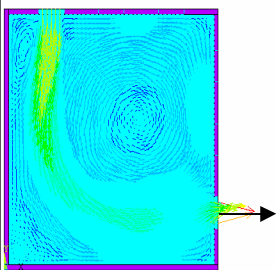
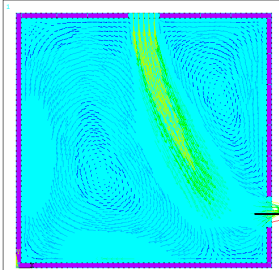
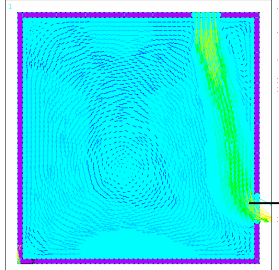
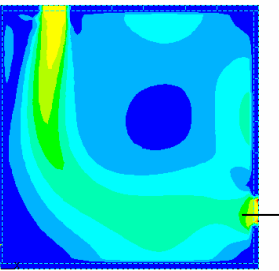
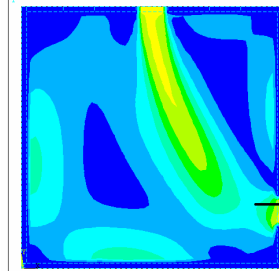
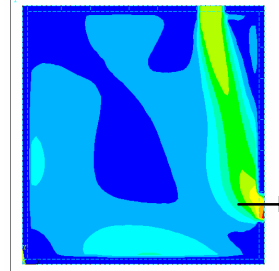
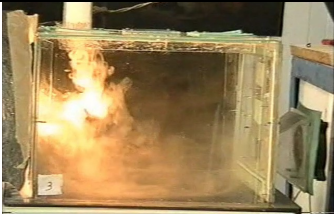
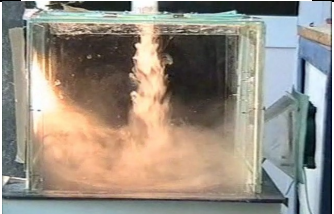
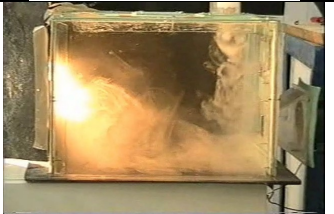
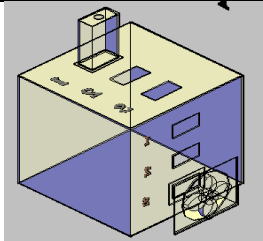
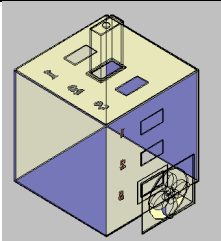
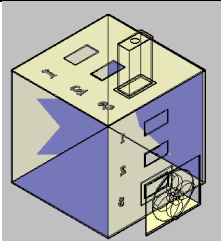


Fig.2: Test model with different locations for supply and extraction ports.

RESULTS AND DISCUSSIONS

As shown in Table 1-a, a comparison is given between experimental visualization using the smoke tunnel and theoretical findings using a CFD ANSYS-FLOTRAN in the form of velocity contours and the streamline vectors for combination (Rs1 We 3), where the suffix (s) denotes supply at ceiling and the suffix (e) denotes extraction at wall at position no.3. The flow enters from the supply and makes a circulation when impacting the adjacent rear wall and the floor before it is extracted from the wall grill. Table 1-b, shows the case (Rs2 We3), in which the circulation above the extraction grill is higher than the circulation in the remaining areas. The case (Rs3 We3) is illustrated in table 1-c, in which the flow passes directly from the supply to the extraction opening. Therefore, case (Rs1 We 3) is the best case.

Table 1 : Comparison Between Experimental and Theoretical Results (different supply locations Rs1,Rs2 & Rs3 with fixed exhaust in the wall We3)

	air flow ↓	air flow ↓	air flow ↓
ANSYS Streamlines			
ANSYS Contours			
Visualization			
Test model			
	(a)	(b)	(c)

In Table 2-a, the location of the extraction was changed to position no. 2. In the first case (Rs1 We2), circulation occurs adjacent the supply and the return openings. For the case (Rs2 We2), the flow passes directly from the supply to the return and there is no circulation inside the test room. In table 2-c, the third case (Rs3 We2), also the flow passes directly from the supply to the return without making any circulation inside the test room..

Table 2 : Comparison Between Experimental and Theoretical Results (different supply locations Rs1,Rs2 &Rs3 with fixed exhaust in the wall We2)

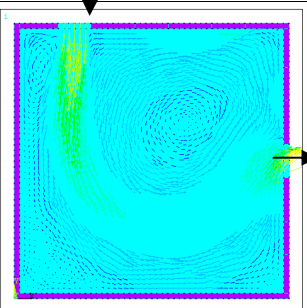
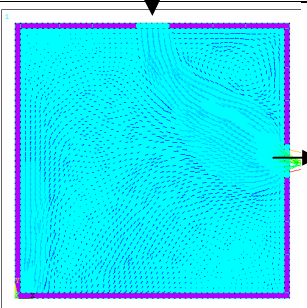
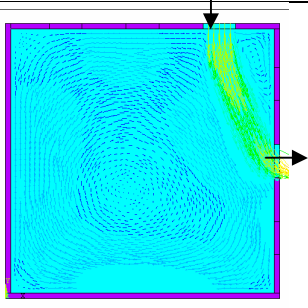
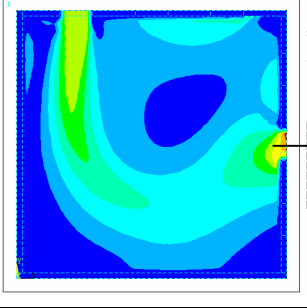
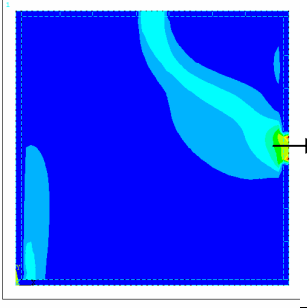
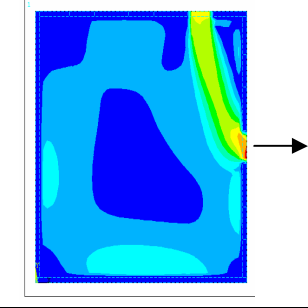
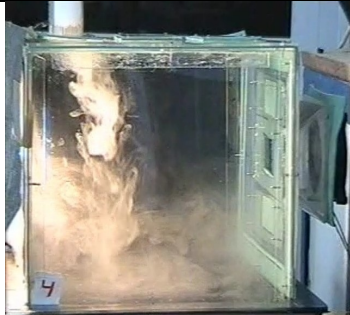

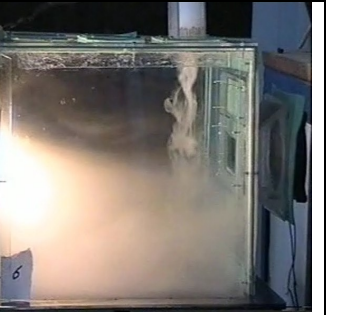
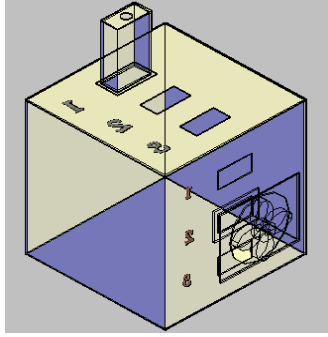
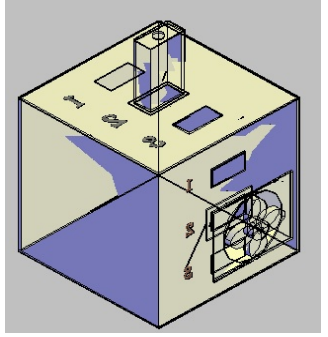
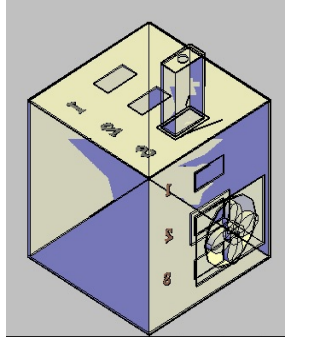
	air flow	air flow	air flow
ANSYS Streamlines			
ANSYS Contours			
Visualization			
Test model			
	(a)	(b)	(c)

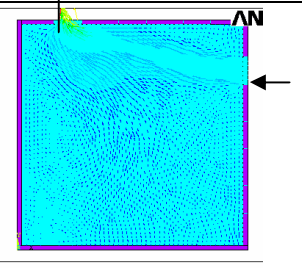
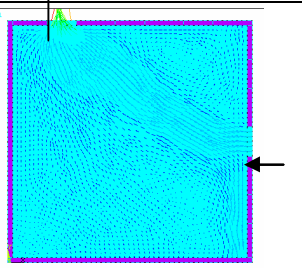
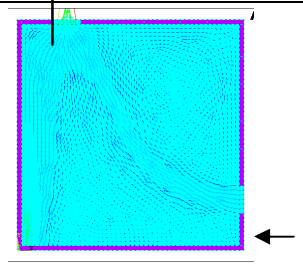
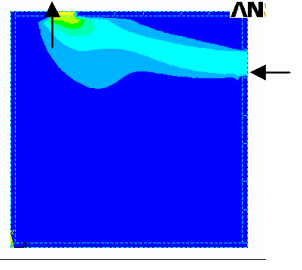
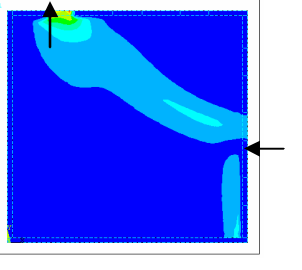
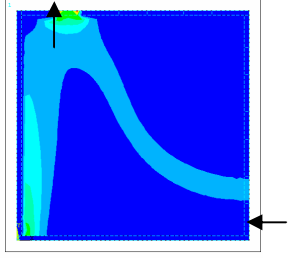
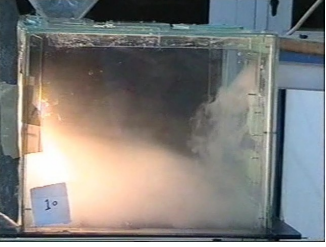


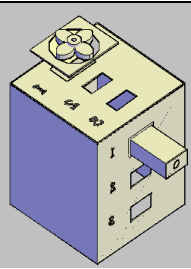
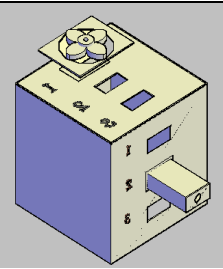
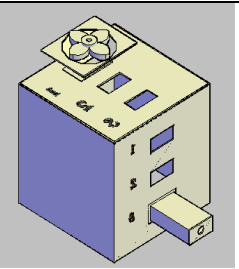
Table 3 shows the last combination for the roof supply. The first case (Rs1 We3), in which as shown in the visualization picture and velocity contour and in the streamlines, the flow passes directly from the supply to the return with a little circulation. For the second case, (Rs2 We3) the flow enters from the supply and divides into two parts the first is extracted and the second part impacting the floor and the rear wall making some circulation and nearly the whole volume covered by the smoke. Finally, the third case (Rs3 We3) as shown in table 3-c, the flow passes directly from the supply to the return without any circulation. Therefore, case (Rs2 We3) is the best in this group of combinations.

Table 3 : Comparison Between Experimental and Theoretical Results (different supply locations Rs1,Rs2 &Rs3 with fixed exhaust in the wall We1)

	air flow	air flow	air flow
ANSYS Streamlines			
ANSYS Contours			
Visualization			
Test model			
	(a)	(b)	(c)

In the second part of this work the extraction was taken from the roof and the supply was made at the front wall. Table 4-a shows the combination (Re1 Ws1). In this case, the flow passes from supply to return directly without making any circulation inside the test room. For the second case (Re1 Ws2), a small circulation occurs adjacent the extraction grill as shown in table 4-b. Table 4-c, shows the third case (Re1 Ws3), in which again a small circulation occurs inside the test room.

Table 4 : Comparison Between Experimental and Theoretical Results (different supply locations Ws1, Ws2 & Ws3 with fixed exhaust in the roof Re1)

	air extraction	air extraction	air extraction
ANSYS Streamlines			
ANSYS Contours			
Visualization			
Test model			

(a)

(b)

(c)

Table 5-a, illustrate the case of (Re2 Ws1), in which nearly no circulation occurs, but the flow was extracted directly from the supply. In table 5-b, for the case (Re2 Ws2) a small circulation occurs inside the tested room. For the last case (Re2 Ws3) Table 5-c, shows that circulation inside the test room is higher than the above two cases but are still a stagnation areas inside the test room.

**Table 5 : Comparison Between Experimental and Theoretical Results
(different supply locations Ws1,Ws2 &Ws3 with fixed exhaust in the roof Re2)**

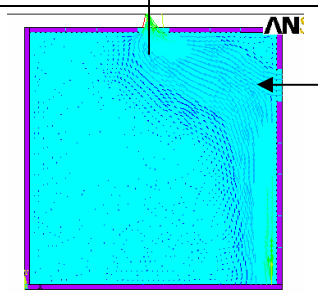
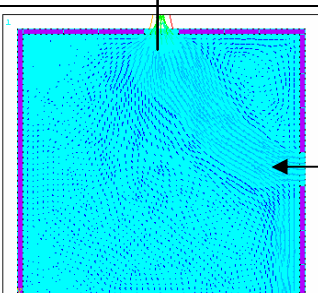
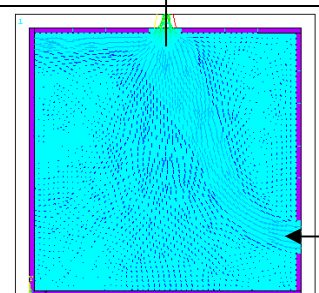
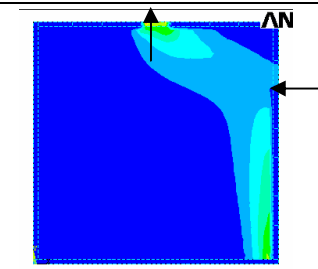
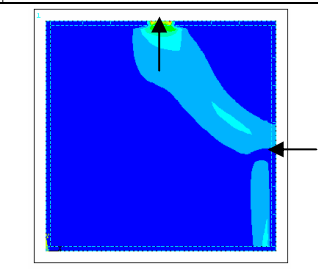
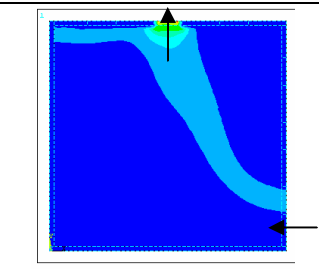
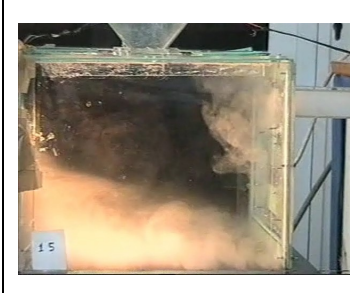

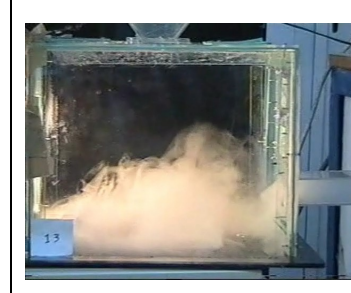
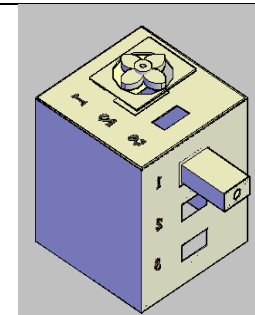
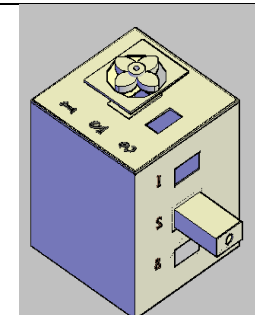
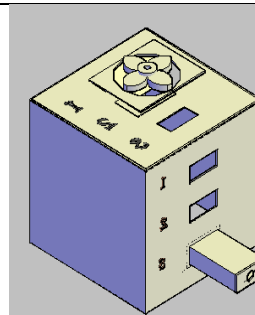
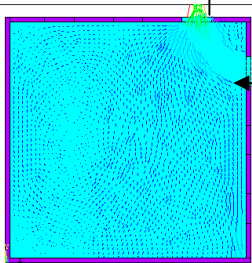
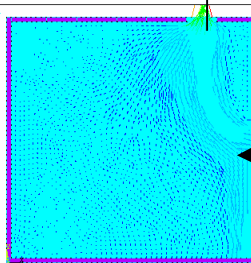
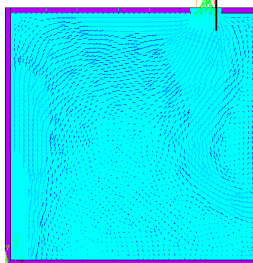
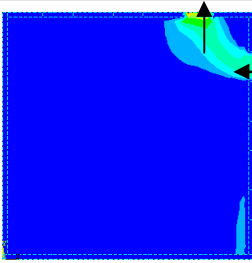
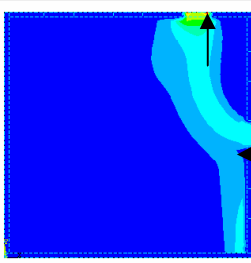
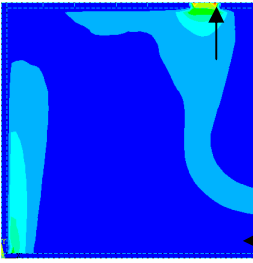

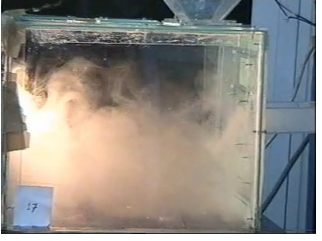
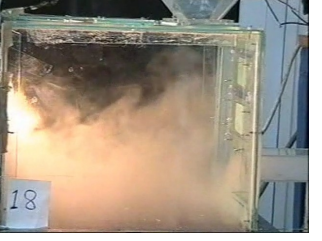
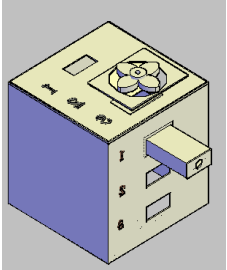
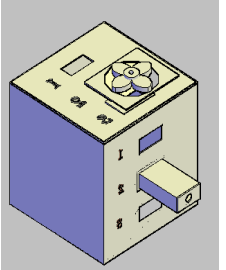
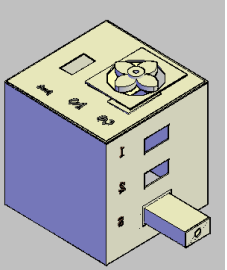
	air extraction	air extraction	air extraction
ANSYS Streamlines			
ANSYS Contours			
Visualization			
Test model			
	(a)	(b)	(c)

Table 6-a, shows the last group of combinations between supply and the return. In the first case, Re3 Ws1), the flow passes directly from the supply to the return resulting in a very small propagation of the smoke inside the tested room. In table 6-b, the case of (Re3 Ws2), indicates that the distance between the supply and the return increased and the flow propagation slightly increased. Finally, as shown in table 6-c, the last case (Re3 Ws3) shows that, the distance between supply and return has largest but the middle area of the test room is in a stagnation state.

**Table 6 : Comparison Between Experimental and Theoretical Results
(different supply locations Ws1, Ws2 & Ws3 with fixed exhaust in the roof Re3)**

	air extraction ↑	air extraction ↑	air extraction ↑
ANSYS Streamlines			
ANSYS Contours			
Visualization			
Test model			
	(a)	(b)	(c)

As shown in Table 7 a summarize the comparisons between the different combination of the supply and the extraction in the test room.

Table 7 Summarize of the Comparisons of Different Combinations of the Supply and the Extraction in the Test Room.

Case description	Case	Circulation status	evaluation
Roof supply at position 1, wall extraction at position 3	Rs1 We 3	good	Highly acceptable
Roof supply at position 1, wall extraction at position 3	Rs2 We 3	Weak	Not acceptable
Roof supply at position 1, wall extraction at position 3	Rs3 We 3	Poor	Not acceptable
Roof supply at position 1, wall extraction at position 3	Rs1 We 2	good	Highly acceptable
Roof supply at position 1, wall extraction at position 3	Rs2 We 2	Weak	Not acceptable
Roof supply at position 1, wall extraction at position 3	Rs3 We 2	Poor	Not acceptable
Roof supply at position 1, wall extraction at position 3	Rs1 We 1	Weak	Not acceptable
Roof supply at position 1, wall extraction at position 3	Rs1 We 1	good	Highly acceptable
Roof supply at position 1, wall extraction at position 3	Rs1 We 1	Poor	Not acceptable
Roof extraction at position 1, wall supply at position 1	Re1 Ws 1	Poor	Not acceptable
Roof extraction at position 1, wall supply at position 2	Re1 Ws 2	Weak	Not acceptable
Roof extraction at position 1, wall supply at position 3	Re1 Ws 3	Weak	Not acceptable
Roof extraction at position 2, wall supply at position 1	Re2 Ws 1	Poor	Not acceptable
Roof extraction at position 2, wall supply at position 2	Re2 Ws 2	Weak	Not acceptable
Roof extraction at position 2, wall supply at position 3	Re2 Ws 3	good	Highly acceptable
Roof extraction at position 3, wall supply at position 1	Re3 Ws 1	Poor	Not acceptable
Roof extraction at position 3, wall supply at position 2	Re3 Ws 2	Weak	Not acceptable
Roof extraction at position 3, wall supply at position 3	Re3 Ws 3	good	Highly acceptable

In the third part of this work the extraction and the supply are taken from the roof and in other two cases at the wall as shown in Table 8. In the first case the supply will be at the position no. 1 on the roof and the extraction at the position no. 3 on the roof (Rs1 Re3). The flow enters from the opening and is extracted directly without any circulation inside the conditioned room. Table 8-b shows the first case when the supply and the extraction are on the wall (Ws3 We1). In this case the propagation of the flow inside the conditioned space unsuitable for good comfort of occupants. Table 8-c shows the second case when the supply and the extraction are on the wall (Ws1 We3). In this case the same behavior as with the previous case will be occurred.

Table 8 : A Comparison Between Experimental and Theoretical Results

	air flow	air extraction	
ANSYS Streamlines			
ANSYS Contours			
Visualization			
Test model			
	(a)	(b)	(c)

CONCLUSION

From the experimental and theoretical results presented above and supported by video movie pictures, the following general comments may be made:

- i) Supply outlets should be located in the ceiling, so architects should provide a total height for the floor of 3.5 m at least. Also, these also should provide one wall without any architectural obstacles to locate the extraction for optimum air distribution.
- ii) It is found that, in vertically downward ventilation, using upper-level extraction may optimize the air flow distribution. In some architectural designs, this option may impossible because of the difficulties of duct network distribution.

RECOMMENDATIONS

One may re-affirm that the above-presented pictures give only a qualitative idea of the flow pattern inside a ventilated space under various conditions of the supply outlets and the extraction locations. They also, serve as first-hand results before going into details of measurement and computation. These pictures are adequate, although needed, to make any solid judgment as whether a certain situation is better than another.

Computational fluid dynamics can successfully replace experimental tools in determining the ventilation characteristics, thus much effort and cost can be saved.

REFERENCES

1. ASHRAE standards, 55 (1966).
2. Gnong N., K.W. Tham, A.K. Melikov, D.P. Wyon, S.C. Sekhar and DKW. Cheong (2006), "the performance for local air movement in the facial regions during long-term exposure in the tropics", proceedings of healthy buildings, Portugal, pp. 63-67.
3. Kempski, D. Van , (2006), "OCA- A new Approach for Evaluating the environment of buildings, healthy building, pp.81-84.
4. Ramiz K and Essam Khalil, (2003), " energy effecicent thermal comfort vs air quality in air conditioned healthcare application, building simulation, Netherlands august, 11-14.
5. Roulet C.A. (2006), " Indoor Air Quality and Energy Performance of Building", Proceeding of Health Building, Portugal, pp. 37-47.
6. Yousof, M.Z.M, A.M. Leman, A. Hussain, S.M.R. Shah, (2006)," the effectiveness of under floor air distribution (UFAD) system in controlling thermal comfort and indoor air quality", healthy building, pp.135-140.
7. Streifel, A.J. Healthcare (2000), " IAQ: Guidance for Infection Control", HPAC Jornal, pp.28-36.

MASTER PLAN FOR THE PHYSICAL DEVELOPMENT OF IBRAHIM BADAMASI BABANGIDA UNIVERSITY (IBBUL), LAPAI, NIGERIA

***Mustapha Zubairu**

*Associate Professor, Department of Urban and Regional Planning,
Federal University of Technology, Minna, Nigeria
Email: mzubairu2002@hotmail.com*

ABSTRACT

The Governor of Niger State, Nigeria inaugurated a Committee for the establishment and development of Niger State University. Among the objectives of the University is to facilitate enhanced access to University education, and transformation of socio-economic lives of Nigerlites. Another Committee was established and charged with the responsibility of evaluating and implementing the Report. IBBUL is scheduled to be fully developed over a fifteen year period, in three phases of five years each. My firm was commissioned to prepare the Master Plan for the University, on the 694.68 hectares of land acquired for the project. The methodology is based on extensive consultation with all stakeholders to give them a sense of ownership. IBBUL is to have a total of nine Faculties; and four Centres of Research on full development, while phase one is to have four Faculties. The projected students' enrolment of IBBUL in the four Faculties is 900, 1,350, 1,850, 2,400, and 3000 respectively. The projected academic staff requirements for phase one is 58, 88, 118, 150, and 196 respectively. A total of eight principles formed the basis of the design of the Master Plan, while the plan itself has the following components: vehicular and pedestrian circulation plan; administration building; academic corridor; research zone; central area; staff housing area; students hostels; sports and recreational area; university farm centre and zoological garden; water supply; and electricity supply. On site, the design and construction of the roads and drainage within the Campus was based on the Master Plan prepared, and the construction of fifty two buildings (Academic, residential etc), in progress, conforms to the Plan. The University has since commenced operation with the admission of the first batch of 350 undergraduate students, in four Faculties. Keywords: academic, circulation, department, faculty, functional, recreational, residential.

INTRODUCTION

On 24th August 2004, the Executive Governor of Niger State, Engineer Abdulkadir Abdullahi Kure, inaugurated a Blueprint Drafting Committee for the establishment and development of Niger State University. The stated objectives of establishing a University in the State include the need to facilitate enhanced access to University education, and the total transformation of social and economic lives of Nigerlites through sustainable development initiatives for human efficiency and productivity among others.

Upon the completion of the work of the Blue print drafting Committee, and the acceptance of its Report by Governor, another committee, known as the Evaluation and Implementation Committee (EAIC) was established and charged with the responsibility of evaluating and implementing the Report. Similarly, the proposed University was named after General Ibrahim Badamasi Babangida, former President and Commander-in-Chief of the Armed Forces of Nigeria. Accordingly, the name of the University is now Ibrahim Badamasi Babangida University, Lapai (IBBUL).

Technical Note

* Corresponding author
Received Date:30/12/07
Acceptance Date:17/4/08

copyright © 2008

The University is scheduled to be fully developed over a fifteen year period, in three phases of five years each. Consequently, the EAIC commissioned a firm of Architect/Planners (Sustainable Human Settlements Consult Limited) in which I am its Principal Partner, to prepare the Master Plan for the University, on the 694.68 hectares of land acquired for the project, along Paiko-Lapai Road, about five kilometres from the town of Lapai.

The objective of this paper is to highlight the core issues addressed in the cause of preparing the Master Plan to guide the physical development of the University.

Administratively, Nigeria has three tiers of government-federal government; thirty six states and one federal capital territory; and 774 local governments.

METHODOLOGY

One of the stated objectives of Niger State Government is to provide a University that all the people of the state (Nigerlites) will be proud of and associate themselves with. As a consequence and also the fact that we had barely two months to prepare the Master Plan, the methodology adopted is summarised as follows:

- i. All stakeholders, representing prominent Nigerlites, traditional rulers, professionals in related fields, NGOs, CBOs, PVOs and other Civil Society organisations were identified, sensitised and made a part of the different consultation groups to generate ideas and the constructively criticise the main issues identified in the process. This is so as to develop a shared understanding of the core issues, and to build a critical mass of supporters of the projects across all political and ethnic persuasions.
- ii. A variety of complementary studies were carried out such as the preparation of Environmental Impact Assessment of the proposed development on the environment and adjoining villages; Soil Investigation; preparation of a digitised topographic map of the site;
- iii. Similarly an extensive consultation was carried out with all stakeholders and professionals, in related fields, of Niger State extraction;
- iv. Drafts of the Master Plan were subjected to independent evaluation by a panel of Town Planners from the State and the Physical Department of the Nigerian Universities Commission (NUC);
- v. Draft Final copy of the Master Plan was approved by the EAIC (client).

PLANNED ACADEMIC PROGRAMMES AND STRUCTURE

The IBB University is to have the Faculty/Department structure. At full development, IBBUL is to have a total of nine Faculties; and four Centres of Research in Agriculture, Policy Analysis and Strategy, Biotechnology, and a Teaching Hospital. The phase one is to have four Faculties-Agriculture, Education and Arts, Applied and natural Sciences and Management and Social Sciences. The first three are to have six Departments each, while the last is to have five. IBBUL is also to construct a befitting Administrative Block and other complementary facilities like staff quarters, students hostels etc.

Staff and Students Projection

The projected students' enrolment of IBBUL of the four Faculties, in the first five years of its existence is 900, 1,350, 1,850, 2,400, and 3000 respectively. The projected academic staff requirements for phase one of the University 58, 88, 118, 150, and 196 respectively. The ratio used is 1 academic staff to 20 students for Arts based faculties and 1:10 for Science based faculties. It is also recommended that the above be distributed among the different ranks as per National Universities Commission norms as follows.

Professors/Associate Professors	-	20%
Senior Lecturers	-	35%
Lecturers I, II and Assistant Lecturers	-	45%

Source: Blue print Committee Report, 2004

EXISTING SITE CONDITIONS

The topographic features and existing land use of the site are summarised in figures 1.0 and 2.0, respectively.

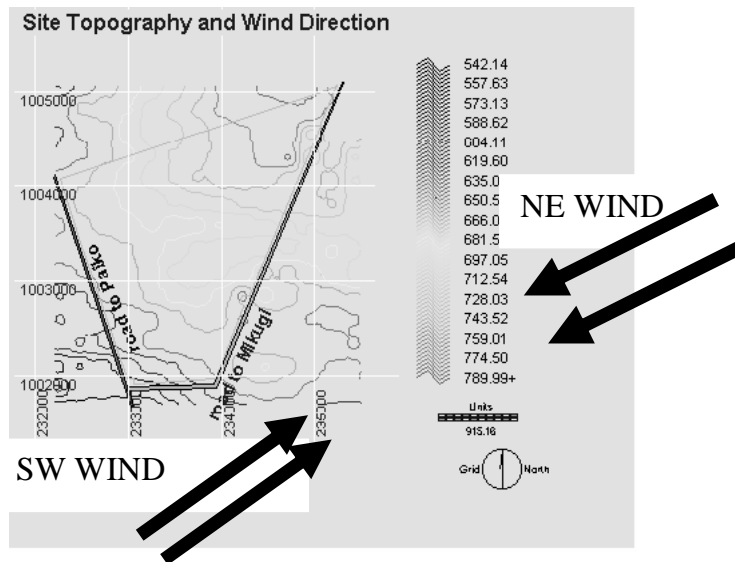


Fig. 1: Site Topography and Wind Direction

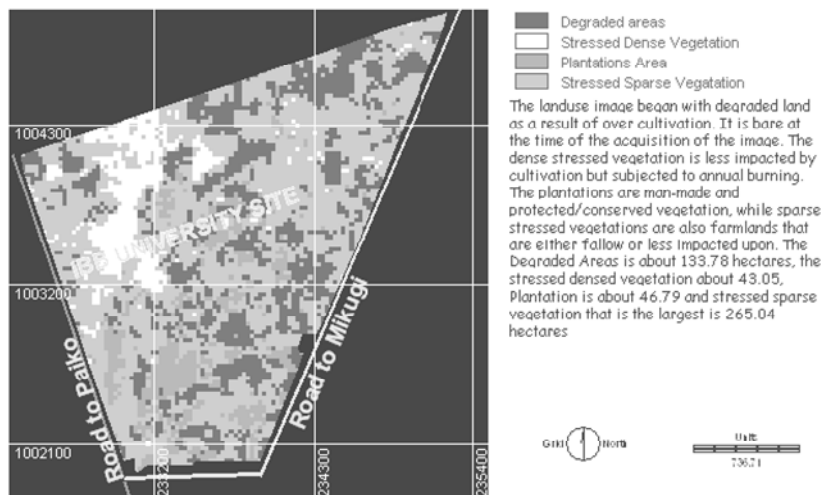


Fig. 2: Land Use Characteristics of Site

EXISTING FACILITIES/SERVICES AND UTILITIES IN LAPAI TOWN

Lapai has the following facilities that can be easily accessible to the university community.

Market

Lapai has a weekly market that operates on every Tuesday and is located about 2km to the university. It has several shops and supermarkets.

Electricity

The town electricity is serviced by Doko feeder (33kva) supply by NEPA. This will soon be augmented by a feeder from Minna which is also 33KVA capacity. Though the 33KVA is adequate there is no stable power supply to Lapai.

Water

The water supply is from the Niger State Water Board system in the town. The capacity of the system is about 1000m³, but the existing plant hardly produces up 77m³ daily. This quantity is grossly inadequate for the present population of the town; in fact even the 1000m³ is inadequate for the town. Presently the supply from the Water Board is augmented with water from boreholes, which have to be up to 70-80m deep to make them effective. Most of the rivers are seasonal and this explains why most of the communities around the university depend on boreholes.

Telecommunication

The existing network by Nigeria Telecommunication is functional only when there is electricity. However, two mobile networks have recently extended their services to Lapai, due to the plan to locate IBBUL there.

Health Service

The community clinic/hospital is less than 1 kilometre from the University gate. It would, however, require up grading in view of the improved status of the town with the coming of the university.

CORE DESIGN PRINCIPLES OF THE MASTER PLAN

The buildings and other physical facilities that comprise a campus play a vital role in achieving the objectives of the University. The quality of the physical facilities contributes immeasurably to the offering of quality educational and research programs and the overall image of the university. Planning succeeds when those who use the campus appreciate its value, understand its power to enhance the educational process and human life, and become active advocates for excellence in the built environment. In designing the Master Plan, account was taken of long-range programme directions of IBBUL, as highlighted in the Academic Brief prepared by the EAIC, and the facilities needed to support those directions.

Accordingly, the following principles were applied during the planning process to provide direction for planning decisions and to help insure the resultant plans include necessary considerations.

- i. To create a unique identify for the University in terms of its planning, architecture and programmes to be offered related to the developmental priorities of Niger State;
- ii. To create a physical environment that contributes aesthetically and physically to the overall educational experience, such as encouraging social interaction, educational discourse etc;
- iii. To plan facilities on the basis of student enrolment and other population levels and distributions over the fifteen-year development period of the University;
- iv. To plan facilities that are responsive to programs and the way they are delivered. Modern methods of teaching and learning, based on Information and Communication Technology (ICT) will be used to facilitate collaborative research of staff and students, teaching and learning by students; To recognize the increasingly diverse (in age, ethnic background, religion etc) student population, and to provide for the needs of these students;
- v. To encourage collaboration, partnerships and innovation in planning, in the form of joint public-private ventures, multi-use facilities, interdisciplinary functions, and other collaborative innovations;
- vi. To ensure community participation in the planning process and benefits to the community in terms of agricultural extension service, transfer of appropriate technology to local farmers in the immediate vicinity of the University and beyond;
- vii. To provide for the transportation needs of the university community and effective segregation of vehicular and pedestrian traffic on the Main Campus (SHSC, 2006).

THE MASTER PLAN

The IBBUL Master Plan has the following components: vehicular and pedestrian circulation plan; administration building; academic corridor; research zone; central area; staff housing area; students hostels; sports and recreational area; university farm and zoological garden; university farm centre; water supply; and electricity supply. These are designed to direct its physical development:

The Land Use Plan

Based on the, present and future, space requirement of the various land uses identified, the land allocation was made, as Land Use Plan proposed, as in Figure 3.0.

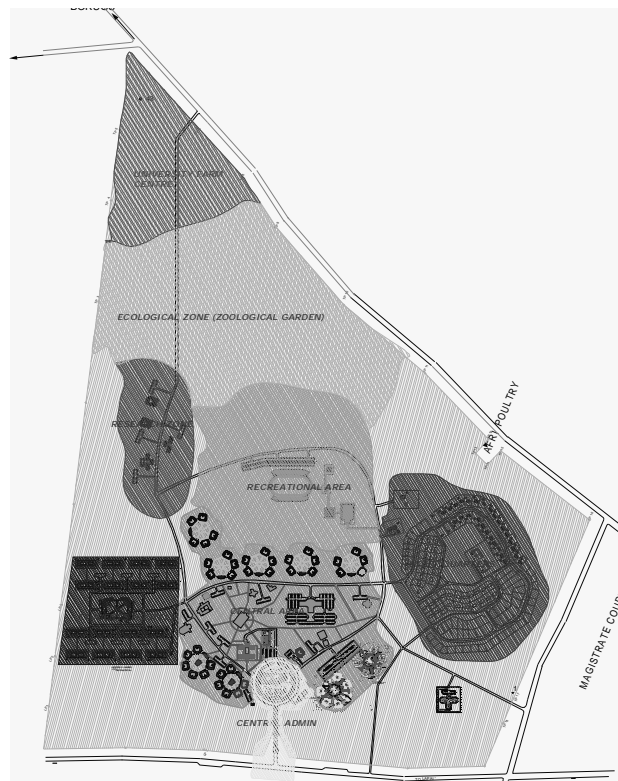


Fig. 3: Land Use Plan of BBUL

Based on schedule of accommodation developed from the physical development brief produced for IBBUL, the land requirement for the facilities now and in the future, out of the 694 hectares acquired for the project, was determined and cleared with EAIC.

ELEMENTS OF THE MASTER PLAN

Our main objective is to create an Eco Campus through the preservation of the numerous orchards of Cashew trees recovered from the farmers who were duly paid compensation. It is hoped that appropriate Department of the University will provide the lead in harnessing the cashews into nuts and juice on a commercial basis, with the revenue accruing to the University. In this respect we intend to encourage the staff and students to walk within the University, through a careful segregation of pedestrian and vehicular traffic. We have also proposed that covered walkways should be constructed to facilitate the movement of people, especially students within the Campus irrespective of the season (dry and wet).

A total of three physical planning concepts were generated for the development of IBBUL. These were subjected to internal and independent review by EAIC, and Town Planners from Niger State, who have been part of the advisory group established to facilitate the process. As a result, a consensus was reached to adopt the site plan shown in figure 4.0.

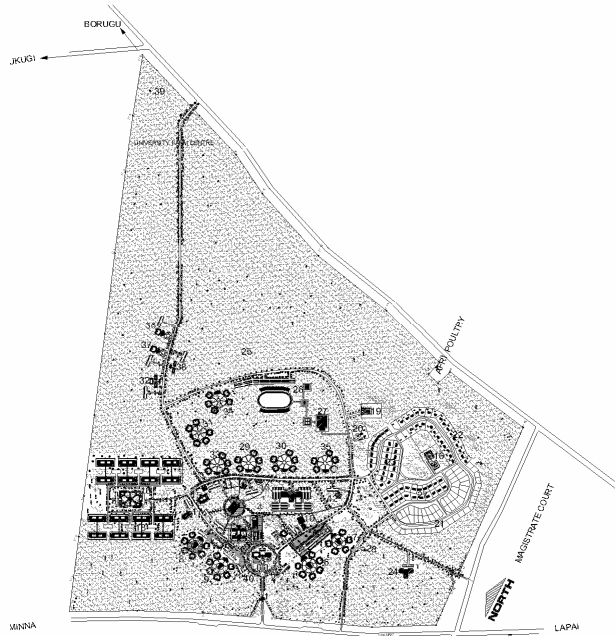


Fig. 4: Site Plan of IBBUL

Vehicular and Pedestrian Circulation Plan

Following facilities were provided: On and Off Campus Bus Stops; and strategically located central parking spaces to be managed on a public-private partnership. Table 5.0 shows the circulation plan. A total of 13km of asphalt road; 9km of surface dressing and 44km of drainage had been constructed as at the time of this report.

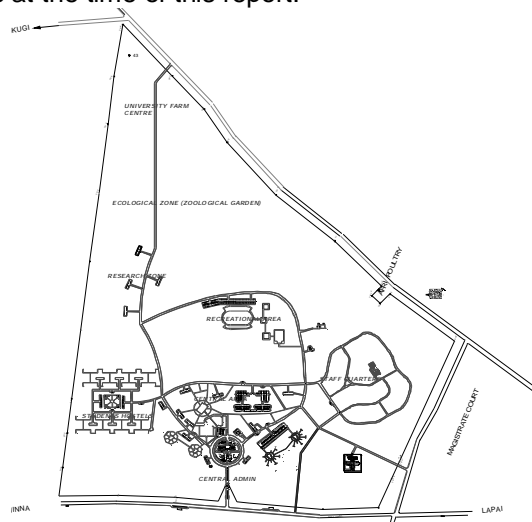


Fig. 5: Vehicular and Pedestrian Circulation

Administration Building

The Administration Building is designed to symbolise the image of the University. This is to be achieved through its architecture and quality of internal and external finishes. The building is designed to be the highest on the Campus. In order to maximise the use to which many of its facilities are to put to, it was recommended to separate the Senate and Council Chambers from the main building. The two components are to be connected by a covered walkway (bridge). It was, also, proposed that the building be located within the main “round about” at the entrance to the Campus, of 200m diameter. The proposal is shown in figure 6.0.

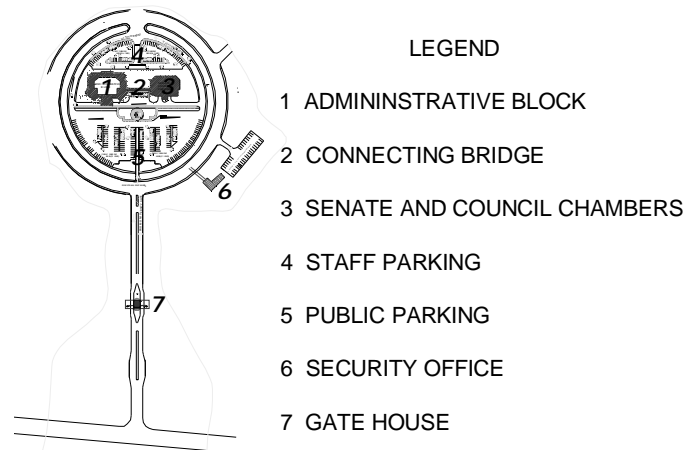


Fig. 6: Central Administration

Academic Corridor

Defines contiguous land area that is intended to guide the siting of academic facilities. Academic Faculties and Departments which share disciplinary interests and desires are located close to one another. Figure 7.0 shows the location of all the nine Faculties planned of the University.

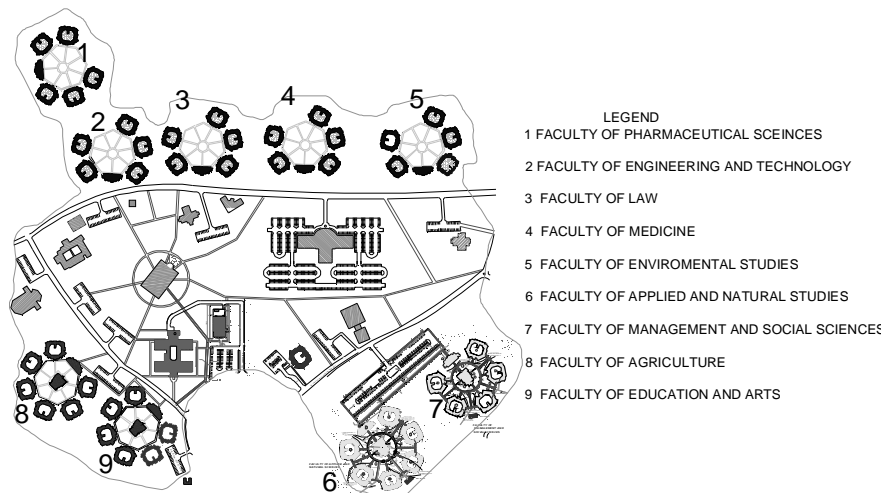


Fig. 7: Academic Corridor

Research Zone

Buildings to house the research facilities of IBBUL are located next to each other, in a slightly secluded part of the University to give the researchers the required serene environment for their work. This is as shown in figures 4.0 and 8.0.

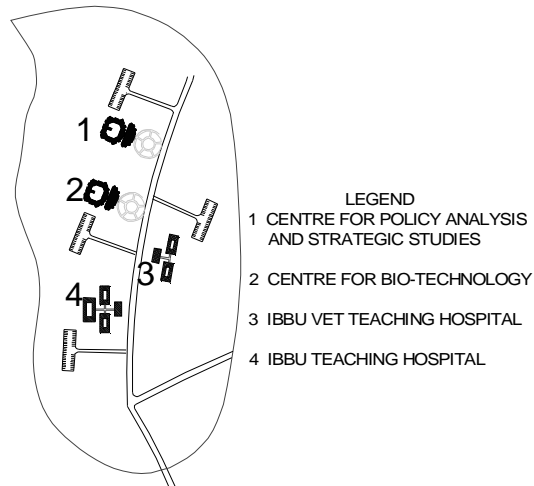


Fig. 8: Research Zone

Central Area

This is the neighbourhood in the centre of Campus which is the heart of campus activity. This area includes academic space, lecture halls, conference centre, cafeteria, library, religious spaces (Mosque and Chapel), ICT Centre, university clinic, bookshop, post office, and printing press. This is as shown in figure 9.0.

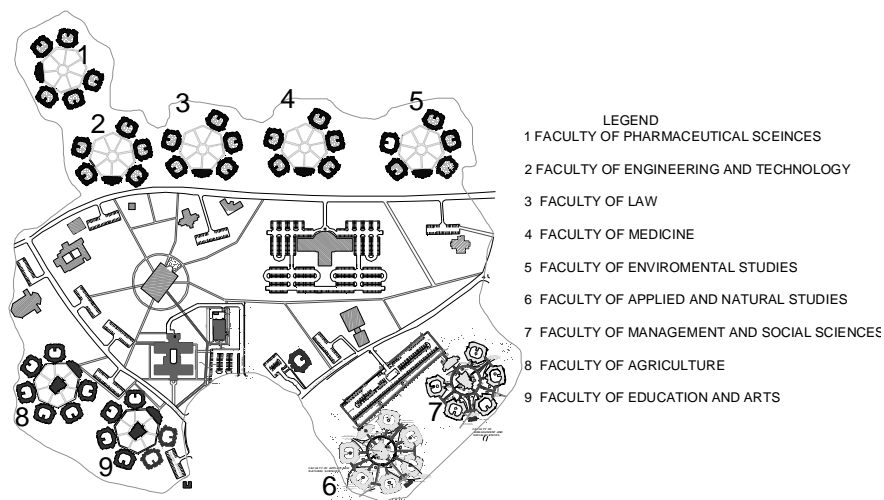


Fig. 9: Central Area

Staff Housing

Even though we are in an era of monetisation of benefits to the staff of University as is the case in Nigerian civil service, it was felt that the IBBUL must have a modest staff quarters to accommodate its pioneering staff, especially, Vice Chancellor, Registrar, Professors and members of the University management, other senior officers and a few junior and intermediate staff. Based on that, a layout was proposed that will facilitate the establishment of a harmonious community. A total of forty units are already under construction, based on the layout, as shown in figure 10.0.

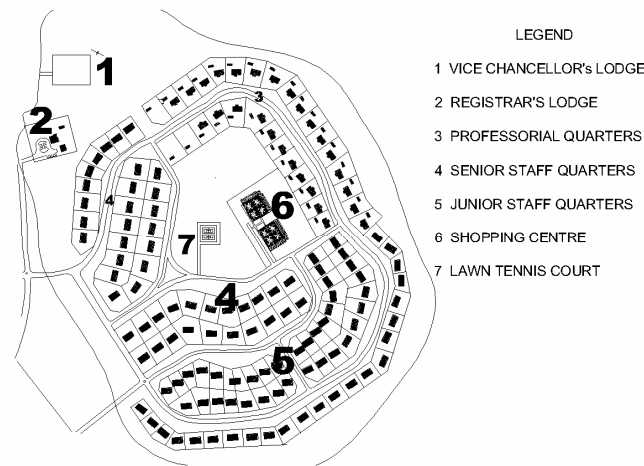


Fig. 10: Staff Quarters

Students Hostel

The layout for the student hostels have been designed such that students will have a sense of identity to their blocks and also belonging to the entire neighbourhood. This should promote a healthy inter hall athletic and games competition. The layout is as shown in figure 11.0.

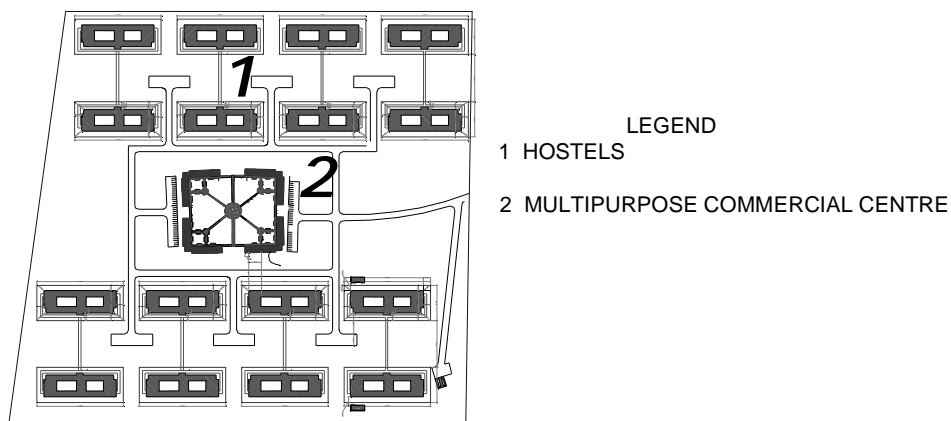


Fig. 11: Layout of Student Hostels

Recreational Area

The location of the recreational area was deliberately chosen, in the middle of the University so as to be inspired by the setting, serenity, architecture and by seeing their peers who are students of the University, at work. The details of the recreational facilities are shown in figure 12.0.

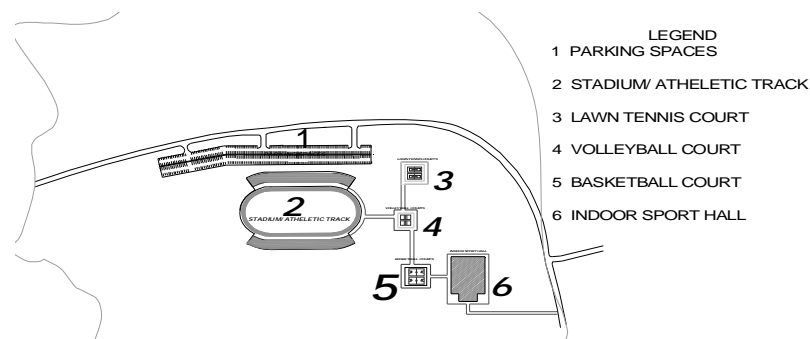


Fig. 12: Recreational Area

Park and Zoological Garden

The Park and Zoological Garden - defines IBBUL's natural resources, includes at least 100 hectares of Cashew nuts plantation and a nature park of 10 hectares to be left, as is. This should facilitate future research.

University Farm Centre

50 hectares of land has been earmarked for the University Farm Centre. This is to enable the students to acquire practical farming experience including the repair of farm implements and equipment, on a demonstration farm. The Farm is in addition to provide extension service to the farmers in the villages around the University and in other parts of the state.

Water Supply

Pending the completion of the, on going Regional Water Project in Lapai by Niger State Government to which IBBUL will be connected, temporary water scheme, involving the sinking of ten industrial boreholes; water treatment plant; ground tank of 500,000 litres capacity; and an overhead tank of 400,000 litres is currently under construction.

Electricity Supply

Electricity from the Power Holding Company of Nigeria (PHCN) will be supplied to the University from both the Bida and Minna supply sources. On the Campus, a provision for five substations each with a 500KVA generator, with automatic changeover facility is currently under construction. There is also a negotiation going on with PHCN for a dedicated supply line to be provided to the University. This will meet the power requirements of the IBBUL now and in the future.

CONCLUSION

It is gratifying to note that the design and construction of the roads and drainage within the Campus was based on the Master Plan prepared. This has made the construction of fifty two buildings (Academic, residential etc), currently in progress, in conformity to the Plan. The University has since commenced operation with the admission of the first batch of 350 undergraduate students, in four Faculties.

REFERENCES

1. Blueprint Drafting Committee, (2004) "Blueprint for the Establishment of Niger State University". Report of the Blueprint Drafting Committee, June.
2. EAIC, (2006) "The Journey So Far" Journal of the Evaluation and Implementation Committee, Ibrahim Badamasi Babangida University, Lapai, No. 1, Volume 1, March.
3. SHSC LTD, 2006: "Master Plan of the Ibrahim Badamasi Babangida University, Lapai".